DESIGN & FABRICATION OF TWO SEATED AIRCRAFT WITH AN ADVANCED ROTATING LEADING EDGE WING

BY

AL AHMARI, SAEED ABDULLAH SAEED

Jumada II 1432 (H)

May 2011 (G)

DESIGN &FABRICATION OF TWO SEATED AIRCRAFT WITH AN ADVANCED ROTATING LEADING EDGE WING

BY

AL AHMARI, SAEED ABDULLAH SAEED

A Thesis Presented to the

DEANSHIP OF GRADUATE STUDIES

KING FAHD UNIVERSITY OF PETROLEUM & MINERALS

DHAHRAN, SAUDI ARABIA

In Partial Fulfillment of the
Requirements for the Degree of

MASTER OF SCIENCE

In

AEROSPACE ENGINEERING

Jumada II 1432 (H)

May 2011 (G)

KING FAHD UNIVERSITY OF PETROLEUM & MINERALS

DHAHRAN 31261, SAUDI ARABIA

DEANSHIP OF GRADUATE STUDIES

This thesis, written by AL AHMARI, SAEED ABDULLAH under the direction of his thesis advisor and approved by his thesis committee, has been presented to and accepted by the Dean of Graduate Studies, in partial fulfillment of the requirements for the degree of MASTER OF SCIENCE in AEROSPACE ENGINEERING.

Thesis Committee

22/9/1432H. 22/8/2011G.

Dr. Ahmed Z. Al-Garni (Advisor)

29/5/2011 G

Dr. Wael G. Abdelrahman (Co-Advisor)

29/5/2011G

Dr. Ayman H. Kassem (Member)

Dr. Edi Prasetyo (Member)

29/5/2011G

Dr. Ahmet Ziyaettin Sahin (Member)

22/9/1432H.
22/8/2011G

Dr. Ahmed Z. Al- Garni
(Chairman, Department of Aerospace Engineering)

Dr. Salam A. Zummo
(Dean of Graduate Studies)

5/10/11

Date

Dedicated to

My beloved

parents, wife, kids, brothers, and sisters

Acknowledgements

"In the name of Allah (God), The Most Gracious, The Most Merciful. Read, In the name of thy lord and Cherisher, Who created man from a [leech - like] clot. Read, and thy Lord Is Most Bountiful, He Who taught [the use of] the pen. Taught man that which he know not. Nay, but man doth Transgress all bounds. In that he looketh upon himself as self- sufficient. Verily, to thy Lord is the return [of all]. " (The Holy QURAN, Surah No. 96)

All praise and thanks are due to Almighty Allah, The Most Gracious, The Most Merciful, for his immense beneficences and blessings. He gave me the extra-ordinary patience to bear the hardships and carry out the work which has resulted in the accomplishment of this research. May peace and blessings be upon Prophet Muhammad (PBUH), his family and his companions.

Acknowledgement is due to King Fahd University of Petroleum and Minerals for the support extended towards my research. Also, I would like to take this opportunity to thank everyone who has helped me to get this master degree in Aerospace Engineering. First, I would like to thank my thesis advisor *Dr. Ahmed Z. AL-Garni*, who has supported me throughout my degree, for his help, advice and valuable suggestions. Also, I would like to thank my co-advisor, *Dr. Wael G. Abdelrahman* for his encouragement, guidance and support. Many thanks and appreciation to my committee members, *Dr. Ayman H. Kassem, Dr. Edi Prasetyo and Dr. Ahmet Sahin* for their help and advice.

My sincere and heartfelt appreciations are dedicated to my parents, my wife, my daughter, my son, my brothers and sisters. My deep gratitude is towards them, for their prayers, support, encouragement and patience during my study.

TABLE OF CONTENTS

List of Tables

List of Figures

Abstract (English)

Name: Al Ahmari, Saeed A.
Title: Design &Fabrication of Two Seated Aircraft with an Advanced Rotating Leading Edge Wing
Degree: Master of Science
Field: Aerospace Engineering (Aerodynamics, Design & Structure)
Date of Degree: Jumada II 1432 (H) - May 2011

The title of this thesis is" Design &Fabrication of two Seated Aircraft with an Advanced Rotating Leading Edge Wing", this gives almost a good description of the work has been done. In this research, the moving surface boundary-layer control (MSBC) concept was investigated and implemented. An experimental model was constructed and tested in wind tunnel to determine the aerodynamic characteristics using the leading edge moving surface of modified semi-symmetric airfoil NACA1214. The moving surface is provided by a high speed rotating cylinder, which replaces the leading edge of the airfoil. The angle of attack, the cylinder surfaces velocity ratio U_c/U, and the flap deflection angle effects on the lift and drag coefficients and the stall angle of attack were investigated. This new technology was applied to a 2-seat light-sport aircraft that is designed and built in the Aerospace Engineering Department at KFUPM. The project team is led by the aerospace department chairman *Dr. Ahmed Z. AL-Garni and Dr. Wael G. Abdelrahman* and includes graduate and under graduate student. The wing was modified to include a rotating cylinder along the leading edge of the flap portion.

This produced very promising results such as the increase of the maximum lift coefficient at $U_c/U=3$ by 82% when flaps up and 111% when flaps down at 40° and stall was delayed by 8degrees in both cases. The laboratory results also showed that the effective range of the leading-edge rotating cylinder is at low angles of attack which reduce the need for higher angles of attack for STOL aircraft.

Master of Science Degree
King Fahd University of Petroleum and Minerals
Dhahran, Saudi Arabia
Jumada'II 1432 H
May 2011

Abstract (Arabic)
ملخص الرسالة

الاســـــــم: سعيد بن عبدالله بن سعيد الأحمري

الــعنـــوان: تصميم وتصنيع طائرة بمقعدين ذات جناح مطور بمقدمة دوارة

الدرجـــــة: ماجستير في العلوم الهندسية

التخصص: هندسة طيران وفضاء (الديناميكية الهوائية والتصميم والهياكل)

الـتـاريـــخ: جمادى الثانية 1432هـ - مايو 2011 م

عنوان هذه الرسالة هو "تصميم وتصنيع طائرة بمقعدين ذات جناح مطور بمقدمة دوارة" وهذا يعطي وصف عام عن ماتم عمله في هذا البحث حيث تم مناقشة وتطبيق مبدأ التحكم في الطبقة المتاخمة بتحريك السطح. وذلك بعمل نموذج لمقطع جناح NACA2412 واختباره في النفق الهوائي ليتم اختبار مدى التغير في خصائص النموذج الديناميكية الهوائية مثل معامل الرفع ومعامل المقاومة الهوائية ونسبة الرفع إلى المقاومة وزاوية الانهيار. هذا النموذج زود بإسطوانة تدور بسرعات عالية في مقدمة الجناح وتم التحكم بثلاثة متغيرات هي : نسبة دوران الاسطوانة إلى سرعة الهواء وزاوية نزول الجنيح (flap) وزاوية الهجوم. وبعد ذللك طبقت هذه التقنية الحديثة على جناح طائرة تم تصميمها وبنائها في قسم هندسة الطيران بالجامعة ، وهذا المشروع بإشراف الأستاذ الدكتور/ أحمد بن ظافر القرني رئيس قسم هندسة الطيران و الفضاء والدكتور/ وائل عبدالرحمن ويضم الفريق عدد من طلاب الدراسات العليا والجامعية.

كانت نتائج الاختبار ممتازة حيث أنه عند نسبة دوران الاسطوانة إلى سرعة الهواء تعادل 3 يزيد معامل الرفع الاقصى بنسبة 83 بالمائه بدون استخدام الجنيح و 111 بالمائه مع استخدام الجنيح عند 40 درجة وتتأخر زاوية الانهيار 8 درجات في كلا الحالتين. وأثبتت الدراسة كذلك أن هذه التقنية تزيد كفائتها عند درجات الهجوم المتدنية وذلك يعني عدم الحاجة إلى درجات هجوم أعلى للطائرات قصيرة الإقلاع والهبوط.

درجة الماجستير في العلوم الهندسية

جامعة الملك فهد للبترول والمعادن

المملكة العربية السعودية – الظهران

جمادى الثانية 1432هـ

مايو 2001 م

NOMENCLATURE

AR	aspect ratio
bhp	shaft brake horsepower
b_{ht}	horizontal tail span
b_{vt}	vertical tail span
b_w	wing span
C_D	drag coefficient
C_{D0}	base drag coefficient
CG	center of gravity
C_L	lift coefficient
C_{ht}	horizontal tail scaling coefficient
c_r	root cord
c_t	tip cord
C_{vt}	vertical tail scaling coefficient
c_w	wing chord
LERC	Leading-Edge Rotating Cylinder
L_f	fuselage length
L_{ht}	distance from wing aerodynamic center to horizontal tail aerodynamic center
L_{vt}	distance from wing aerodynamic center to vertical tail aerodynamic center
L/*D*	lift to drag ratio
MAC	wing mean aerodynamic chord
MSBC	Moving Surface Boundary- Layer Control
n	load factor
P	performance parameter
q	dynamic pressure
RPM	revolution per minute
S_{ht}	horizontal tail area
STOL	short takeoff and landing
S_{vt}	vertical tail area
S_w	wing area

t/c	thickness ratio
U	freestream velocity
U_c	cylinder tangential velocity
U_c/U	cylinder surface velocity ratio
V	aircraft velocity
V_H	level full-throttle speed
V_s	stall speed
Vz	rate of climb
W	total weight
W_e	empty weight
W_{TO}	takeoff weight
W_u	useful weight
X	the actual center of gravity position
X_F	the most forward position of the center of gravity
X_R	the most rearward position of the center of gravity
Z_{max}	service ceiling
α	angle of attack
δ	flap deflection angle
λ	taper ratio
ρ	density
ω_c	angular velocity of the cylinder

CHAPTER 1

Introduction

1.1Objectives

The major objective of this research is to study and characterize the effect of a leading edge rotating cylinder on the aerodynamic characteristics of a semi-symmetric NACA 2412 and to design and build a 2-seat light-sport aircraft equipped with rotating cylinder at the leading edge along the flap portion of its wing. This aircraft will be used as a platform for testing the rotating cylinder technique. In this regard, the effect of the cylinder on the aerodynamic characteristics of airfoil section such as lift, stall angle, drag and pressure distribution will be investigated. The ultimate objective of the present work is to use flow control to delay leading edge separation from the airfoil, which in practical terms will allow the removal of the leading edge slat devices.

1.2 Introduction

The challenge to aircraft engineers and designers since Ludwig Prandtl (1904) introduced the concept of boundary layer has been to find ways to minimize the adverse effects of boundary layer. To meet the new generation of high performance airplanes, demand and requirements for improved performance, aerodynamics and less environmental impact, much research work has been conducted on ways to reduce

drag. The adjustment of the pressure gradient by shaping and using laminar boundary-layer control are two powerful and effective ways to reduce drag [1]. Aircraft manufacturers are under economic and environmental pressures to produce aircrafts which are more efficient, simpler in design and have reduced manufacturing and maintenance costs [2]. There is a need to achieve larger increase in lift to drag ratio for a given angle of attack in order to increase the overall efficiency which will be transformed into improvements in fuel burn and cheaper, simpler and lighter aircraft. This will lead to lower operating, maintenance and purchase costs. If the aircraft is to use a leading edge device, the choice of device will depend on the exact demands required by the design mission. The general objective in high lift system design is to match the airfield performance requirements in terms of approach speed, take off field length and climb rate. Also, maximum flight safety must be guaranteed, which implies good handling qualities, moderate approach speeds and "normal" controllable stall characteristics [3]. The high lift design process involves the basic wing design and the development of target design parameters such as C_{Lmax} and *L/D* ratio. Simultaneously, there is a need to achieve larger increases in lift coefficient for a given angle of attack and an increase in maximum lift for greater payload over a specified range [4]. Improvements in high lift performance will allow the pilot to take off and land with less noise levels.

Using traditional high lift systems to achieve the aircraft performance required in modern busy airports will increase the high lift system complexity and hence the weight and cost of the product. The complexity of high lift systems probably peaked on the Boeing 747, which has a variable camber Krueger flap and triple slotted, inboard and outboard trailing edge flaps. Since then the tendency in high lift has been

to achieve higher levels of lift with simpler devices in order to reduce fleet acquisition and maintenance costs [5]. Maximum operating loads occur mostly during low speed maneuvers with the devices deployed. However, failure of the system can have serious consequences on the controllability of the aircraft. An important consideration for a safe design and one that supports the argument against increased complexity is to minimize the probability of failure by minimizing the number of parts and joints in series.

Flow control technologies can, in general, be divided into those that are passive, active and reactive [2]:

1. Active system: can be classified as a system that requires an external energy source and would include traditional high lift systems, suction or blowing through slotted or perforated surfaces and moving surface boundary layer control.
2. Passive system: does not require a power input for their operation such as, static vortex generators and Gurney flaps, stall strips, wing fences and natural laminar flow.
3. Reactive systems: possess some intelligence and are either predetermined or actuate proportion to the signal that is supplied from the sensor.

The concept of Moving Surface Boundary- Layer Control (MSBC) appears quite promising. It has already proved successful in lift augmentation, drag reduction (by as much as 80%) of bluff bodies as well as suppression of flow-induced vibrations. An innovative step change is required to improve or replace the existing mechanically deployed leading edge high lift systems with the future technology based on flow

control. The existing mechanically deployed systems are very sensitive to deployment location and that sensitivity requires expensive, complicated and heavy mechanical systems [2].

Throughout the last century many boundary-layer control methods have been studied and employed with a varying degree of success, including shaping, blowing, wall suction, wall heating cooling, wave cancellation, vortex generators, streamlining and the moving wall effect. Boundary-layer control is used with many devices involving fluid flow, such as diffusers, compressors and wings. Boundary-layer control, applied to an aircraft wing, can lead to greater maneuverability, longer range, and/or shorter take-off and landing runs. The concept of moving surface boundary-layer control (MSBC) has proved quite successful in increasing lift and delaying stall of streamlined bodies like airfoil sections.

The turbulent boundary layer is more resistant to separation and more lift can be obtained at higher incidence, but there is a higher skin friction drag compared to a laminar boundary layer. Lower skin friction as well as lower flow-induced noise can be achieved if transition from laminar to turbulent flow is delayed. The laminar boundary layer, however, can only support a very small adverse pressure gradient without separation and loss of lift and a subsequent increase in form drag. The typical aerodynamic flow control goals are to reduce drag, enhance lift, and suppress flow induced noise or a combination of them.

Many ways of achieving these goals for either free shear or wall-bounded flows include:

• The delay or advancement of transition from laminar to turbulent flow,

• The prevention or provocation of flow separation and

• The suppression or enhancement of turbulence levels [6].

The delay or prevention of boundary-layer separation and the enhancement of the lift-to-drag ratio of an airfoil are always important to the control of the boundary-layer flow. A moving surface attempts to accomplish this in two ways [7]:

- It retards growth of the boundary-layer by minimizing relative motion between the surface and the free stream.
- It injects momentum into the existing boundary-layer.

The use of MSBCs will both delay flow separation on the upper surface by adding to the flows momentum, thereby reducing drag and also maintain the increased static pressure on the lower surface. Flow control technologies applied to the leading edge of an airfoil are more effective on an airfoil that demonstrates a leading edge separation than on one that demonstrates a trailing edge separation. When a cylinder rotates in a uniform flow, one half of the cylinder moves along the stream whereas the other moves against it. This creates asymmetry in the velocity and pressure fields around the rotating cylinder, which in turn, leads to asymmetry in the boundary layer separation and a force normal to the flow direction [8]. In the presence of a wall boundary in the flow, the shear effect makes the velocity of the approaching stream vary in the direction normal to the cylinder, affecting the behavior of the vortex shedding behind the cylinder. The vortex generating mechanism consists of a positive vortex being shed from the lower side of the cylinder and two negative vortices generated from the upper side of the cylinder and the plane (stationary) wall, respectively. The wall-side wake couples with the boundary layer vorticity of opposite sign on the plane wall while the actual wake is dominated by the vorticity shed from the other side of the cylinder. The

vortex separating from the lower side of the cylinder is stretched by the vorticity of opposite sign on the plane wall. This vortex is oblate in shape and does not initially detach from the cylinder due to the flow through the gap being suppressed, thus the vortex is unable to be efficiently swept downstream by the freestream. It should be noted at this juncture that the flow in the gap, being the tangential or local velocity, is not equal to that of the freestream. In the case of a moving wall, the wall boundary will be at the same velocity as that of the freestream. The local velocity will be higher than that of the freestream and moving boundary, caused by the venture effect of the gap. What this means is that a negative vortex, albeit a smaller one will exist due to the presence of the wall.

There are several applications of rotating cylinders as a flow control device, for example [2]:

- counter-rotating cylinders as a steering device
- cylinder (in front of) and rudder combination to reduce cavitations, replacing a conventional ship rudder
- improves lift and reduces cavitations on hydrofoils
- airfoil and leading edge rotating cylinder combinations to elongate the lift curve slope, thereby improving the airfoils stall characteristics
- airfoil and trailing edge rotating cylinder combinations to shift the lift curve to the left, generating higher lift at lower angles of attack
- flap and rotating cylinder combination to improve aircraft's handling qualities at low speed
- rotating cylinders utilized as a high lift device, both at the leading and trailing edges

- fin and rotating cylinder combination to improve torpedo control
- drag reduction on high-sided vehicles by adding momentum to the separating boundary layer
- incorporating rotating cylinders at step change in area of diffusers to avoid flow separation
- rotating cylinders to improve the flow in air-curtain wall applications

In summary, the potential of a leading-edge rotating cylinder (LERC) as a boundary-layer control device has been investigated by researchers elsewhere; however, most of the work has focused primarily on exploratory studies or force measurements.. In this research, I am going to study the application of a rotating cylinder at the leading edge as a high lift device. And I will focus on leading edge rotating cylinder and flap combination to improve aircraft's handling qualities at low speed. See the rotating cylinder configuration in Figure 1-1.

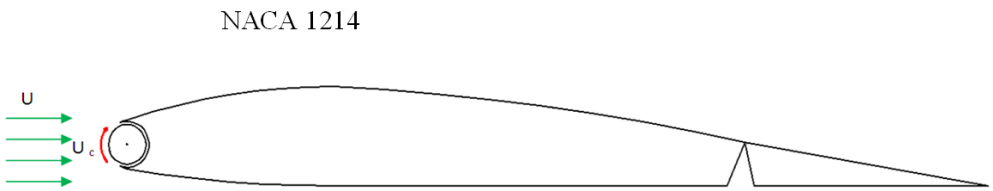

Figure 1-1: The rotating cylinder layout.

1.3 Literature Review

The use of boundary-layer control to increase lift of an airfoil is quite well known. A comprehensive review over the years on concept of Moving Surface Boundary- Layer Control (MSBC) has been done by several authors including Goldstein [9], Lachmann [10], Rosenhead [11], Schlichting [12], Chang [13], and others. This concept has a long and interesting history dating back to more than a century including contributions by Magnus, Prandtl, Flettner and others. Magnus (1852) first recognized the presence of an aerodynamic force produced by an unsymmetrical pressure distribution due to the Bernoulli's effect [14]. He studied the lift generated by circulation and utilized the effect to construct a ship with a vertical rotating cylinder replacing the sail which is referred to as Magnus lift. Swanson has presented excellent reviews of literature on the Magnus effect [15]. The leading edge jet effect of the moving wall can be seen in Figure 1-2 with a cylinder in place [16]. The Magnus lift is generated mainly by the downstream moving wall effect on the topside moving the separation from the subcritical (laminar) position towards the supercritical (turbulent) position. In the turbulent case the main effect is that of the upstream moving wall on the bottom side promoting separation, moving the separation from the supercritical towards the subcritical position [16]. The association of this effect with the name of Magnus was due to Rayleigh (1877) who studied the case of a rotating cylinder in a uniform flow [17]. His paper is credited as the first true explanation of the so-called Magnus effect. Magnus found that a rotating cylinder moved side way when mounted perpendicular to the flow. Rayleigh gave a simple analysis that the side force was proportional to the free-stream velocity and the spinning speed of the cylinder.

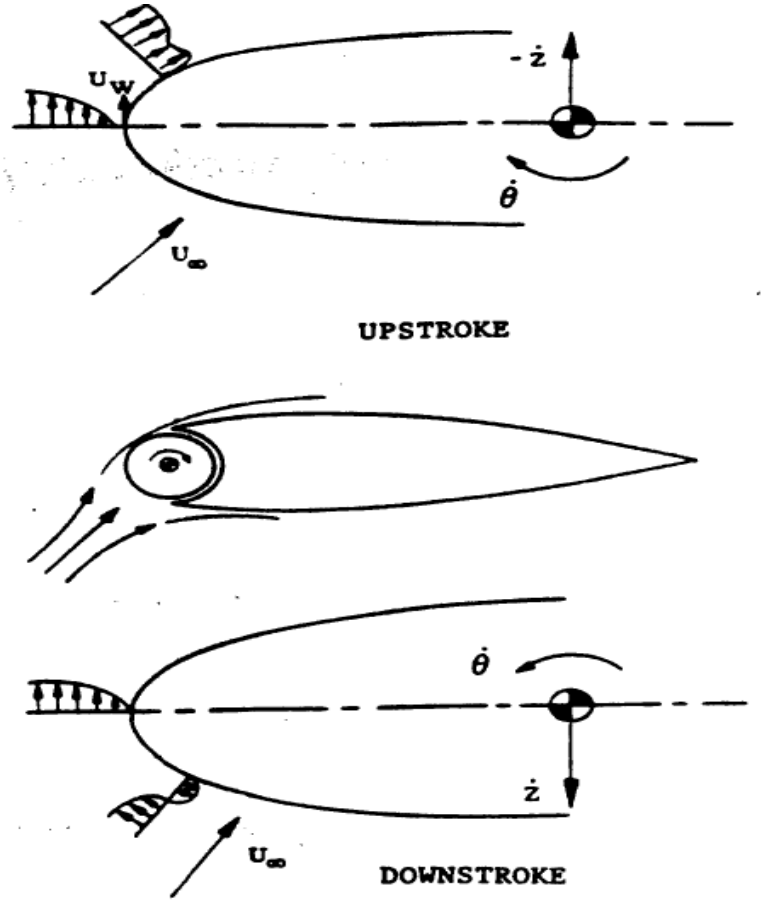

Figure 1-2: The leading edge jet effect of the moving wall [2].

In 1904, the boundary-layer concept was introduced by Prandtl [18]. Since then, the Magnus effect has been attributed to asymmetric boundary-layer separation. After that, Prandtl demonstrated his "ship of zero resistance" (Figure 1-3) through flow around two counter-rotating cylinders [18]and later Flettner (1924) applied this concept to a ship where he replaced the sail by rotating cylinders[19,20]. He fitted large vertical rotating cylinders on the deck of the "Buchau".

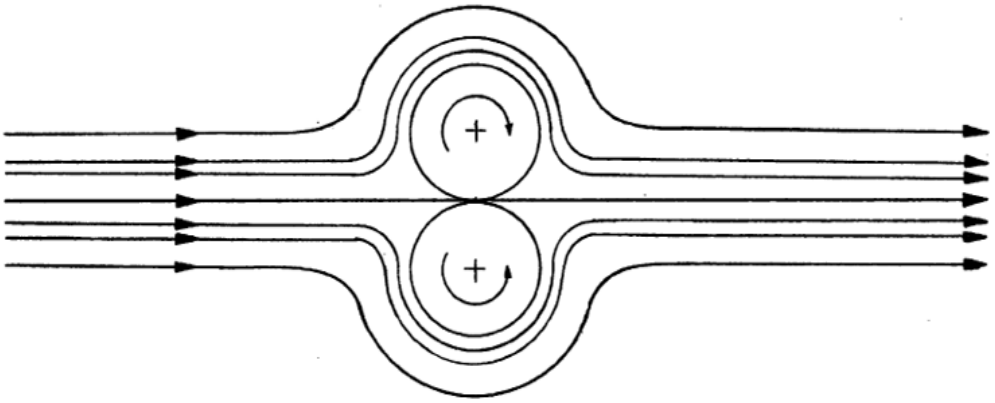

Figure 1-3: Prandtl demonstrated his "ship of zero resistance" through flow around two counter-rotating cylinders in a uniform flow display [20].

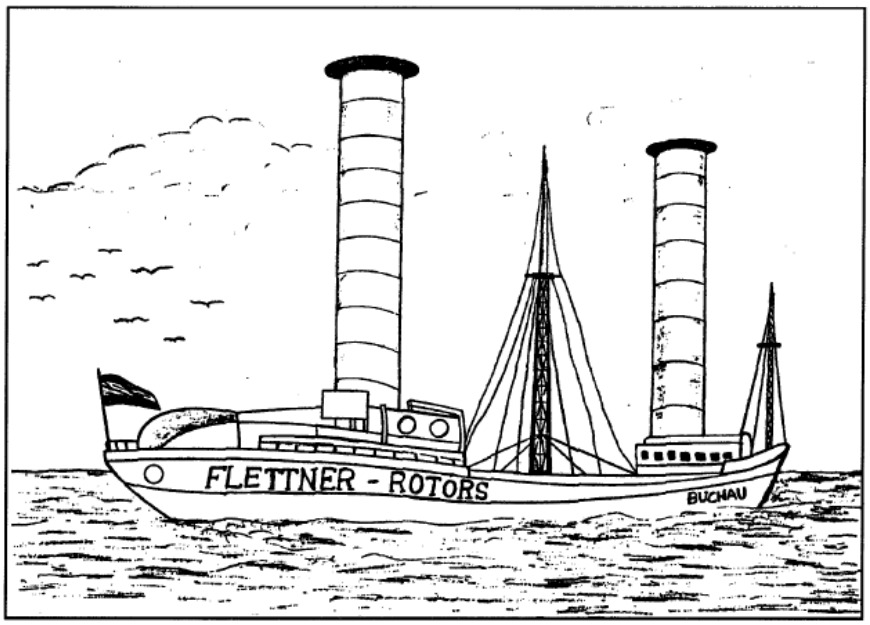

Figure 1-4: Flettner (1924) applied this concept to a ship where he replaced the sail by rotating cylinders [20].

The first aeronautical experiments and the most practical application of a moving wall for boundary-layer control was demonstrated by Favre 1938 [21]. Using a belt moving over two rollers as an airfoil's upper surface, he successfully delayed boundary-layer separation up to an angle of attack of 58°, with a maximum lift coefficient of 3.5 but because of the mechanical difficulty of its implementation, the idea was ignored. See Figure 1-5.

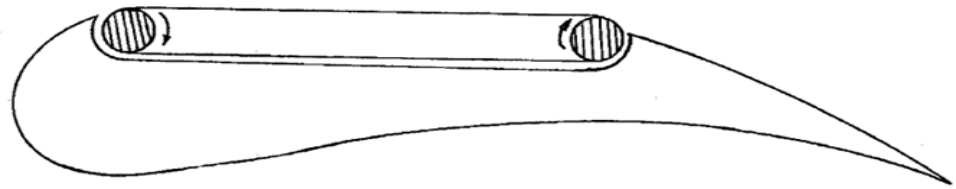

Figure 1-5: Favre used a belt moving over two rollers as an airfoil's upper surface.

The MSBC principle was also illustrated by Goldstein [9] using a rotating cylinder at the leading edge of a flat plate. The application of a clockwise rotating cylinder on the upper surface of an airfoil was investigated by Alvarez-Calderon and Arnold in 1961. Their investigation covers a vertical takeoff and landing configuration and a short takeoff and landing (STOL) configuration [22]. They carried out tests on a rotating cylinder flap to evolve a high lift airfoil for STOL-type aircraft. The system was flight tested on a single engine high-wing research aircraft designed by Aeronautical Division of the Universidad Nacional de Ingenieria in Lima, Peru [20, 23].

In 1963, Brooks [24] studied the effect of a rotating cylinder at the leading and trailing edge of a hydrofoil. For the leading edge configuration only a small increase in lift was observed, however, for the latter case a substantial gain in lift resulted. Motivation for the test-program was to assess improvement in the fin performance for torpedo control. Along the same line, Steele and Harding [25] studied the application of rotating cylinders to improve ship-maneuverability. Extensive force measurements and flow visualization experiments were conducted using a water tunnel and a large circulating water channel. Three different configurations of rudder were used. The rotating cylinder:

1. in isolation;
2. at the leading edge of a rudder;
3. combined with a flap-rudder, the cylinder being at the leading edge of the flap.

The North American Rockwell designed OV-10A twin-engine aircraft which was flight tested by NASA's Ames Research Center [26,27]. Cylinders were located at the leading edges of the flaps and rotated at high speed with the flaps in lowered position (see Figure 1-6). The main objective of that test program was to assess handling qualities of the propeller powered STOL type aircraft at higher lift coefficients. The aircraft was flown at speeds of 29-31 m/s, along approaches up to -8°, which corresponded to a lift coefficient $C_{Lmax} \approx 4.3$. In the pilot's opinion any further reductions in approach speed were limited by the lateral-directional stability and control characteristics. Flight tests of the system showed great improvement in handling qualities and control characteristics of the aircraft.

Figure 1-6: The North American Rockwell OV-10A Aircraft.

In 1971, Tennant et al replaced the trailing edge with a rotating cylinder on a symmetrical airfoil type NACA-EPH and reported that, at a zero angle of attack, a coefficient of lift of 1.2 was obtained for a normalized cylinder rotation U_c / U = *3* (where U_c is the cylinder surface speed and U is the freestream velocity) [23,28]. Hence, lift was achieved on the cylinder-forebody combination by an adjustment of the trailing wake which is initiated at the location of the separation points on the upper and lower surfaces of the body. By means of boundary-layer control, these separation points are moved, and the wake takes on a new trailing direction. What is unique here, is that lift may be produced by a symmetrical body at zero angle of attack, and the amount of lift can be controlled by variation in the amount of boundary-layer control applied, namely by the cylinder rotation speed.

Tennant applied the moving wall to an air flow through a diffuser with a step change in area [29]. The diffuser incorporated rotating cylinders to form a part of its wall at the station where the area change took place. Experimental results showed no separation for the appropriate ratio of the moving surface to the diffuser inlet velocity, and the moving surface provided a high area ratio diffuser with a short overall length.

Tennant and Johnson also, tested different possibilities for the rotating cylinder-airfoil combination. Tennant et al.[30] conducted tests with a wedge-shaped flap having a rotating cylinder as the leading edge. The angle of attack, in their study, was limited to 15 deg, and the cylinder speed necessary to reattach the flow was determined. Their study included the effect of the gap between the rotating and fixed surfaces on the effectiveness of the boundary-layer control technique. They concluded that the gap should be kept at its minimum value to minimize the cylinder speed required for effective boundary-layer control.

Ericsson [16] found that the moving wall effect on laminar to turbulent transition is quite straight forward. However, when the moving wall effect influences flow separation via the boundary layer transition mechanism, the total moving wall effect becomes much more complicated and, in general, it also has a larger influence on the unsteady aerodynamics than is the case of the purely laminar or turbulent boundary layer separation. In most full-scale flight cases, it is the more complex form of the moving wall effect that has to be dealt with.

Modi [5, 31, 32, 33, 34] entered this field in 1979 and was the first, to generalize the concept of a rotating cylinder as a versatile boundary-layer control

device for diverse applications such as high-lift airfoils, drag reduction of static as well as moving bluff bodies, control of wind induced instabilities of civil engineering structures, reduction in snow deposition over a roof, suppression of wave and current, induced oscillations of offshore platforms and marine risers, etc. A comprehensive wind tunnel test program involving a family of airfoils such as NACA 63-218 and multi-sectional symmetric Joukowsky airfoil, using combinations of rotating cylinders at various locations forming moving surfaces, complemented by the surface singularity numerical approach, surface pressure measurement, six-axis force balance and flow visualization, was investigated by Modi. He has shown spectacular effectiveness of the MSBC concept, which increased the maximum lift coefficient by more than 200% and delayed the stall angle to 48°. As a further application of the MSBC concept at a more fundamental level, a flat plate and several rectangular prisms with momentum injection through rotating cylinders were also studied. A drag reduction of about 75 % was achieved for a normal flat plate with twin cylinders, one at each edge $(U_c/U = 3)$. Modi developed and studied various two-dimensional airfoil (Joukowski) having one or two rotating cylinders acting as momentum injecting elements as shown in Figure 1-7.

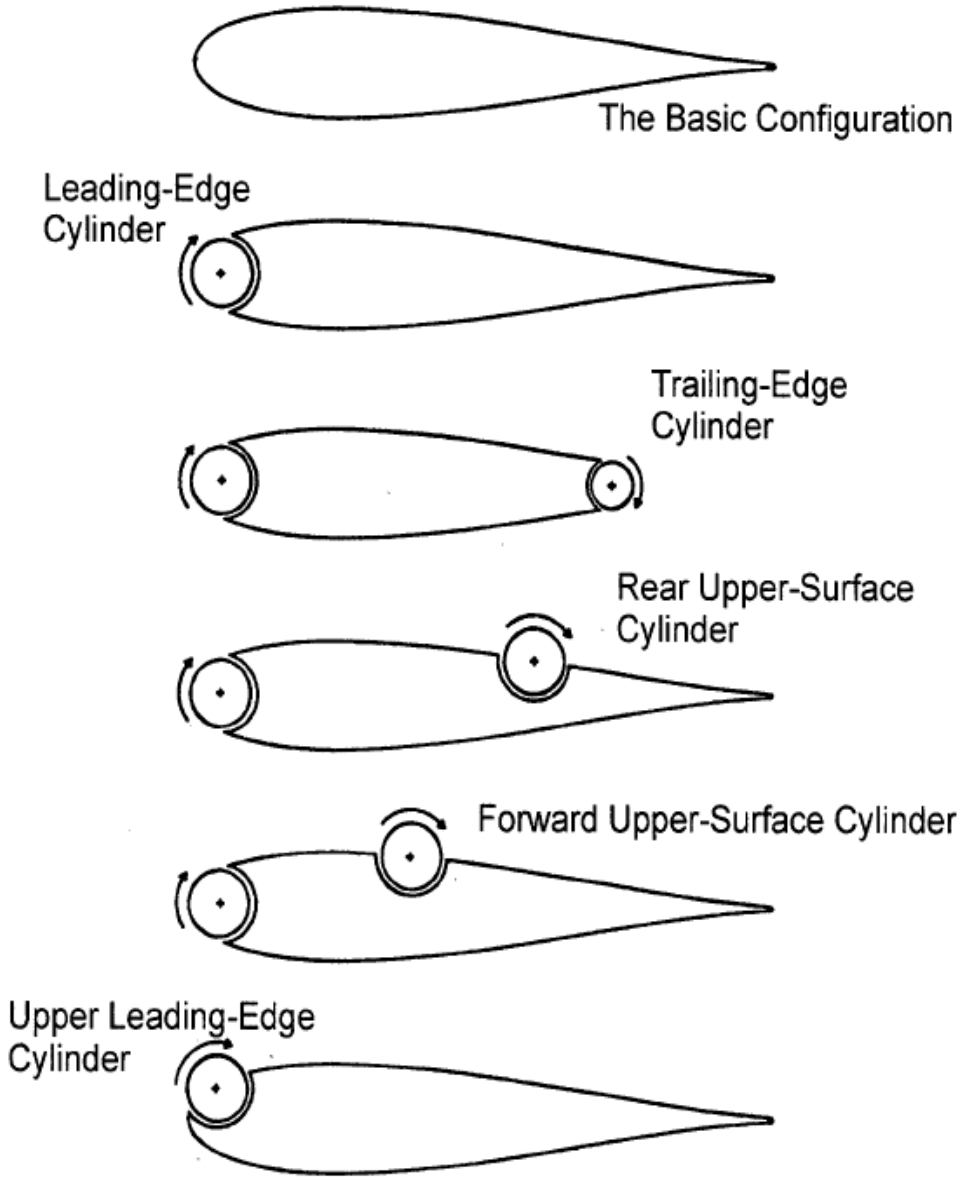

Figure 1-7: Rotating-cylinder configurations studied by Modi with a 2D Joukowski airfoil [35].

Modi et al. [36] described the technology as semi-passive in character due to the low power requirements. This definition is actually a further category to those suggested in the introduction. Within the constraints of those categories this technology would be described as active. The cylinders can be hollow and therefore light and, in a steady state, the power requirements are those required overcoming the

losses of the bearings supporting the cylinders [31]. A comparison between the power required by the moving surface boundary layer and that required by a control method with boundary layer suction for increases in C_L and α_{stall} was made by Modi et al [34] shows that MSBLC offers more value in terms of the power consumed from the aircraft's system. Increased manufacturing complexity is due to a wing's span wise chord reduction requiring a cylinder with a diameter that reduced in diameter accordingly. A further potential design problem was encountered in the wind tunnel. Modi stated that the main objective of a boundary-layer control procedure is to prevent, or delay the separation of the boundary layer from a wall by:

- preventing the initial growth of the boundary layer by minimising the relative motion between the surface and the freestream.
- injecting momentum into the existing boundary layer.

Modi tests were conducted at a Reynolds number of $4.62x10^4$, for a range of angles of attack from 0 to 45 and with cylinder rotation speeds from 0U to 4U. The results suggested that there is a critical speed ratio between the cylinder surface velocity (U_c) and the free stream velocity (U) and that the gap size between the cylinder and the airfoil is important. Too large a gap has an adverse effect on the flow [31]. A large unsealed gap would allow communication between the high and low pressure regions [32]. The presence of the leading edge flap cylinder considerably degenerated the performance as compared to the single cylinder case. When used in conjunction, leading edge and trailing edge cylinders can produce an increase of around 195% in C_{Lmax}. The trailing edge cylinder rotation gives an improvement in the lift coefficient, at a given angle of attack, before stall. The drag co-efficient increases directly as the cylinder rotation increase. The surface roughness of the cylinder has an effect on both the boundary layer control and the control of the drag coefficient. An

increase of 210% in the lift co-efficient is associated with the axial splined surface roughness condition compared to the smooth cylinder.

The importance of the location of the cylinder on the airfoil has been investigated [31]. Modi, by designing the model in sections enabled the study of each configuration as follows:

1. Base airfoil
2. Leading edge cylinder
3. Trailing edge cylinder
4. Leading and trailing edge cylinder

Base airfoil: Pressure distribution plots were in good agreement with that expected at $0 \leq \alpha \leq 12$, with stalls occurring at around 10° - 12°. Maximum lift coefficient at $\alpha = 10^{\circ}$ is 0.88.

Leading edge cylinder: As expected, there is a penalty associated with the nose geometry and gap, but even at $(U_c/U = 1)$, the lift and stall characteristics are significantly improved. The maximum lift coefficient measured with $U_c/U = 4$ was around 2 at $\alpha = 28^{\circ}$, more than double the base airfoil. What occurs is that the flow separates as the angle of attack increases and the point of separation moves closer to the leading edge. However, as the rate of rotation is increased, the size of the separation region is reduced, with the point of separation moving downstream. Table 1-1 below, reflects the expected separation points, measured along the chord from the leading edge at $\alpha = 16^{o}$.

$\alpha = 16^{o}$	X/C = 0	X/C = 25%	X/C = 50%	X/C = 100%
U_c/U	1	2	3	4

Table 1-1: The effect of the rotation speed on the flow separation points [28].

The effect of the leading edge cylinder is to extend the lift curve slope without significantly changing its slope. This means that both the maximum lift coefficient is increased and the stall angle is delayed.

Trailing edge cylinder: Improves the lift over a range of low to medium angles of attack ($\alpha = 20^{\circ}$) The suction over the airfoil upper surface as well as compression on the lower surface are increased, more so with higher rotation speeds. Referring to the coefficient of lift at $Uc/U_{\infty} = 4$, the C_L has increased from zero to 1.05 at $\alpha = 0^{\circ}$, effectively shifting the lift curve to the left. The maximum lift coefficient is 192% higher at 1.7 but at a lower angle of attack (8°).

Leading and trailing edge cylinder: In combination, the lift curve slope has moved upwards, with a maximum lift coefficient of 2.5 and a stall angle of 18°. Figure1-8 shows all the configurations tested by Modi.

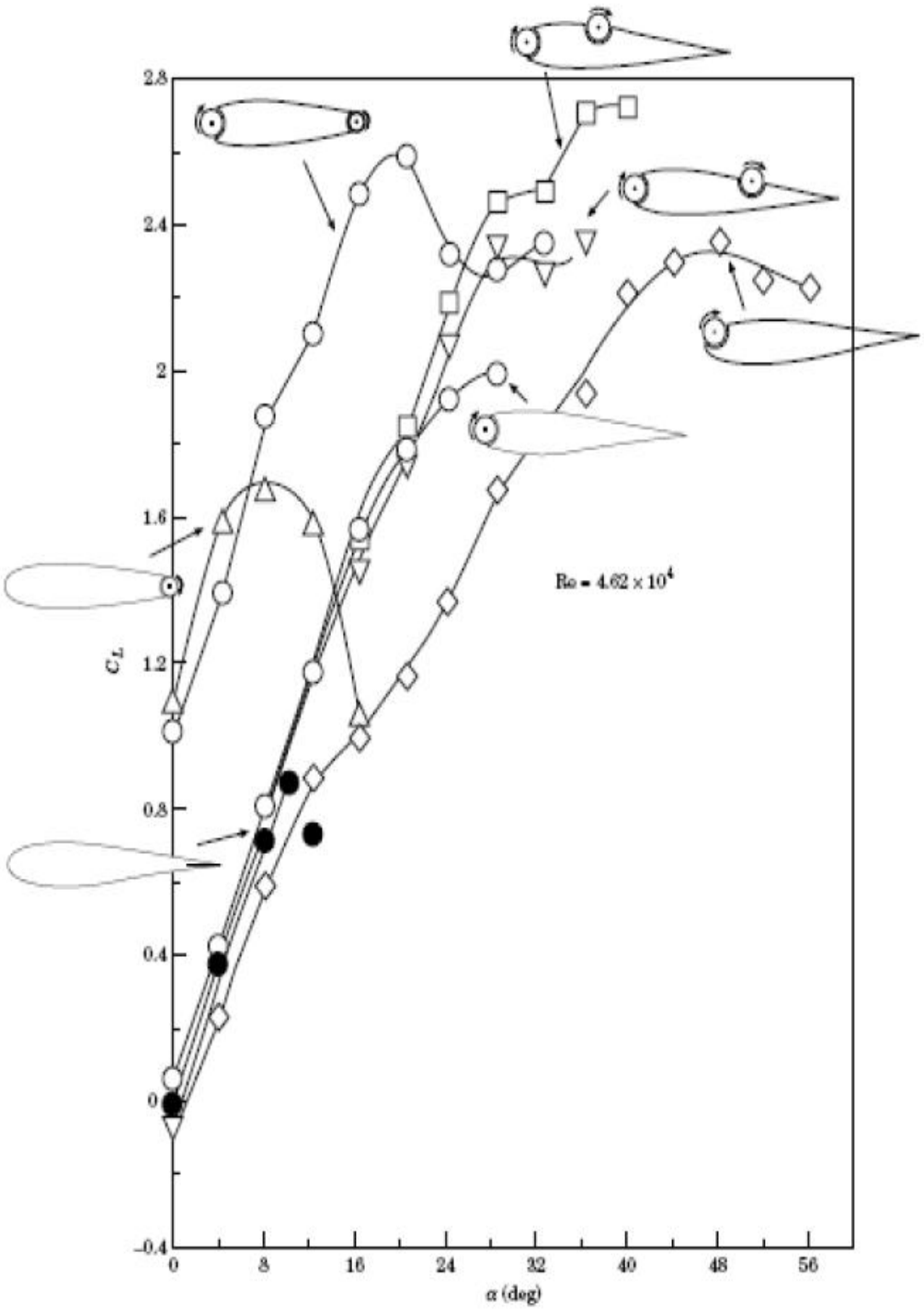

Figure 1-8: Plots to assess the relative performances of the various configurations as tested by Modi. All cylinder rotation speeds are at 4 [35].

Theo Thomson examined the impact of an underlying surface on the aerodynamic characteristics of a symmetrical airfoil section and compared it to the same section modified to include moving surface boundary-layer control devices located at the leading and trailing edge (MSBC)[28]. An experimental and numerical model was constructed and compared to determine the aerodynamic characteristics of a plain and modified NACA0012 symmetrical airfoil for both in and out of ground effect cases.

Hassan and Sankar carried out a purely numerical study of MSBC [37]. They found that the benefits gained from the introduction of vorticity in the leading edge region tend to decrease with the increase in the flow angle of attack. For separated flows, the early formation of a leading edge shock wave inhibits the beneficiary effects of the additional momentum introduced into the boundary layer through the rotating leading edge. They contend that the accompanying rapid increase in the drag forces does not warrant the use of this device as a means to control the boundary layer at supercritical or perhaps critical onset flow conditions. They argue that previous experiments, mentioned above, although quantitative in nature provide information about the character and behavior of the boundary layer only in a general sense and the technique is limited to flows that do not contain massive boundary layer separation and is therefore not suitable for the analysis of flows at angles of attack approaching or exceeding the static stall angle. Hassan and Sankar modeled compressible flow past an airfoil with a leading edge rotating cylinder using the full Reynolds averaged Navier-Stokes equations with body fitted curvilinear grid and an implicit finite difference scheme. For realistic values of the Reynolds number this would require significant computer effort and cost.

Gerontakos and Lee [38] took the previous work a step further by examining the effects of the cylinder rotation on the fluid dynamic process, by measuring and characterizing the effects of a leading-edge rotating cylinder (LERC) on the growth, development, and separation of the boundary layers and wake structures developed on and behind a symmetrical airfoil. Sayers [39] presented lift coefficients and stall angles of a rudder with a leading-edge rotating cylinder. Results of the study showed that the leading-edge rotating cylinder increases the lift coefficient and stall angle and, thus, increases the maneuverability of a vessel fitted with such a rudder.

Bin Ying [7] studied the application of the two concepts: Moving Surface Boundary-layer Control (MSBC); and trip fences; to a two-dimensional wedge airfoil and tractor-trailer truck configurations. His extensive wind tunnel test program, complemented by a flow visualization study, investigates effectiveness of:

1. the MSBC for 2-D wedge airfoil;
2. the MSBC for 3-D tractor-trailer truck;
3. the trip fences when applied to the upstream face of a rectangular prism and the trailer; and
4. combinations of the MSBC and fences as applied to a tractor-trailer truck configuration.

An important parameter is the ratio of the cylinder surface velocity to the free stream velocity, which was systematically varied during the test-program conducted in the smooth flow condition. In the fence study, the variables of interest are the fence width and height *(bf* and *hf, respectively*) and their locations

that have led to a maximum reduction in drag. A schematic diagram of the configurations studied is presented in Figure 1-9.

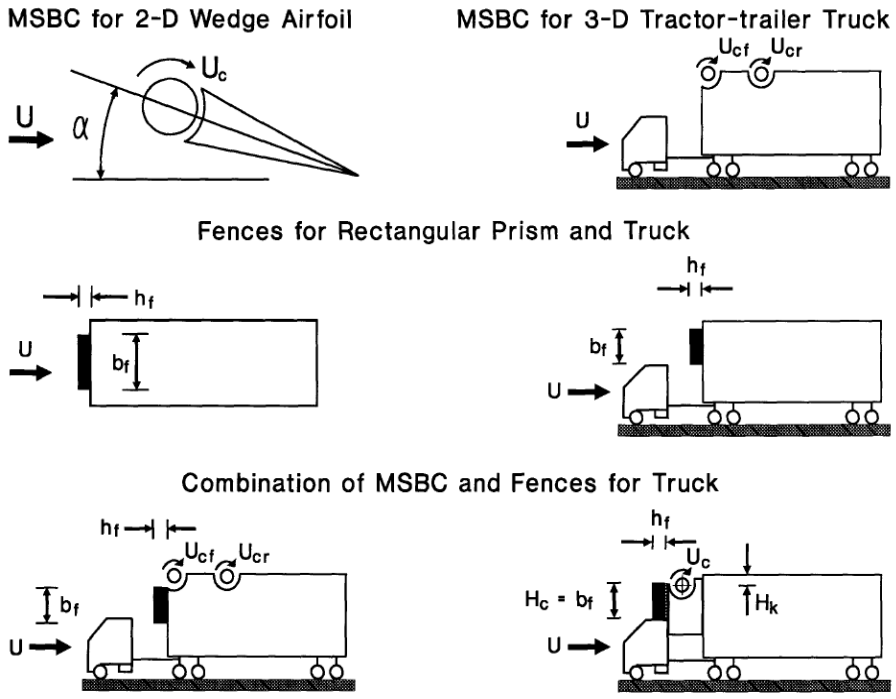

Figure 1-9: A schematic diagram of the configurations studied during the test program [7].

An experimental investigation undertaken by Al-Garni et al. has been carried out in King Fahd University of Petroleum and Minerals (KFUPM) on a two-dimensional NACA 0024 airfoil equipped with a leading-edge rotating cylinder [40]. The airfoil was tested for different values of leading-edge rotations and deflection angles. The effects of the angle of attack, the cylinder surface to the free stream velocity ratio U_c/U, and the flap deflection angle on lift and drag coefficients, the size of the separated flow region, and the stall angle of attack were investigated. The experimental results showed that the leading-edge rotating cylinder increases the lift

coefficient of a NACA 0024 airfoil about 92% and delays the stall angle of attack about 160%. In addition, the lift-to-drag ratio increased from 0 to a value of around 20 at zero angle of attack, hence reducing the need for higher angles of attack for STOL. This increase in the lift coefficient, lift-to-drag ratio, and stall angle of attack would make an airplane fitted with such an airfoil more maneuverable and improve its performance in terms of STOL.

The study shows also that the total percentage of increase in the maximum lift coefficient is about 130% due to the combined effects of $U_c / U = 4$and $\delta = 30$ degrees. Although the flap was successful in increasing the lift coefficient, it reduced the lift-to-drag ratio of the leading-edge rotating cylinder airfoil.

Smoke-wire flow visualization was also used to show the large reduction of the size of the separated flow region see Figure 1-10. Results of the boundary-layer measurements showed that the leading-edge rotating cylinder reduced the boundary-layer thickness and the turbulence intensity in the vicinity of the airfoil surface. The flow visualization studies showed that an increase in the speed of the leading-edge rotating cylinder would delay the separation on the upper surface of the airfoil or perhaps forces the flow to reattach. Considering the changes in the lift coefficient vs U_c / U_∞ along with flow visualization results, suggests that the effect of the leading-edge rotating cylinder becomes less at higher U_c / U . The effect of the flap on the flow pattern over the upper surface of the airfoil is shown in Figure 1-11. Note that the deflection of the flap moves the separation point upstream toward the leading edge of the airfoil.

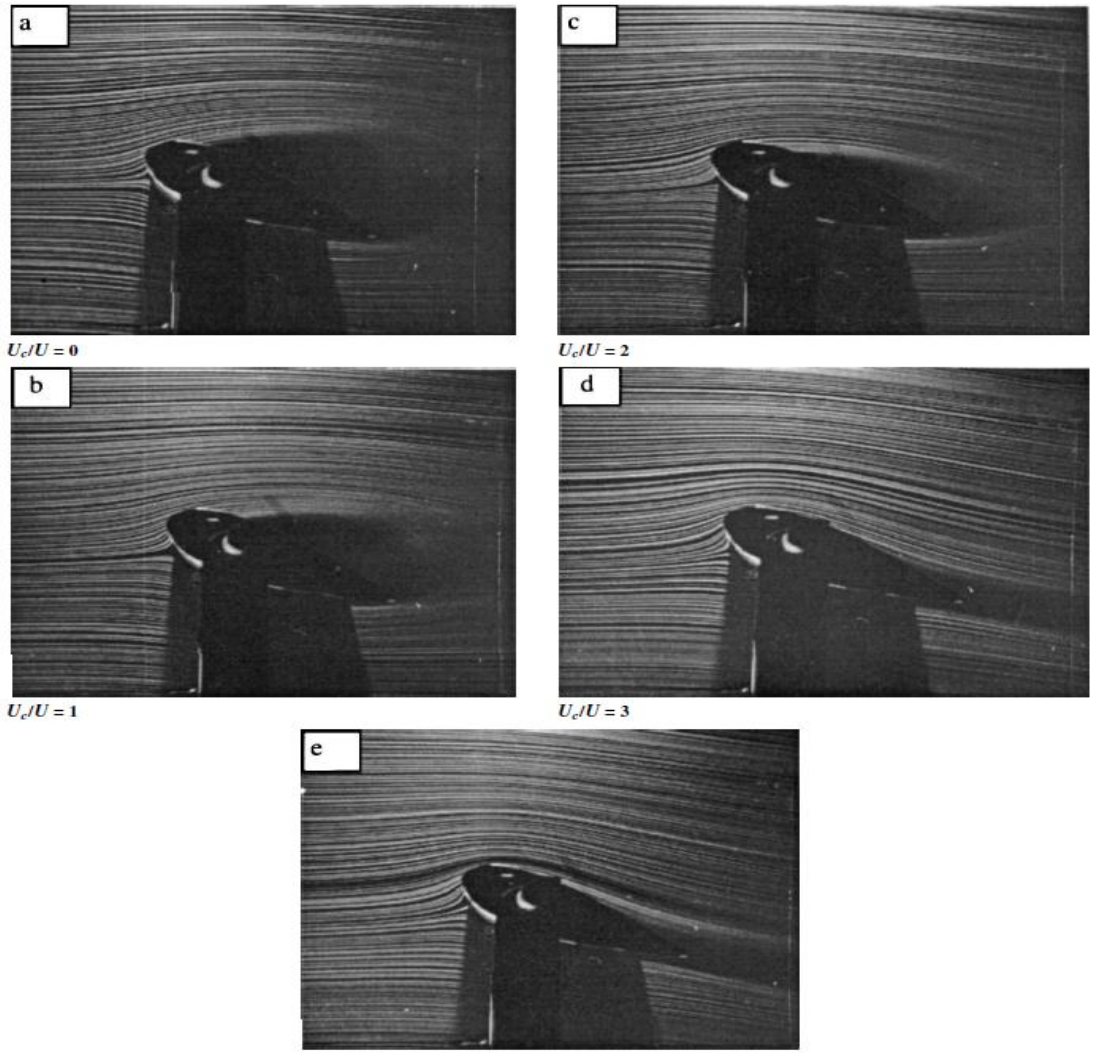

Figure 1-10: Smoke-wire flow visualization shows the effect of the rotating cylinder the size of the separated flow region [40].

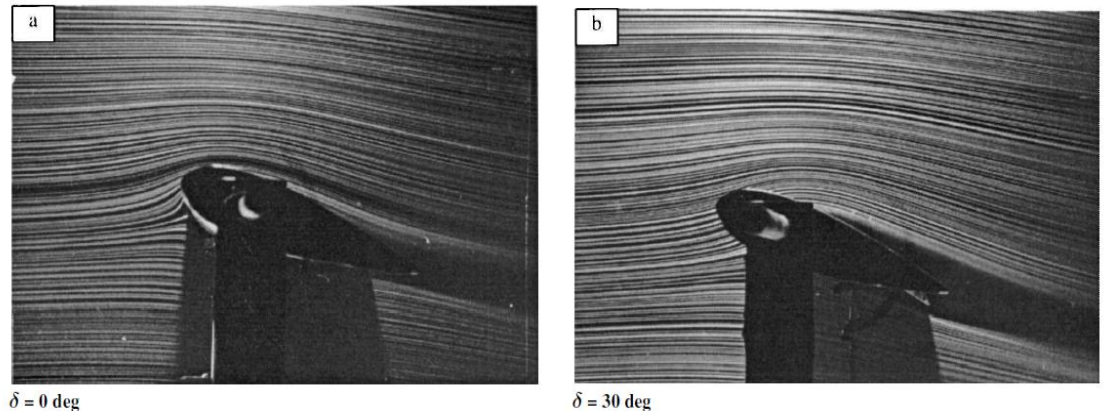

Figure 1-11: The effect of the flap on the flow pattern over the upper surface of the airfoil [40].

One year after the research done by Al-Garni and his team (in 2000), the leading edge rotating cylinder concept was applied to a remote control airplane (Saqr Al Jazerah 1) in the Aerospace Department Labs at this university and I was one of the construction team. The application of the leading edge rotating cylinder showed an excellent improvement of the aircraft's handling qualities and maneuverability (see Figure1-12).

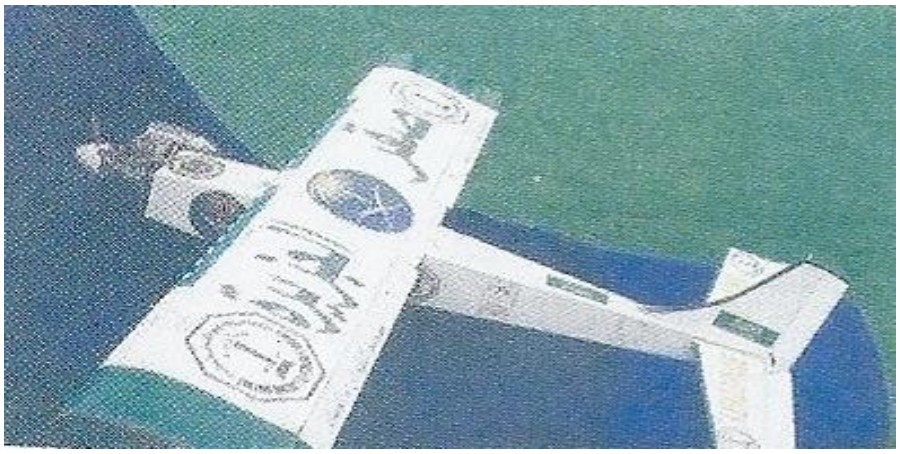

Figure 1-12: Saqr Al Jazerah 1- remote control airplane equipped with leading edge rotating cylinder.

In 2005, Chaplin investigated the moving surface boundary layer control (MSBC) over a streamlined body [41]. A NACA 0015 airfoil was modified to include a rotating cylinder along the leading edge. He studied the effect on the airfoil's aerodynamic characteristics of varying the speed, gap distance and surface roughness of the cylinder. A low speed wind tunnel was used to measure the lift and drag using an under floor balance. This produced very promising results; in one case the maximum lift coefficient increased by 197% and delayed stall by 6 degrees. The optimum distance for maximum lift was 4mm and for minimizing drag was 2 mm. The fine sand paper increased the lift by 30% and the coarse paper slightly reduced the drag. Then computational and experimental results were compared using a CFD

model. The computational lift results were very similar to the experimental testing and the CFD model was very successful at capturing the re-circulation effect during stall. The paper concluded with a basic flow visualization study showing the dramatic effects of Moving Surface Boundary Layer.

After that, he investigated the applications of Moving Surface Boundary Layer Control (MSBC) as a leading edge high lift device by modifying the wings of a small model aircraft (1.55m wing span) in order to include a rotating cylinder along the leading edge grove. This will provide momentum injection to the incoming airflow and thus energizing the boundary layer. Various Flight tests were conducted on the model aircraft to assess its performance, stability and control characteristics.

The encouraging results of the MSBC concept open the vision towards the future implementation of this technology in the industrial and civil works [27]. Figure 1-13 shows possible future application of this technology to a bridge-tower and a super tall building.

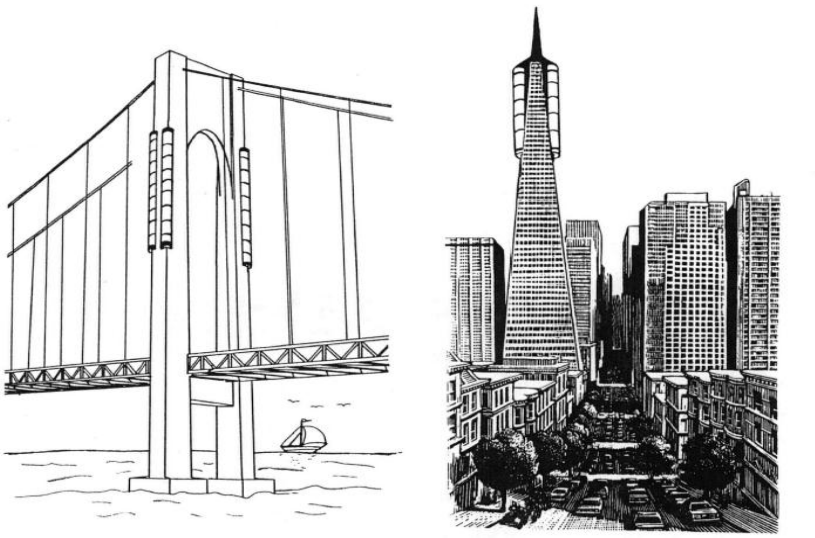

Figure 1-13: The possibility of applications to next generation of civil engineering structures [27].

1.4 Current Work

Starting from what has been achieved in the laboratories by the above teams, an experimental model was constructed and tested in the wind tunnel to determine the aerodynamic characteristics using the leading edge moving surface concept of modified semi-symmetric airfoil NACA2412. The moving surface is provided with a high speed rotating cylinder, which replaces the leading edge of the airfoil. From the literature review we can observe that all the previous work has been done on symmetrical airfoils. In this research cambered airfoil is used. After that, we apply this advanced technology to a 2-seat light-sport aircraft that is designed and built in the Aerospace Engineering Department at KFUPM. The project team is led by the Aerospace Engineering department chairman Dr. Ahmed Z. Al-Garni and includes a graduate and an under graduate students. It embodies the works of M.S thesis, senior design projects, Coop projects and other undergraduate activities.

The embodiment of the rotating cylinder along the flap portion of the wing should be taken into consideration during the design and building stages. The wing was modified to include a rotating cylinder along the leading edge. Two cylinders each 2.15 meters long each were fitted to the leading edge of the flap portion of the wing (one on each side).

CHAPTER 2

Conceptual Design

2.1 Introduction

The creation of anything has different phases, and so does the creation of an aircraft. In the earliest aviation years the pioneers had a vision before the first ever airborne machine was built. This vision remains in the mind of the aircraft designer, although not always as ground breaking, to create an aircraft that can handle new tasks or existing tasks better than before.

In the process of the production, the design phase is the most important part. An aircraft design consists of three phases: conceptual design phase, preliminary design phase, and detail design phase. In the conceptual phase, there is a need to evaluate many different approaches to the problem and hence the need of a tool where this evaluation can take place. In the preliminary design stage, fine tuning of the conceptual design should be made through parametric wind tunnel tests of scale model of the design or by computational flow simulations. The detailed design stage involves generating the detailed structural design of the aircraft and every detail needed for building the aircraft. Figure 2-1 describes the design process in general.

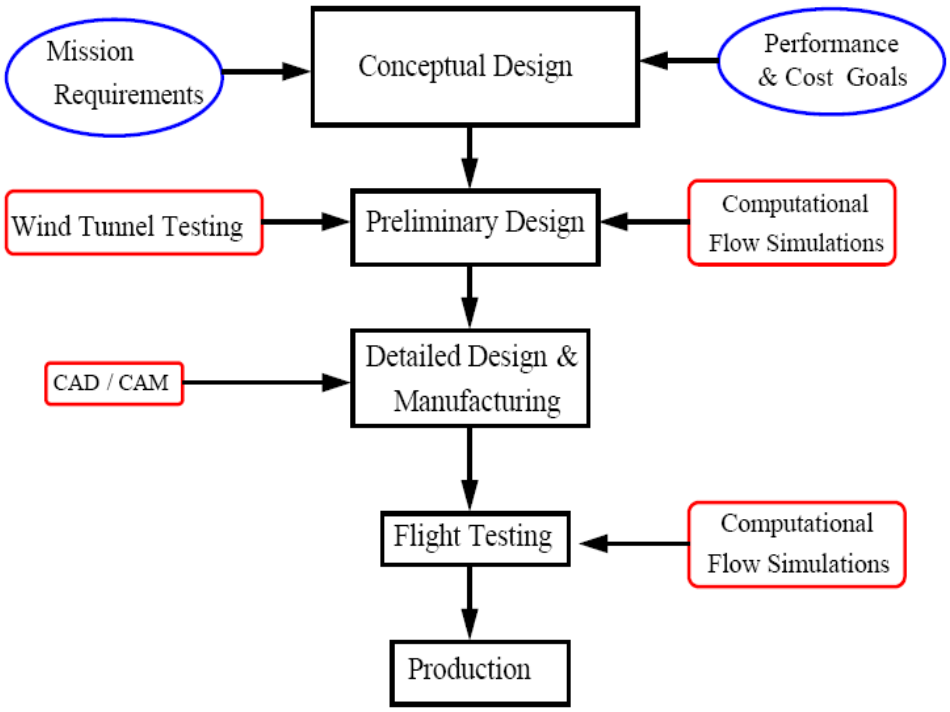

Figure 2-1: Design process flow chart [42].

This aircraft matches the performance capabilities of current similar light-sport aircraft and also satisfies the mission design and associated Federal Aviation Regulations (FAR) requirements. Table 2-1 represents some aircraft specification of the same category. The mission profile for this aircraft is shown in Figure 2-2.

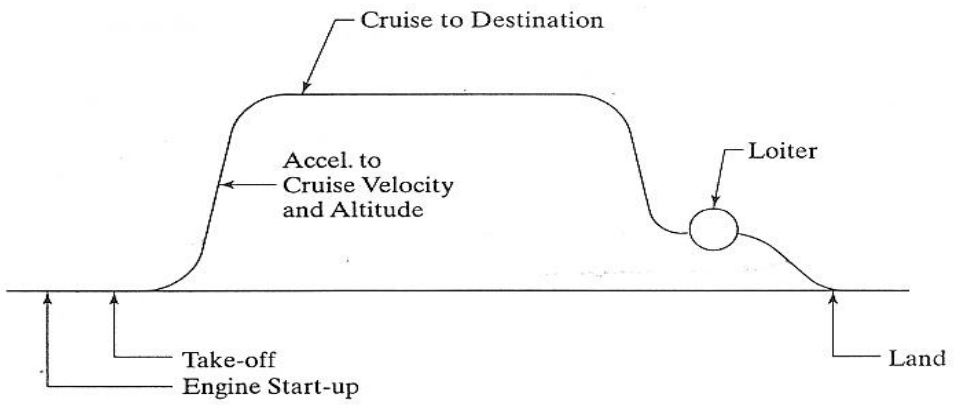

Figure 2-2: Mission Profile.

SPECIFICATIONS	Jabiru 2200	Breezer	Elitra-202	Skylark	The Tecnam P92	Beechcraft Model 77	APOLLO FOX
General							
seats	2	2	2	2	2	2	2
Weights							
Empty Weight	617 lbs	704 lbs	476 kg	653 Ibs	670 lbs	1,100 lb	715 Ibs
Gross Weight	1245 lbs	1320 lbs	730 kg	1320 Ibs			680 feet
Fuel Capacity	24.8 Gallons	18.5 Gal	100	24 US Gal			60 L (15.5 USG
Useful Load	628	655		525 Ibs	650 lbs	580 lb	1265 Ibs
Geometry							
Wing Span	31.5 ft	28.5 ft	8.3 m	26 ft	28 ft 6 in	30 ft	9.15 m (30 feet)
Wing Area	142 ft^2	127 ft^2		101 ft^2	129 ft2	129.8 ft^2	(122.7 sq. ft)
Aspect ratio	7.01	6.4		6.69	6	6.93	7.33
Length	18.6 ft	21 ft	5.7 m	21.7 ft	20 ft 11 in	24 ft	6.25 m (20.2 feet)
Height (At Wing)	6.23 ft	6 ft	2.1 m	7.4 ft	8 ft 3 in	6 ft 11.1 in	1.7 m (5.58 feet)
Engine	2200	Rotax 912 UL 2	Rotax 912 ULS	Rotax912	Rotax 912	Lycoming O-235	Rotax 912UL (80 HP)
Horse Power		100		100			
Fuel Consumption (80%)	3.75 Gal/hr	3.5Gal/hr					60 L (15.5 USG
Performance							
Stall speed	44 Knots	36 Knots	90 km/h	42 mph	30 mph	54 mph	39.75 MPH
Cruise Speed	95 mph	125 mph	200 km/h	mph	135 mph	121 mph	129 MPH
Maximum Speed	105 mph	109 mph	240 km/h	179 mph	146 mph	165 mph	132 MPH
service celling				14000 ft	14,760 ft	12,900 ft	
Range (with reserve)	~670 miles	497 miles	800-1500 km	625 miles	500 mi	719 km	600 km (375 miles)
wing laoding						12.9 lb/ft^2	
Rate Of Climb	1000 ft/min	900 ft/min	4.5 m/s	1200 fpm	1,161 ft/min	720 ft/min	1000 FPM
Take Off Roll	328 ft	410 ft	220 m	500 ft	460 ft		750 feet
Landing Ground Roll	328 ft			530 ft	330 ft		

Table 2-1: Some light sport aircraft specifications.

Light-Sport Aircraft category as defined in the FAA's proposed Sport Pilot Light-Sport Aircraft Category which is defined as simple, low-performance, low-energy aircraft that are limited to:

1. 1,320 pounds maximum takeoff weight for aircraft not intended for operation on water; or
2. 1,430 pounds maximum takeoff weight for aircraft intended for operation on water.
3. A maximum airspeed in level flight with maximum continuous power of not more than 120 knots CAS under standard atmospheric conditions at sea level.
4. A maximum seating capacity of no more than two persons, including the pilot.
5. A single, reciprocating engine.
6. A fixed or ground-adjustable propeller if a powered aircraft other than a powered glider.
7. A non-pressurized cabin, if equipped with a cabin.
8. Fixed landing gear, except for an aircraft intended for operation on water or a glider.
9. A maximum stalling speed or minimum steady flight speed without the use of lift-enhancing devices (Vs1) of not more than 45 knots CAS at the aircraft's maximum takeoff weight and most critical CG.

In the conceptual design phase, the aircraft will be designed in concept without the precise calculations. The conceptual design develops the first general size and configuration for a new aircraft. It involves the weight estimation and balance and the choice of the aerodynamic characteristics that will be best suited to the mission requirement or category regulations.

2.2 Aircraft Purpose

This aircraft has a low stall speed which means that it can be used effectively for new pilot training, borders security and aerial surveillance and sightseeing. This aircraft will be used as a platform for researches and modifications in the department. It also can be used as a laboratory for the design, Structure, Aerodynamics, Propulsion, Maintenance Flight stability and control courses in addition to senior projects or courses projects. It may be used for illustration of the structural repairs schemes and construction material. It may be used in cooperation with industry for production and modification of this design in future. Finally, it helps and gives confidence to introduce the aircraft industry in our country.

2.3 Aircraft Configuration Selection

We have Chosen to go with the high un-tapered wing with a conventional tapered tail, tricycle landing gears arrangement and Single engine at nose (tractor configuration) as shown in Figure 2-3.

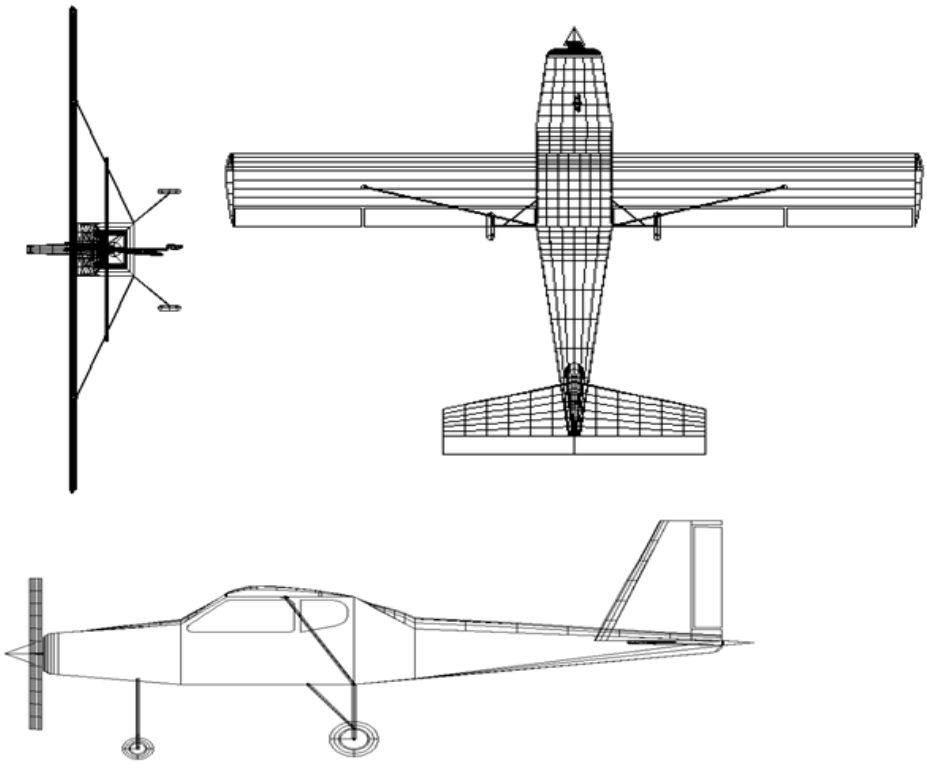

Figure 2-3: Aircraft configuration

2.4 Aircraft weight estimation

The total takeoff weight is divided into useful and empty or structure weight.

1. Useful Weight (Wu)

The useful weight includes the crew, fuel and baggage weight:

$Wu = W_{crew} + W_{fuel} + W_{baggage}$

This airplane is intended to carry two persons (a pilot and one passenger). Table 2-2 gives the average weight per passenger. The weight of the crew was assumed to be for average adult male in summer which is 200 lb.

No	Passenger	Weight Per Passenger (*lb*)	
		Summer	Winter
1	Average adult	190	195
2	Average adult male	200	205
3	Average adult female	179	184
4	Child weight (2 years to less than 13 years of age)	82	87

Table 2-2: The average weight per passenger at deferent conditions [45].

The fuel consumption is at a rate of 4 gallons per hour (gph) per 80 hp installed engine [43]. Fuel weighs approximately 6 pounds per gallon, thus we'll need 24 pounds of fuel per hour endurance for 80 bhp. A practical airplane needs two to four hours' endurance, so let's choose three hours as our goal.

The weight of fuel required for three hours endurance will be:

3 (hours)× 30(pounds)×0.8(bhp)= 72 pounds.

This airplane, equipped with a 80 bhp engine and 15 gallons of fuel (three hours endurance) will need a useful load of

Wu = 2 × 200+72= 472 pounds.

If we want to carry baggage, fly far or if the weight of the occupants is heavier than 200 pounds, then we'll have to adjust Wu to what is required.

2. Empty Weight (We)

Next we have to estimate the empty weight of our new airplane. We do this by choosing one of the columns in Table 2-3.

	1	2	3	4	5	6
We/ Wu	0.8	2	1.2	1.4	1.7	2
W_{TO} / *Wu*	1.8	2	2.2	2.4	2.7	3
We/ W_{TO}	0.444	0.5	0.545	0.583	0.642	0.667

Table 2-3: Weight ratios for light sport aircraft [43].

-Column 1 is for a very basic airplane with a very good design.

-Column 2 or 3 equates with a simple airplane and a good design.

-Column 4 equates to a classic airplane, simple to build and with adequate strength.

-Column 5 or 6 equates to either a single seat aircraft or a very strong (aerobatic) airplane with heavy equipment and fairings. The design is compromised somewhat for ease of manufacturing.

We pick column 5 as our guide to obtain our maximum weight:

$We + Wu = Wu[1 + We/Wu]$

W_{TO} *= 472 (1+ 1.7) =1274 pounds*

This allows us an error of 1320 pounds (the proposed weight for a Light-Sport Aircraft) minus 1,274 pounds, leaving us 46 pounds of 'room for error," that is, being heavier than planned.

We could increase the useful load by 17 pounds to 489 pounds:

Wu =472+17=489 pounds

Then:

W_{TO} = *489* (1 + 1.7) = 1320 pounds

That's exactly the proposed W_{TO} = 1,320 pounds for a Light-Sport Aircraft

$We = W_{TO} - Wu = 1320 - 489 = 831\ lb.$

2.5 Engine Selection

In this step, some searches have been done through the internet for the suitable engine for this aircraft. The search for engines specifications was focused on power (from 80 to 100 hp), weight, fuel consumption and the total price. AeroVee 2.1 was chosen which is a complete Conversion Engine Kit Package, by AeroConversions. The AeroVee 2.1 package is a 2180 cc, 80 hp @ 3400 RPM (Continuous) Aero-Engine that can be run on AvGas or Auto Fuel. The complete package weighs only 161 Ibs which within the acceptable limits of today's technology that is about two pounds per hp. The fuel consumption is low about 3.5 gph in cruise (see Figure 2-4). The AeroVee 2.1 engine price is only $6,495 and the full package (including engine, exhaust, propeller, and other accessories) costs about 10,000$ with shipping. Time Before Overhaul of the AeroVee between 700 and 1200 hours depending upon how well be treated.

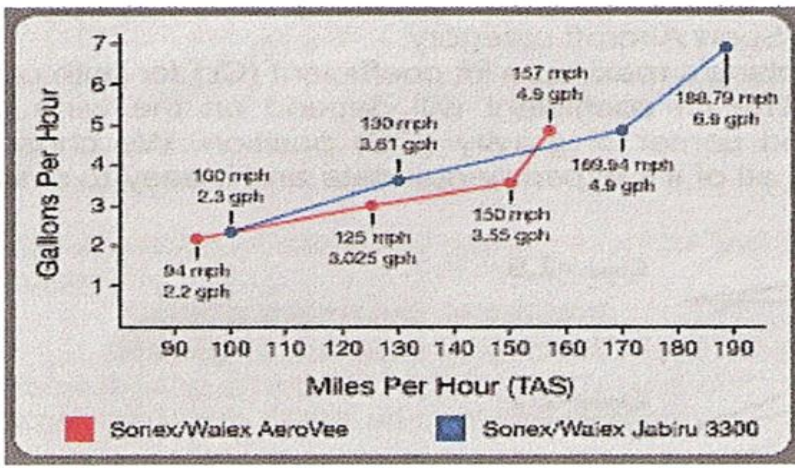

Figure 2-4: The fuel consumption for AeroVee 2.1 comparing to Jabiru 3300 [46].

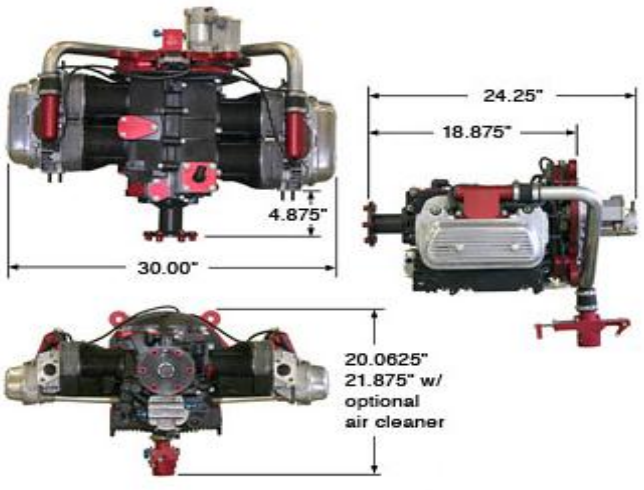

Figure 2-5: AeroVee 2.1 engine dimensions [46].

Engine	Specifications
Make/model	AeroVee 2.1
Horsepower (hp)	80
Number of cylinders	4 (4 strock)
RPM	3400
Altitude (ft)	SL
Weight	161 Ib
Propeller	Specifications
Make/model	Sensenich
Number of blades	2
Type	Fixed Pitch
Max. Diameter (in)	55

Table 2-4: Propulsion system specifications.

2.6 Wing Sizing

Having selected the weights, we now have to select the maximum stall speeds. The proposed Light- Sport Aircraft category prescribes these as:

Vso=39knots=45mph (flaps down)

Vs=44knots=50mph (clean configuration)

At these speeds, the airplane will be easy and relatively safe to land, which is one of the purposes of creating the Light-Sport Aircraft category. Next, we have to know the airplane's maximum lift coefficient (C_L) for both configurations –flaps down and flaps up (clean). The lift coefficient will depend on the wing planform, Reynolds number, airfoil roughness, and center of gravity (CG) position. We chose the airfoil section NACA 2412 because we have all of it's characteristics and it easy to manufacture where the lower surface is almost flat see Figure 2-6.

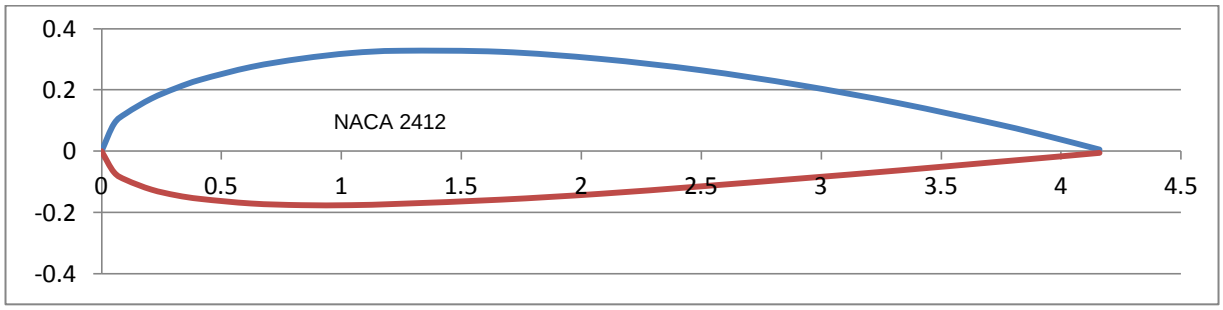

Figure 2-6: Airfoil NACA 2412.

For a simple design, we choose a simple, plain flap, and we do not forget that the flap portion of the wing is only about one-half of the wingspan (the ailerons occupy the outboard one-half span approximately).

C_{Lmax} flaps down = C_{Lmax} clean + 1/2 C_{Lmax} with flaps where C_{Lmax} clean= 1 .6

= [1.6/2] + [2.1/2] = 1.85

With these values we find the required wing area (Sw) to meet the selected stall speed requirements:

W= q x S_w x C_{Lmax}

Where: $q = \frac{\rho v^2}{2} = \frac{v^2}{391}$ at sea level conditions

(*q* is in 'psf' Pounds per square feet. when V is In mph)

For V= *50* mph $\rightarrow q = \frac{50^2}{391}$ = 6.4 psf

$$S_w = \frac{W_{TO}}{q \times C_L} = \frac{1320}{6.4 \times 1.6} = 129\ feet^2$$

For V= *45* mph $\rightarrow q = \frac{45^2}{391}$ = 5.18 psf

$$S_w = \frac{W_{TO}}{q \times C_L} = \frac{1320}{5.18 \times 1.85} = 138\ feet^2$$

If the design has to fit in the Light-Sport Aircraft category, our wing area must be 138 square feet.

If we choose (wing span) bw = 32 feet for our airplane.

$AR = \frac{bw^2}{Sw} = \frac{32^2}{138} = 7.42$

And the wing aerodynamic chord (c_w):

$c_w = \frac{S_w}{b_w} = \frac{138}{32} = 4.313ft.$

Thickness ratio is: t/c = 0.12

Wing loading at cruise is:

$$(\frac{W}{S_w}) = q \times C_L = 6.4 \times 1.6 = 10.24\ qsf$$

The wing shape is high rectangular and fitted above the cockpit. It contains two flaps, two ailerons and two rotating cylinder. Figure 2-7 shows the wing dimensions in feet.

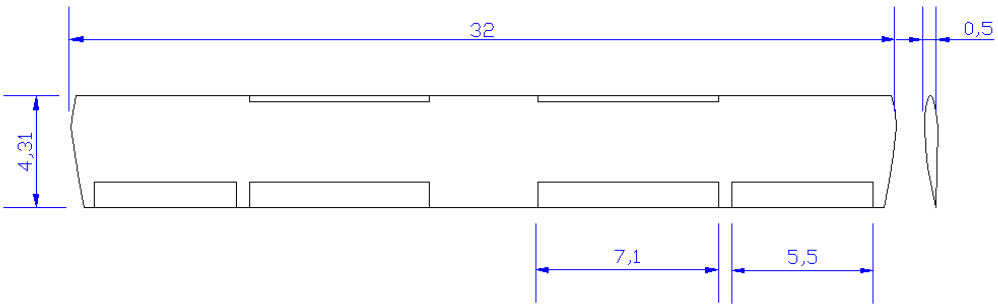

Figure 2-7: The wing shape and dimensions in feet.

The wing tip is Horner wing tip as shown in Figure 2-8. If the wing tip is cut at 45-degrees with a small radius at the bottom and a relatively sharp top corner, the air from the lower surface travels around the rounded bottom but can't go around the sharp top corner and is thus pushed outward[44].

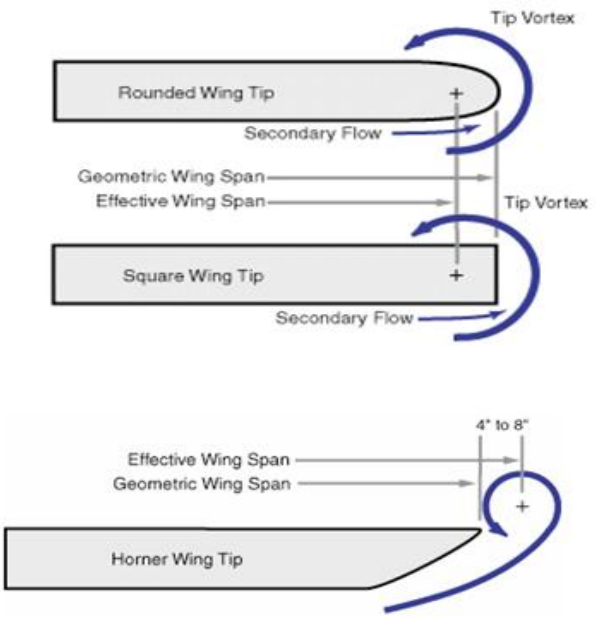

Figure 2-8: Wing tip vortices [44].

The performance of the aircraft depends on the distance from the right to the left tip vortices (the effective wing span), and not the actual measured geometric span. Horner wing tips provide the largest effective span for a given geometric span or a given wing weight.

2.7 Horizontal and Vertical Tail Sizing

1. Horizontal Tail Sizing

The area of the horizontal tail is found from the equation:

$$S_{ht} = C_{ht}\frac{c_w S_w}{L_{ht}}$$

Where C_{ht}=0.7 (the horizontal tail scaling coefficient for general aviation-single engine) [42].

And L_{ht} (the distance from the wing aerodynamic center to the horizontal tail aerodynamic center) for front mounted propeller engine is about 60 percent of the fuselage length.

If we choose fuselage length L_f = 23 feet

$L_{ht} = 0.6 \times L_f = 0.6 \times 23 = 13.8ft$

$$S_{ht} = (0.7)\frac{4.18 \times 138}{13.8} = 41.8ft^2$$

Next, we determine the shape of the horizontal tail. The shape is defined by the aspect ratio 'AR' and the taper ratio 'λ'. For the horizontal tail, the aspect ratio (AR) = 3 – 5, and the taper ratio (λ) = 0.3 – 0.6.

Let us take: AR = 4, λ = 0.6

$$AR = \frac{{b_{ht}}^2}{S_{ht}} \quad \gg \quad b_{ht} = \sqrt{AR \times S_{ht}} = \sqrt{4 \times 41.8} = 12.93ft$$

The root cord is $c_r = \frac{2S_{ht}}{b_{ht}(1+\lambda)} = 4.04ft$

The tip cord is $c_t = \lambda\, c_r = 2.42$ft

Thickness ratio is: t/c = 0.075

The horizontal tail shape and dimensions are shown in Figure 2-9.

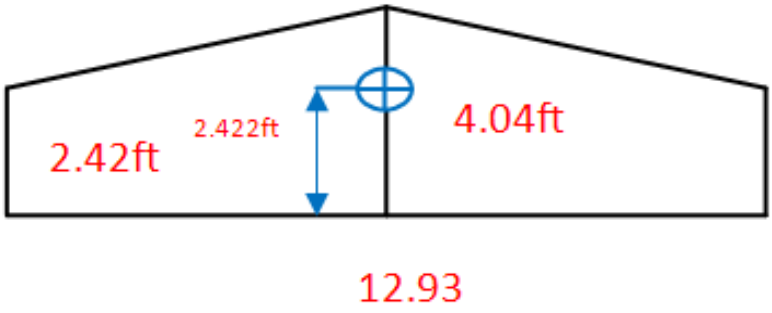

Figure 2-9: The horizontal tail shape and dimensions.

2. Vertical Tail Sizing

The area of the vertical tail is found from this equation:

$$S_{vt} = C_{vt} \frac{b_w S_w}{L_{vt}}$$

Where C_{vt} = 0.04 (the vertical tail scaling coefficient for general aviation-single engine) [42].

If we choose L_{vt} =13 ft (the distance from the wing aerodynamic center to the vertical tail aerodynamic center).

Then:

$$S_{vt} = (0.04)\frac{33 \times 138}{13} = 14ft^2$$

Next, we determine the shape of the vertical tail.

For the vertical tail, the aspect ratio (AR) = 1.3 – 2, and the taper ratio (λ) = 0.3–0.6 [42].

Let us take: AR = 1.7, λ =0.45

$$b_{vt} = \sqrt{AR \times S_{vt}} = \sqrt{1.7 \times 14} = 4.88ft$$

The root cord is $c_r = \frac{2S_{vt}}{b_{vt}(1+\lambda)} = \frac{2\times14}{4.88(1+0.45)} = 3.96\ ft$

The tip cord is $c_t = \lambda \times c_r$ =1.78 ft

Thickness ratio is: t/c = 0.08

The vertical tail shape and dimensions are shown in Figure 2-10.

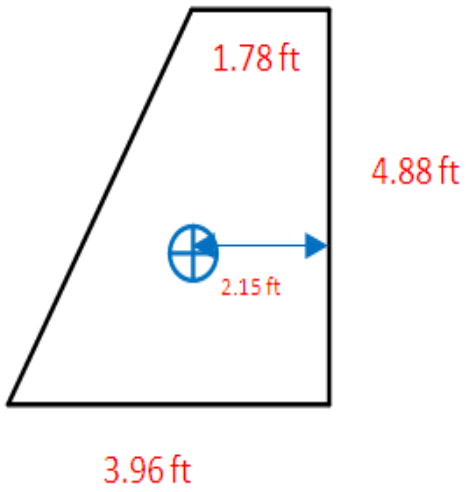

Figure 2-10: The vertical tail shape and dimensions.

The airfoil sections for the horizontal and vertical stabilizers are symmetric (NACA 0008) and having a low base drag coefficient (C_{D0}). During an uncontrolled spin, the vertical stabilizer is caught in the wake of the horizontal stabilizer. This makes the rudder ineffective. The solution is to move the horizontal stabilizer either

forward or aft the vertical stabilizer position. In our case the horizontal stabilizer is aft the vertical stabilizer position.

2.8 Control Surfaces Sizing

All control surfaces are rectangular and hinged to the fixed parts by an aluminum hinge along the span length apart from the rudder which is hinged to an aluminum torque pipe. The used control method is purely manual using both solid and flexible push-pull mechanical components such as control cables and rods. Table 2-3 shows the dimensions of the control surfaces.

Flaps		**Elevator**	
Flap Type	Plain	Elevator chord (%c)	40
Flap Chord (%c)	25	Elevator span (%b)	100
Span Ratio	0.45	Elevator span	12.47 ft
Span	14.4 /2 ft	Elevator chord	0.97 ft
Chord	1.05 ft		
Ailerons		**Rudder**	
Aileron chord (%c)	25	Rudder chord (%c)	45
Aileron span (%b)	33	Rudder span (%b)	9
Aileron span	10.6/2 ft	Rudder span	4.4 ft
Aileron chord	1.05 ft	Rudder chord	0.97 ft

Table 2-5: Control Surfaces Dimensions

2.9 Landing Gears Sizing

Based on the weight of the aircraft, the landing gears where designed to withstand this weight. Table 2-4 represents the size of the landing gears.

The weight on each wheel of the main landing gear:

$$W_{main} = \frac{0.9W_{TO}}{N_{wheels}} = 594\ lb$$

Main wheel diameter (in) = $1.51 \times {W_{main}}^{0.349} = 12.7\ in$

Main wheel width (in) = $0.715 \times {W_{main}}^{0.312} = 6\ in$

Nose landing dimensions are 40 percent smaller

For operation on unpaved runways the values of all the wheels should be increased by 30 percent.

Component	Value
Main wheel height	3 ft
No. of nose wheels	1
No. of main wheels	2
Nose wheel width	3.6 in
Nose wheel diameter	7.6 in
Main wheel width	6 in
Main wheel diameter	12.7 in

Table 2-6: Landing Gears Dimensions

2.10 Performance

To estimate the maximum level full-throttle speed of our aircraft, we simply calculate:

$V_H = 160\sqrt[3]{\frac{bhp}{S_W+100}} = 160\sqrt[3]{\frac{80}{138+100}}$ =111 mph for a comfortable wide

$V_H = 180\sqrt[3]{\frac{bhp}{Sw+100}} = 180\sqrt[3]{\frac{80}{138+100}}$ =125 mph for an average design

$V_H = 200\sqrt[3]{\frac{bhp}{Sw+100}} = 200\sqrt[3]{\frac{80}{138+100}}$ =139 mph for a very clean design

Because the proposed light-sport aircraft category limits the maximum level flight speed to 120 Knots, or 138 mph, we will be quite happy with the "average design". Then, the maximum level flight speed is125 mph. The usual 75 percent power setting cruise speed at sea level will be:

(0.9)*(V_H) = 0.9 * 125 =112.5 mph

The cruise speed will increase to 0.95 x V_H = 119mph at 7,000 or 8,000 feet where we will have 75 percent power at full throttle. Above this altitude the cruise speed will decrease (unless we have a turbo charger), and we will fly very close to the indicated stall speed when we reach the airplane's ceiling.

A simple way of estimating whether our airplane will have good takeoff and climb performance is to calculate the wing loading *(W/S)* and power loading (W/bhp) and multiply:

$\frac{w}{Sw} \times \frac{w}{bhp} = P$

if *P smaller than200* $\frac{pounds^2}{ft^2 bhp}$, the above performance parameters outlined for weight and speed are acceptable[43]. The smaller "P" is, the better the takeoff and climb will be:

$$P = \frac{w}{Sw} \times \frac{w}{bhp} = \frac{1320}{138} \times \frac{1320}{80} = 158$$

This airplane will take off easily. We can easily estimate the rate of climb (Vz) in fpm when W is in pounds:

Vz = $\frac{7000}{w/bhp} \times \sqrt[4]{AR}$

Vz = $\frac{7000}{1320/80} \times \sqrt[4]{7.89}$ =711fpm

The service ceiling will be close to:

$Z_{max} = 16 \times Vz = 16 \times 711 = 11350ft$

2.11 Structural Analysis

A *V-n* diagram shows the flight load factors that are used for the structural design as a function of the air speed. These represent the maximum expected loads that the aircraft will be experience. These load factors are referred to as the limit load factors. Load factor standards for aircraft are covered by FAR-23 for normal, utility, acrobatic and commuter aircraft. The maximum load factor in according to FAR-23 for normal general aviation is (-1.25≤ n ≥ 3.1) [41]. Load factor limits was specified to be

(+3 / -1 g) as a maneuver loads. Figure 2-11 gives the V-n diagram for this aircraft which shows the aircraft limit load factor as a function of airspeed.

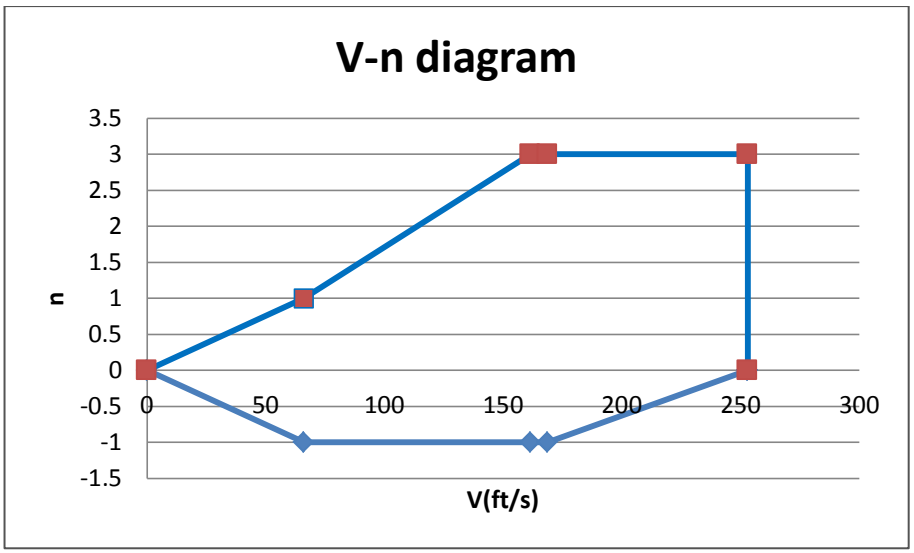

Figure 2-11: V-n diagram for the aircraft

The variation of gust velocity ($\hat{u}$) with altitude for different flight conditions is shown in Figure 2-12. The effects of the loads experienced when the aircraft encounters a strong gust exceed the maneuver limits of this aircraft are shown in Figure 2-13.

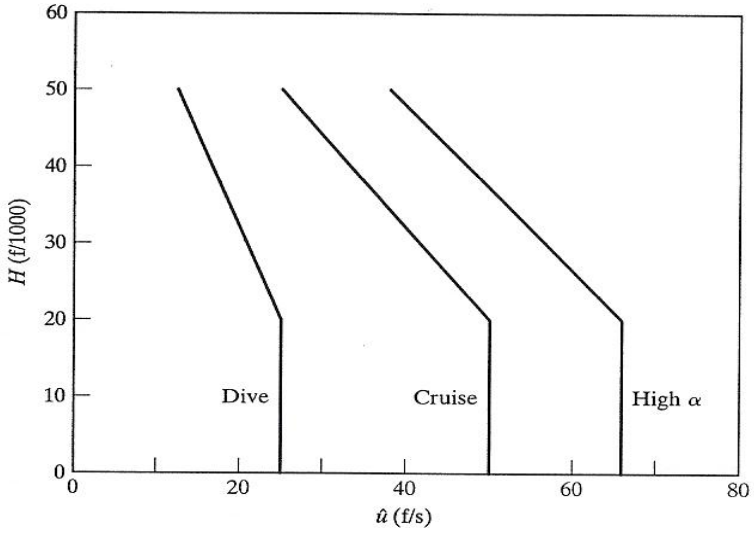

Figure 2-12: Variation of gust velocity with altitude for different flight conditions [42].

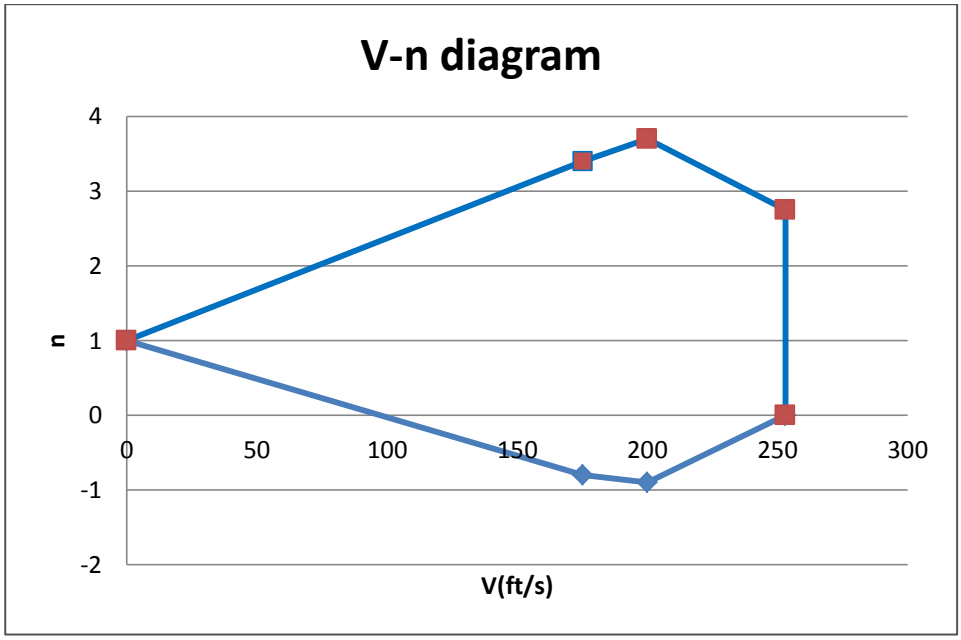

Figure 2-13: V-n diagram with gust loads

The limit load factor value should be multiplied by 1.5 as a safety factor.

$n_{design} = 1.5 n_{limit}$

This results in +4.5 / -1.5 g. Design Load Factor.

2.12 Static Stability and Control

2.12.1 Refined weight estimation

The refined weight estimates are based on formulas that relate different characteristics of aircraft to their components weights. These formulas involve coefficients found by minimum error fit to a large set of aircraft. We will use the method of calculating weights of each part independently using these equations. Table 2-7 shows the estimated weights. (For equations see ref. [42] eq. # 11.1 to 11.6).

Component	Weight(lb)
wing	169.426
horizontal tail	25.45
vertical tail	14.79
fuselage	136.91
main landing gear	42.97
nose landing gear	10.23
Installed engine	220
Other components(fuel system, flight controls, avionics, furnishings)14%of the TOGW	185 (acting @x/L=0.5 of fuselage)
Total weight	804.78

Table 2-7: The estimated weights of the aircraft components.

If we compare this result to what has been calculated before - the empty weight is We =831 lb., the error is only -3.2%. Therefore, the baggage or the empty weight can be increased by 26 lb.

2.11.2 Weight and Balance

Aircraft weight and balance process is important to adjust the center of gravity in the allowed range around the aerodynamic center which is about 25% of the wing by moving components and the useful load. Table 2-8 shows the weight of the aircraft

components and location from the nose and the moment caused by these weights. The table gives also the center of gravity of the aircraft which is 6.5 feet from the nose.

Components	Weight lbs	Loc ft	Moment ft-lbs
STRUCTURES	**419.8**		**3552**
Wing	169.43	6.0	1017
Horizontal Tail	25.45	21.0	534
Vertical Tail	14.79	19.0	281
Fuselage	136.9	9.0	1232
doors	5	6.0	30
cowling	5	2.0	10
engine Mount	10	3.0	30
Main Landing Gear	42.97	9.0	387
Nose Landing Gear	10.23	3.0	31
PROPULSION	**215.0**		**437**
Engine	162	2.0	324
Air Induction	2	2.0	4
Cooling	1	2.0	2
Exhaust	9	2.0	18
Engine Controls	4	3.0	12
Misc. Engine Inst	10	2.0	20
Propeller	7	1.0	7
Starter	10	3.0	30
Fuel System	10	2.0	20
EQUIPMENT	**97.0**		595
Flight Controls	50	6.0	300
Instruments	5	4.0	20
Electrical	5	7.0	35
Avionics	5	4.0	20
Rotating cylinder	12	5.0	60
Furnishings & Equipment	20	8.0	160
Empty Weight Allowance	73.2	6.3	458
TOTAL WEIGHT EMPTY	**804.9**	**6.3**	5042
USEFUL LOAD	**515.1**		
Crew	200.0	8.0	1600
Fuel	72.0	4.5	540
Oil	6	5.0	30
Passengers	200	8.0	1600
Payload	0	10.0	0
TAKEOFF GROSS WEIGHT	**1320.0**	**6.5**	8560

Table 2-8: The weight of the aircraft components and location from the nose.

2.11.3 Static stability

The static stability of the aircraft is presented in three directions of motion (longitudinal, lateral and directional) separately. The longitudinal stability is the measure of the response of the aircraft due to the change in the pitch angle. Because this aircraft flies mainly with its wings, the wing leading edge is the reference for measuring **X** and $\mathbf{X_R}$ (see Figure3-12) [44]. The graph helps us to design a stable aircraft and shows that a high wing aircraft, due to the pendulum effect, is slightly more stable than a low wing aircraft. $\mathbf{X_R}$ is the most rearward position of the center of gravity where the aircraft is still stable. If **X**, which is the actual center of gravity position, is smaller than $\mathbf{X_R}$, the aircraft is stable and can be flown hands off.

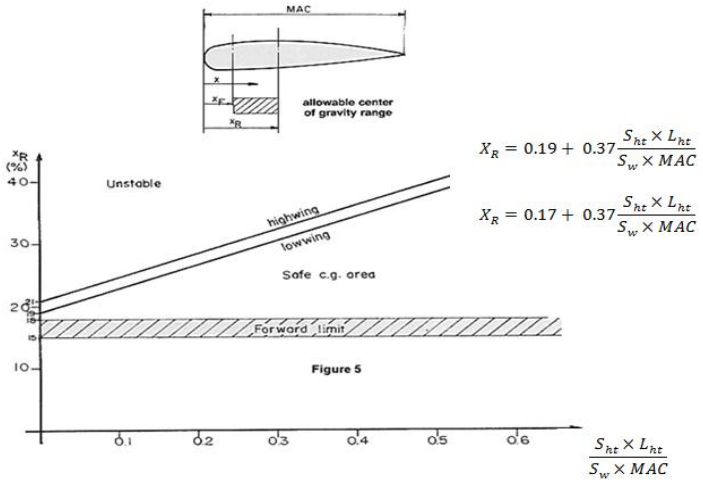

Figure 2-14: Longitudinal stability.

The two lines in the diagram represent the following formulas:

$X_R = 0.17 + 0.37\ S_{ht}\ x\ L_{ht}/(\ S_w\ x\ MAC)$ - Low Wing (1)

$X_R = 0.19 + 0.37\ S_{ht}\ x\ L_{ht}/(\ S_w\ x\ MAC)$ - High Wing (2)

where:

S_{ht} horizontal tail area

S_w wing area

L_{ht} distance from the aerodynamic center of the wing to the center of lift of the horizontal tail

MAC wing mean aerodynamic chord

(S_{ht} x L_{ht}) is sometimes called horizontal tail volume

For this aircraft (high wing), we use equation 2:

$$X_R = 0.19 + 0.37 \times \frac{S_{ht} \times L}{S_w \times MAC} = 0.19 + 0.37 \times \frac{41.8 \times 13.8}{138 \times 4.31} = 0.55 \quad (3)$$

$$X_F = 0.15 \times X_R = 0.082 \quad (4)$$

The allowable center of gravity should be kept in the range of 8.2 to 55 percent of the MAC which is from 0.356 to 2.37 ft from the leading edge of the wing. If the aerodynamic center is at 25 percent of the wing, it will be at 1.08ft from the leading edge and 6.6ft from the aircraft nose.

The forward CG allowable limit= 1.08-0.356 = 0.713ft = 8.6 in

The aft ward CG allowable limit= 2.37 – 1.08 =1.29 ft =15.4 in

The empty weight and the useful weight of the aircraft should be adjusted by moving the aircraft components, crew seats and fuel tanks locations. From Table 2.8, the center of gravity is in between the allowable limits. Because of the aircraft symmetry about X axis of the aircraft and the high wing configuration, the aircraft will be laterally stable due to the pendulum effect.

CHAPTER 3

Preliminary Design

3.1 Introduction

In the preliminary design stage, fine tuning of the conceptual design should be made through parametric wind tunnel tests of a scale model of the design. It involves a more detailed analysis of the aerodynamic loads, components weights and costs. From that, the structural design is further refined. Additional conformation of estimates may require building and testing some of the proposed structural components.

A scale model (1:16) was built to be used for wind tunnel test to find the aerodynamic coefficients (see Figure 3-1). The model was installed in the wind tunnel to get coefficients of the aerodynamic characteristics that were used in the spreadsheets. This model helped us a lot in the initial design of the aircraft and its components before the building stage.

Figure 3-1: The scale model of the aircraft in the wind tunnel.

3.2 Aircraft dimensions

A 3D drawing was done using AUTOCAD software. Some of the dimensions were taken from the aircraft component sizing which was done in the conceptual design and some details were taken from the scale model. These general dimensions will be used in the stability analysis, detail design step and structural details. See Figure 3-2 and Figure 3-3.

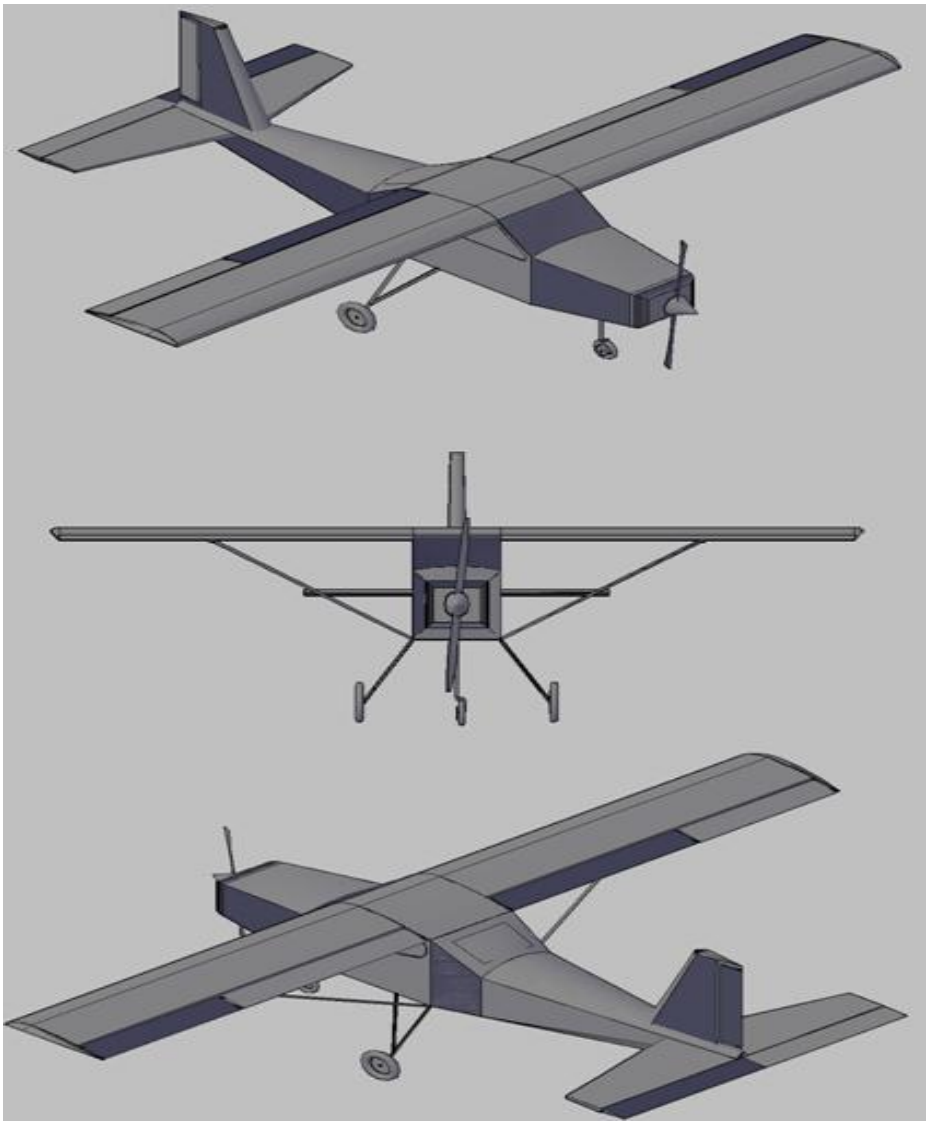

Figure 3-2: 3D drawing for the aircraft.

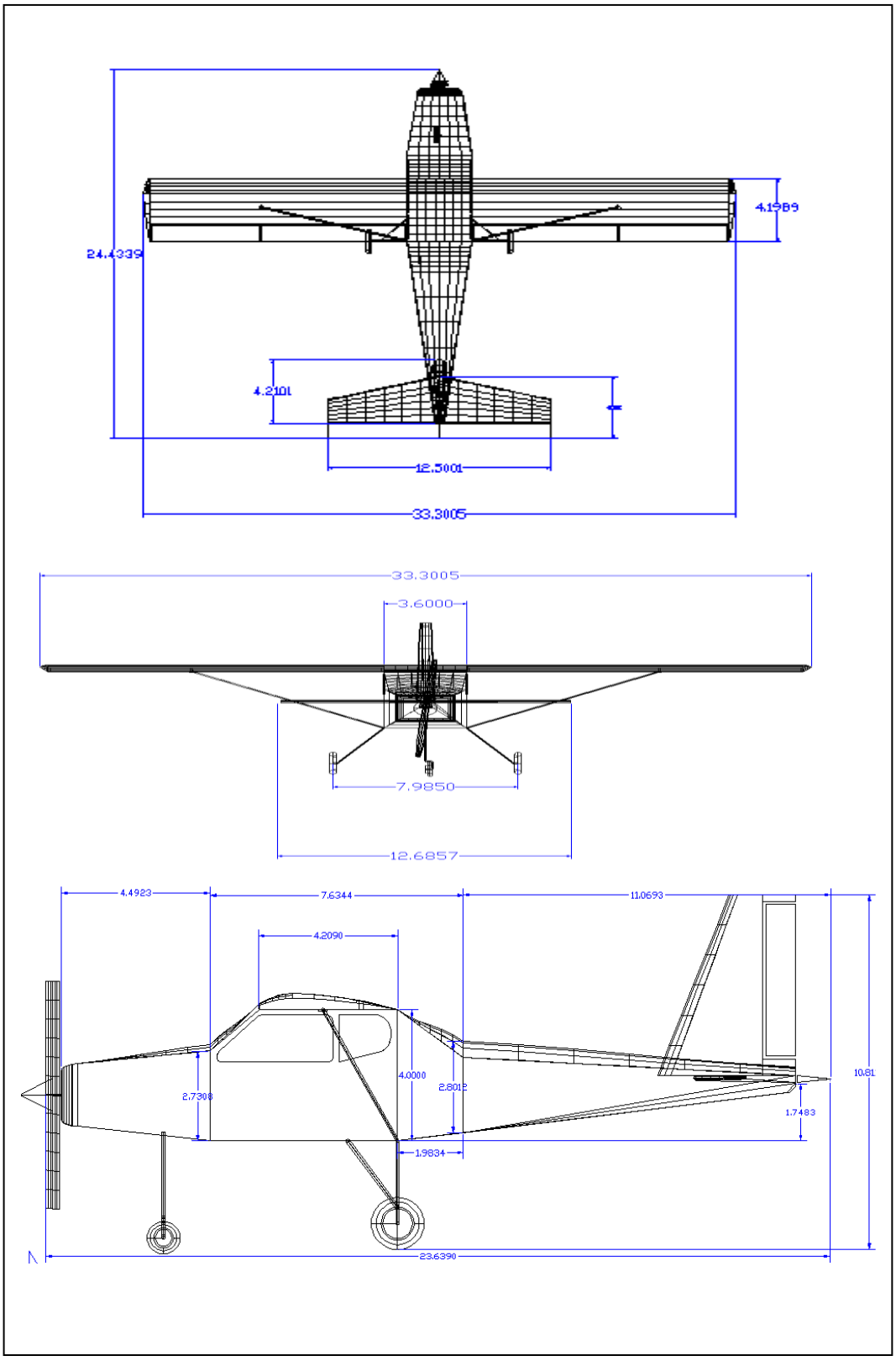

Figure 3-3: General dimensions for the aircraft.

3.3 Performance

A spreadsheet called master 1 performance and Raymer Simplified Aircraft Design Spreadsheet for Homebuilders were used to analyze the performance of this aircraft. Figure 3-4 represents variation of the total drag, cruise thrust and total thrust with airspeed in knots. The intersections of the total drag curve with the total thrust curve and with the cruise thrust curve are the maximum and cruise speed limits. Figure 3-5 shows the lift to drag ratio as a measure of the aerodynamic efficiency of the aircraft at different airspeeds.

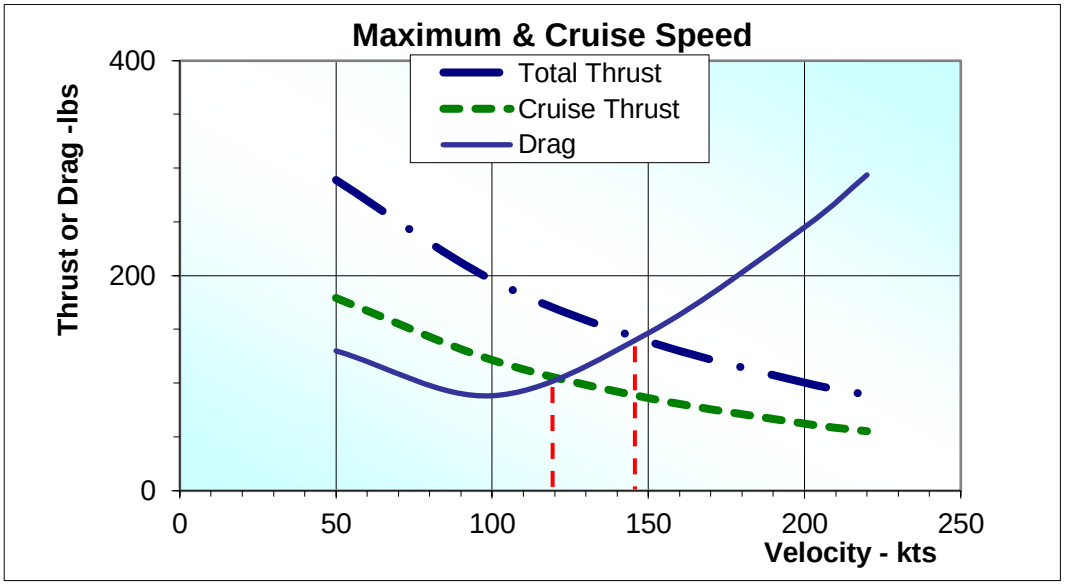

Figure 3-4: The thrust and drag curves.

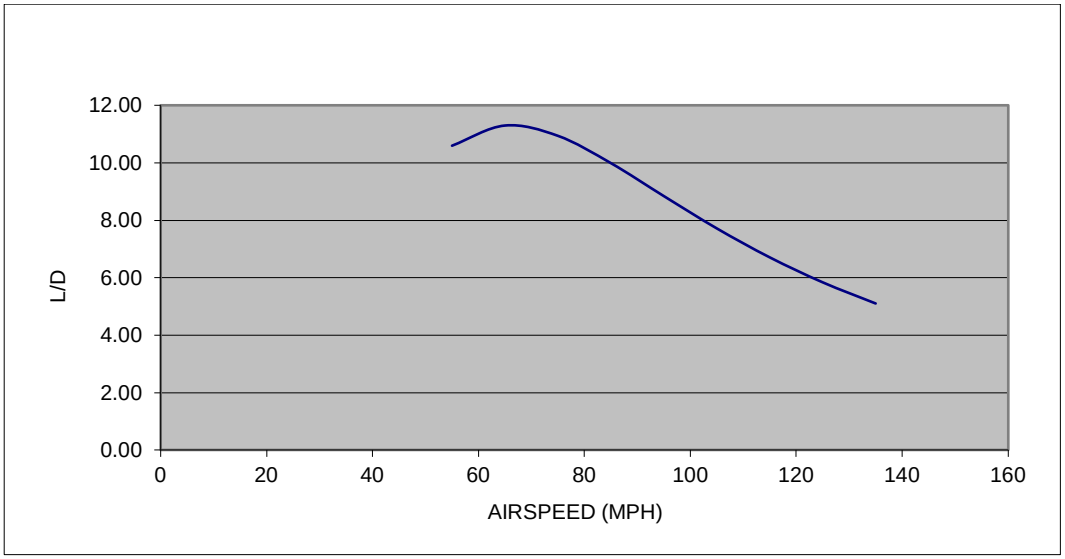

Figure 3-5: The variation of induced, profile, parasite and total drag with airspeed.

The cruise performance is represented in Figure 3-6 as a function of the power required and the airspeed. Figure 3-7 gives the required shaft horse power and the corresponding rate of climb in feet per minute at 1.3 Vs. The best rate of climb is at the sea level which decreases as the altitude increases (see Figure 3-8). Figure 3-9 shows the takeoff run distance as a function of engine horsepower at sea level.

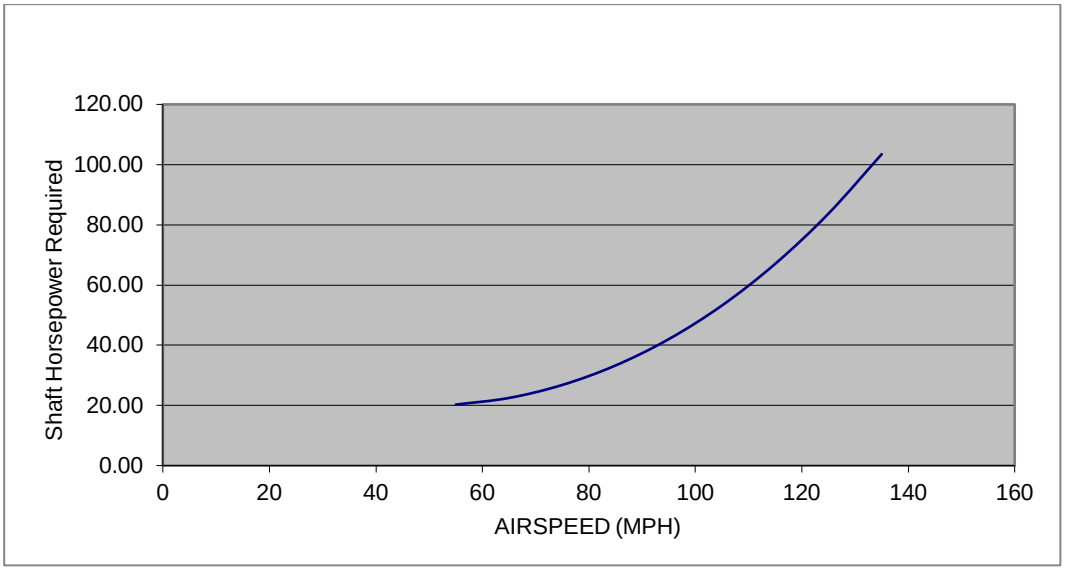

Figure 3-6: The required power at cruise.

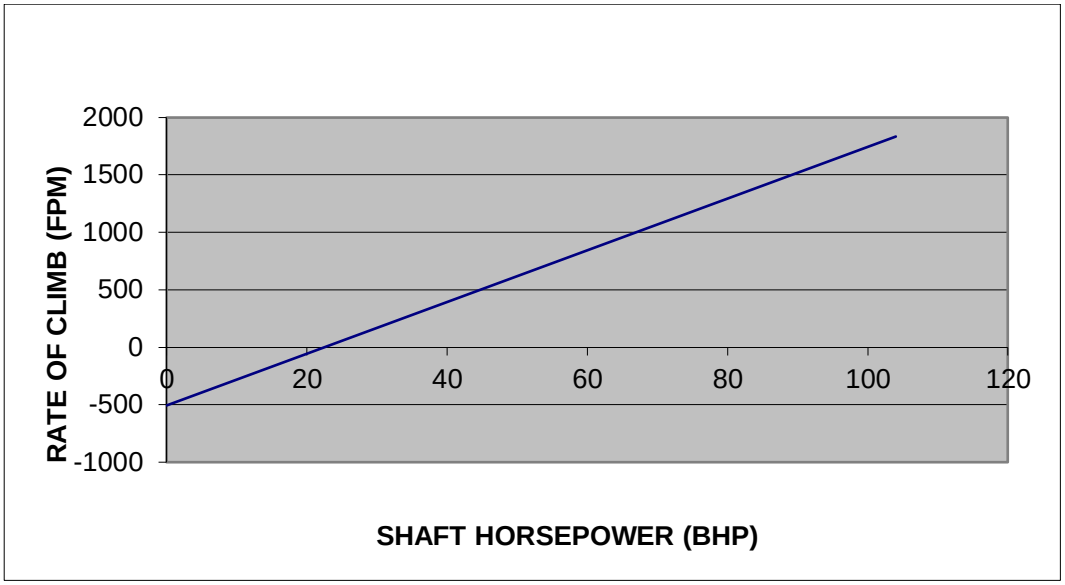

Figure 3-7: The variation of rate of climb with power at 1.3 Vs.

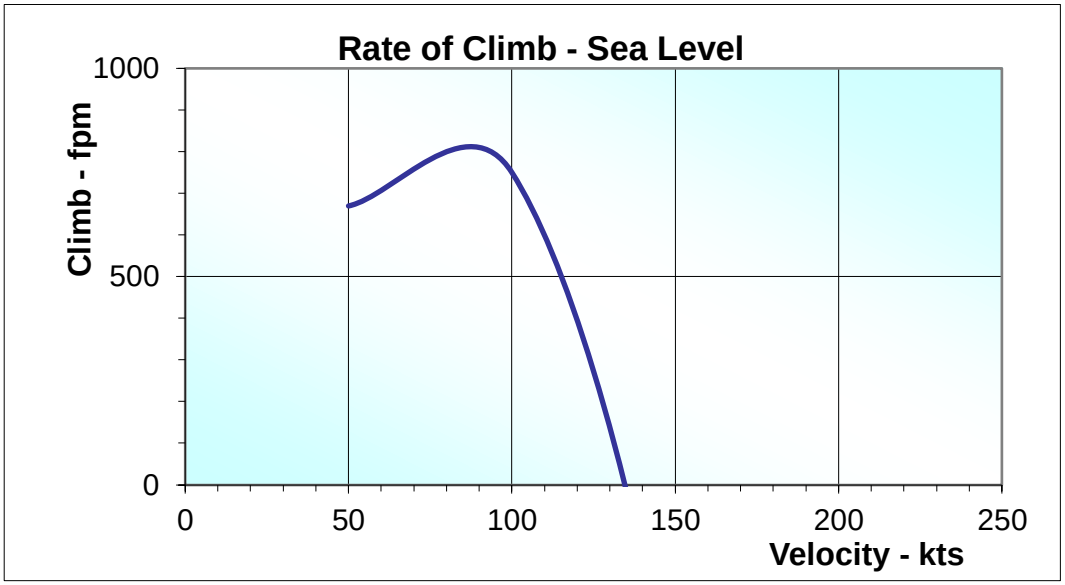

Figure 3-8: Rate of climb vs. airspeed at sea level.

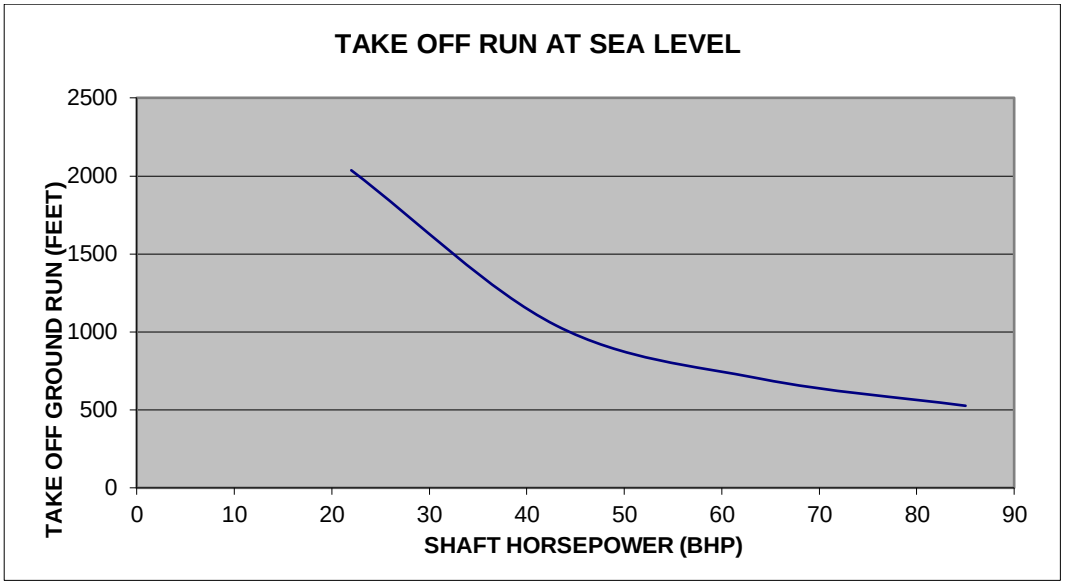

Figure 3-9: Takeoff run at sea level vs. shaft horsepower.

From the performance codes, we got the following performance results:

- Takeoff ground run at sea level is 560 feet.
- Take off distance to a 50ft obstacle is 732 feet
- Rate of climb at 1.3 Vs is about 843 feet per minute at sea level.
- Maximum level speed is 124 mph.
- Cruise speed at 75% power is 112 mph.
- Glide descent rate at 1.3 Vs is 506 feet per minute.
- The landing distance is 687 feet.
- The Range is 370 mile.
- The Endurance is 3.4 hours.

3.4 Estimating stability and control characteristics

The method used for this purpose is the USAF Stability and Control **DATCOM** software. The fundamental purpose of this program is to provide a systematic summary of methods for estimating stability and control characteristics in preliminary design applications [47]. The Digital DATCOM program uses aircraft-unique configuration and geometry parameters to predict aircraft performance by utilizing classical aerodynamic equations. The Digital DATCOM program calculates static stability, high lift and control, and dynamic derivative characteristics, and is applicable to subsonic, transonic, supersonic, and hypersonic vehicles, for traditional body-wing-tail or canard-equipped vehicles.

For those speed regimes and configurations where DATCOM methods are available, the Digital DATCOM output provides the longitudinal coefficients C_L, C_D, C_m, C_n, and C_A (body axis), and the derivatives $dC_L/d\alpha$, $dC_m/d\alpha$, $dC_Y/d\beta$, $dC_n/d\beta$, and $dC_l/d\beta$. Output for configurations with a wing and horizontal tail also includes downwash and the local dynamic-pressure ratio in the region of the tail. The pitch, roll, yaw and angle-of-attack rate derivatives dC_L/dq, dC_m/dq, $dC_L/d(\alpha\text{-dot})$, $dC_m/d(\alpha\text{-dot})$, dC_l/dp, dC_Y/dp, dC_n/dp, dC_n/dr, and dC_l/dr are also computed for most configurations.

Dimensions of the aircraft and some inputs from the wind tunnel or from the performance program were used. Figure 3-10 shows the 3D approximation model that was constructed in DATCOM code for our aircraft.

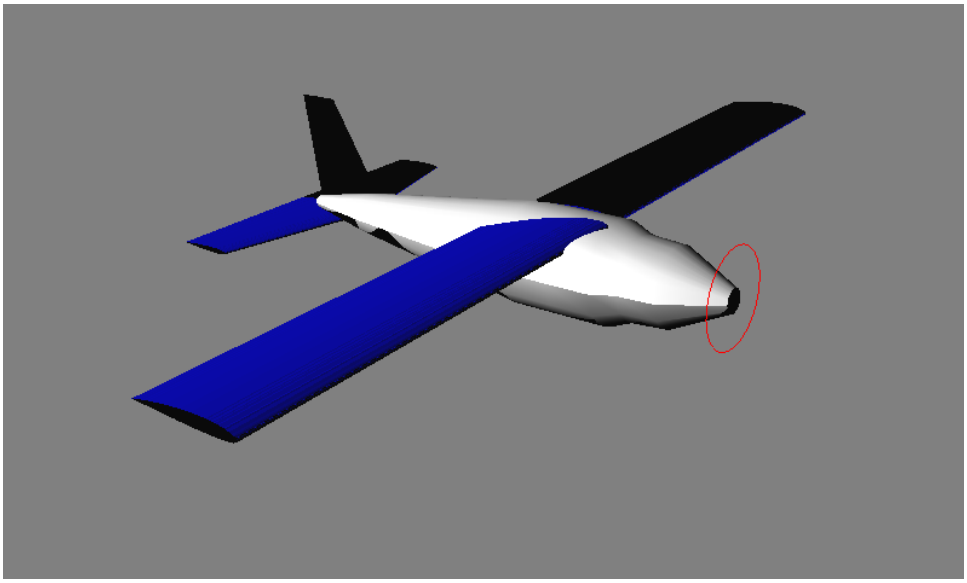

Figure 3-10: 3D approximation model.

After running the DATCOM program, we got the following output parameters:

- Lift coefficient due to:

  - basic geometry (C_{L_α})

  - flap deflection ($C_{L_{\delta f}}$)

  - elevator deflection ($C_{L_{\delta e}}$)

  - pitch rate derivative (C_{L_q})

  - angle of attack rate derivative ($C_{L_{\alpha dot}}$)

- Drag coefficient due to:

  - basic geometry (C_{D_α})

  - flap deflection ($C_{D_{\delta f}}$)

  - elevator deflection ($C_{D_{\delta e}}$)

- Side force coefficient due to:

  - sideslip (C_{n_β})

  - roll rate derivative (C_{n_p})

- yaw rate derivative (C_{n_r})

- Pitching moment coefficient due to:

  - basic geometry (C_{m_α})

  - flap deflection ($C_{m_{\delta f}}$)

  - elevator deflection ($C_{m_{\delta e}}$)

  - pitch rate derivative (C_{m_q})

  - angle of attack rate derivative ($C_{m_{\alpha dot}}$)

- Rolling moment coefficient due to:

  - Aileron Deflection ($C_{l_{\delta a}}$)

  - Sideslip (C_{l_β})

  - roll rate derivative (C_{l_p})

  - yaw rate derivative (C_{l_r})

- Yawing moment coefficient

  - aileron deflection ($C_{y_{\delta a}}$)

  - sideslip (C_{y_β})

  - roll rate derivative (C_{y_p})

  - yaw rate derivative (C_{y_r})

- Horizontal tail downwash angle (ε)

- Derivative of downwash angle ($\delta\varepsilon/\delta\alpha$)

- Elevator-surface hinge-moment derivative with respect to alpha (C_{h_α})

- Elevator-surface hinge-moment derivative due to elevator deflection (C_{h_δ})

Where the output was in Excel charts form (see Figures from 3-12 to 3-37)

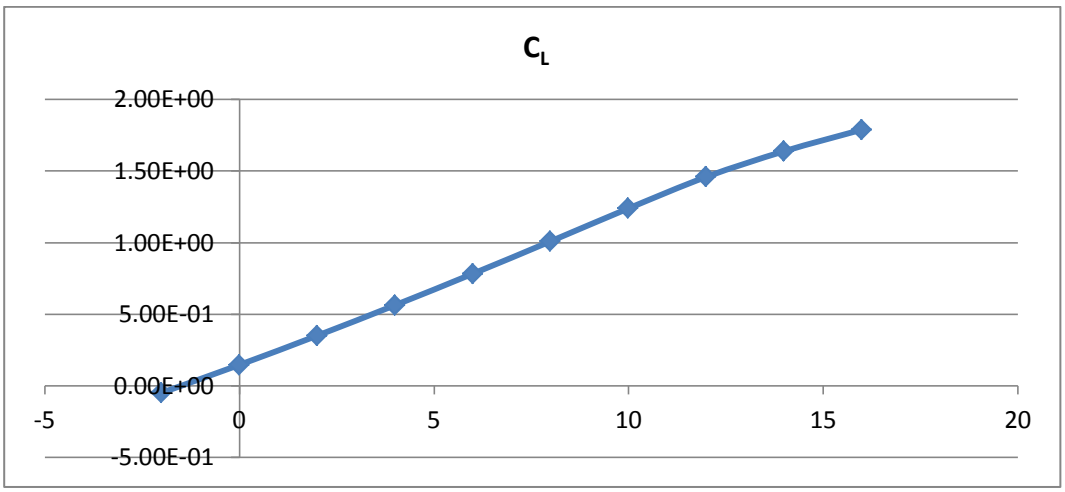

Figure 3-11: Lift coefficient due to basic geometry (C_{L_α}).

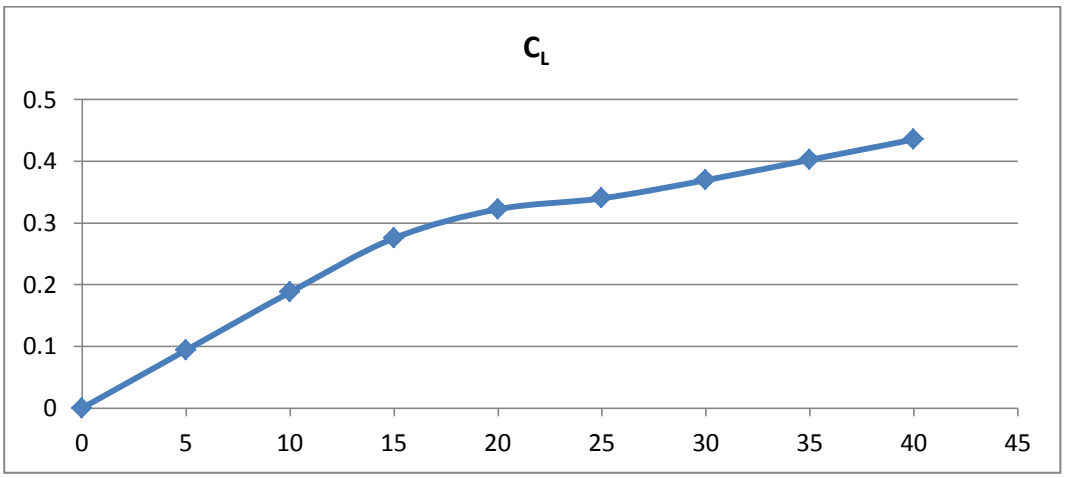

Figure 3-12: Lift coefficient due to flap deflection ($C_{L_{\delta f}}$).

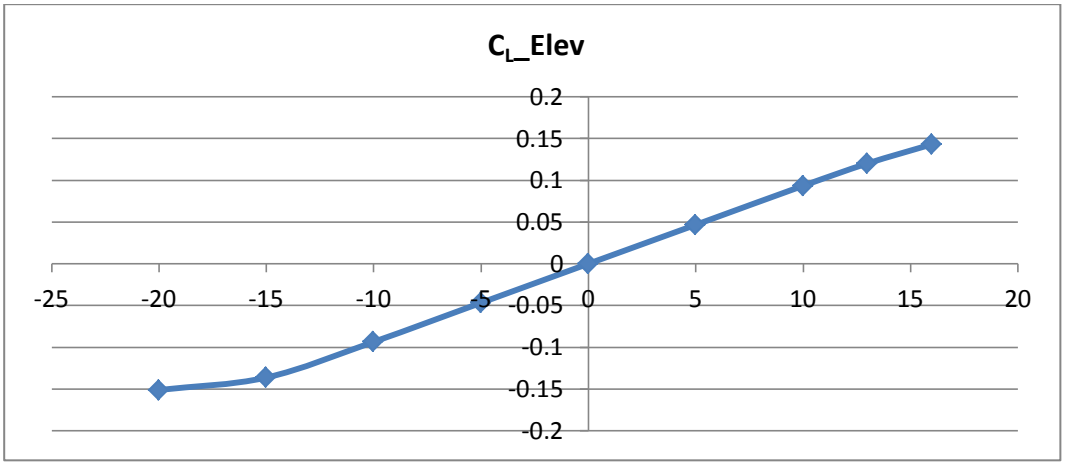

Figure 3-13: Lift coefficient due to elevator deflection ($C_{L_{\delta e}}$).

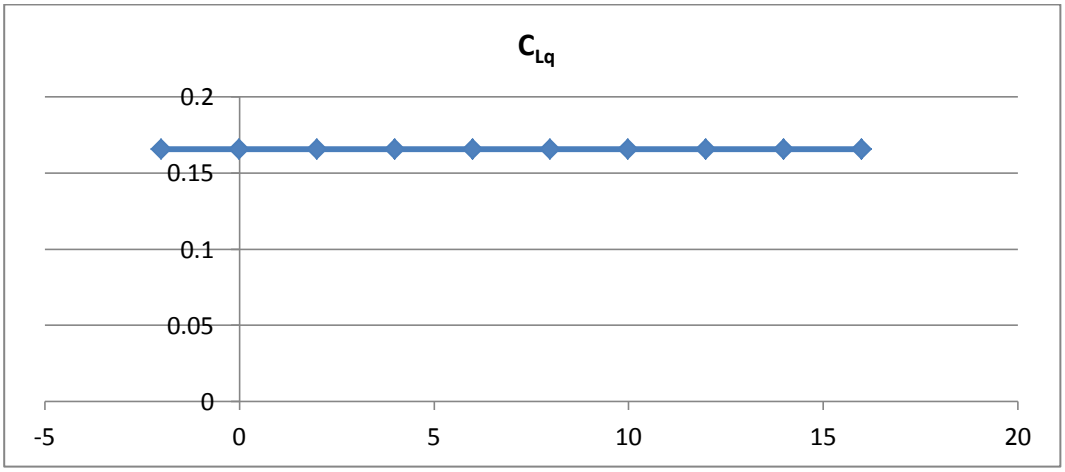

Figure 3-14: Lift coefficient due to pitch rate derivative (C_{L_q}).

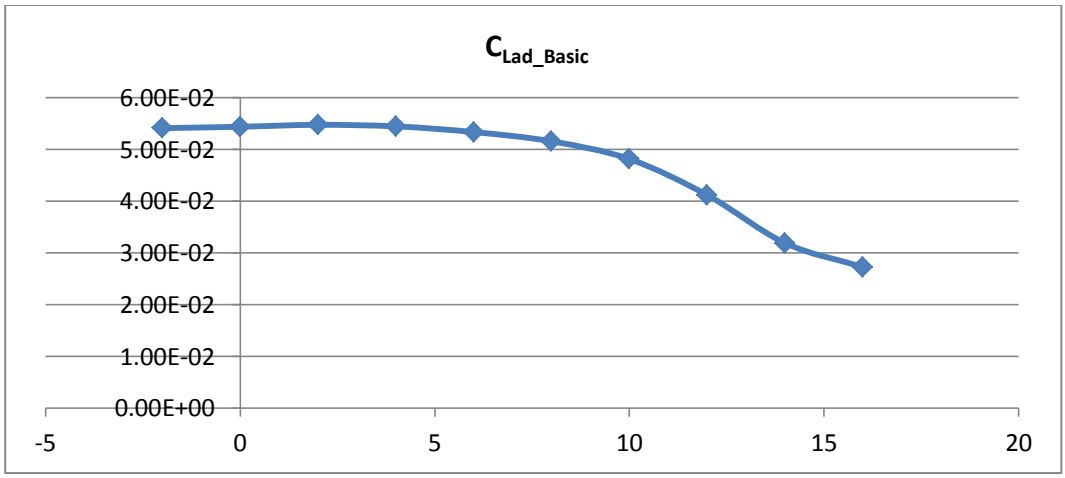

Figure 3-15: Lift coefficient due to angle of attack rate derivative ($C_{L_{\alpha dot}}$).

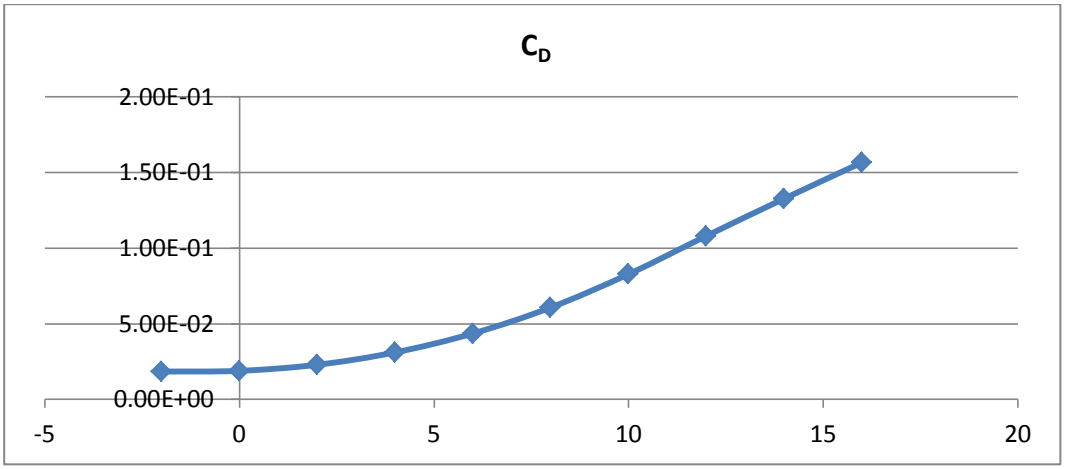

Figure 3-16: Drag coefficient due to basic geometry (C_{D_α}).

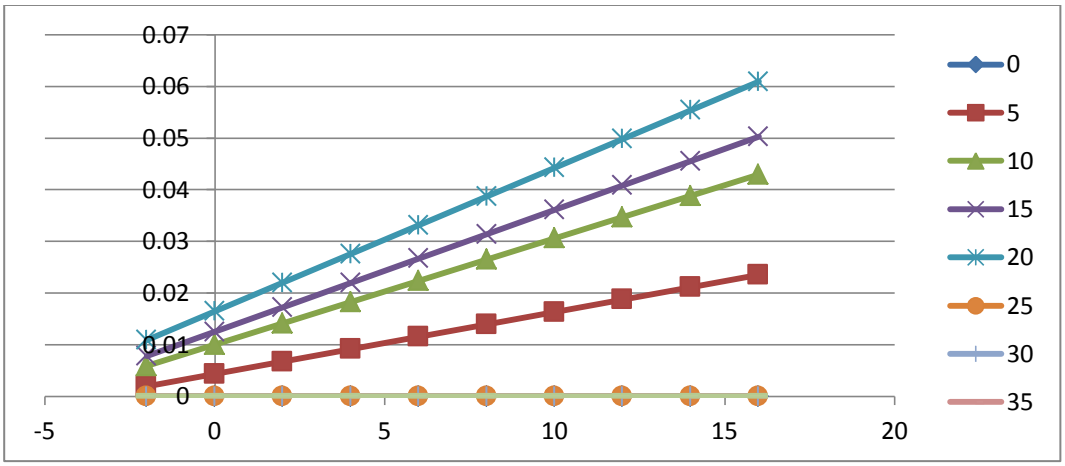

Figure 3-17: Drag coefficient due to flap deflection ($C_{D_{\delta f}}$).

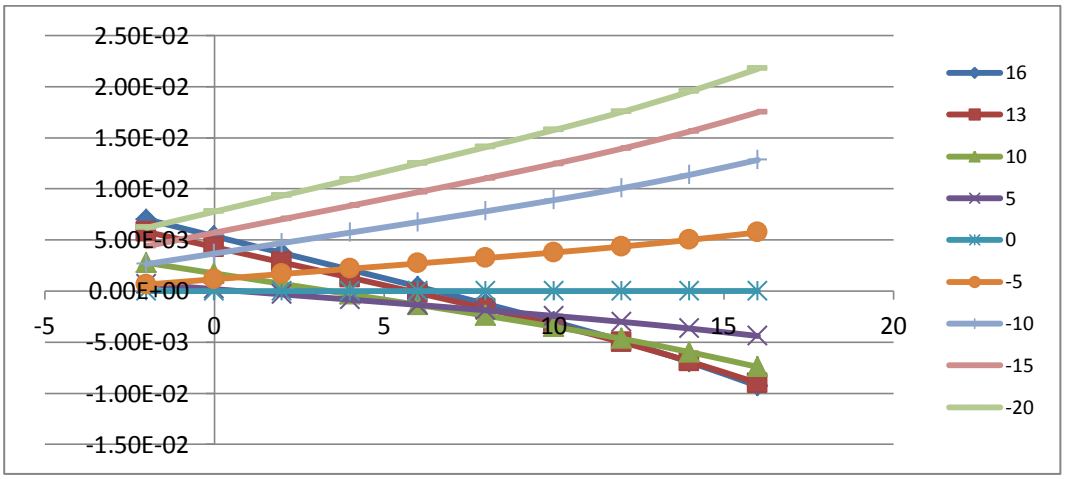

Figure 3-18: Drag coefficient due to elevator deflection ($C_{D_{\delta e}}$).

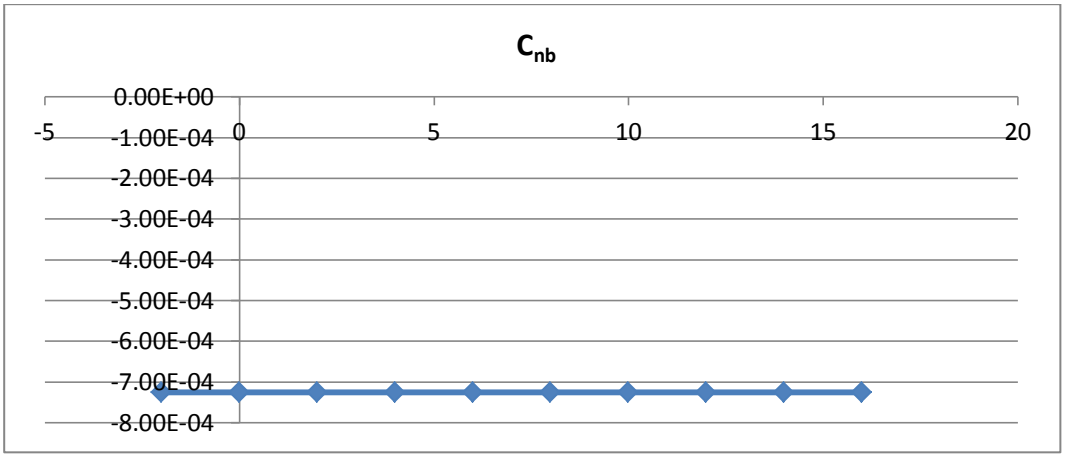

Figure 3-19: Side force coefficient due to sideslip (C_{n_β}).

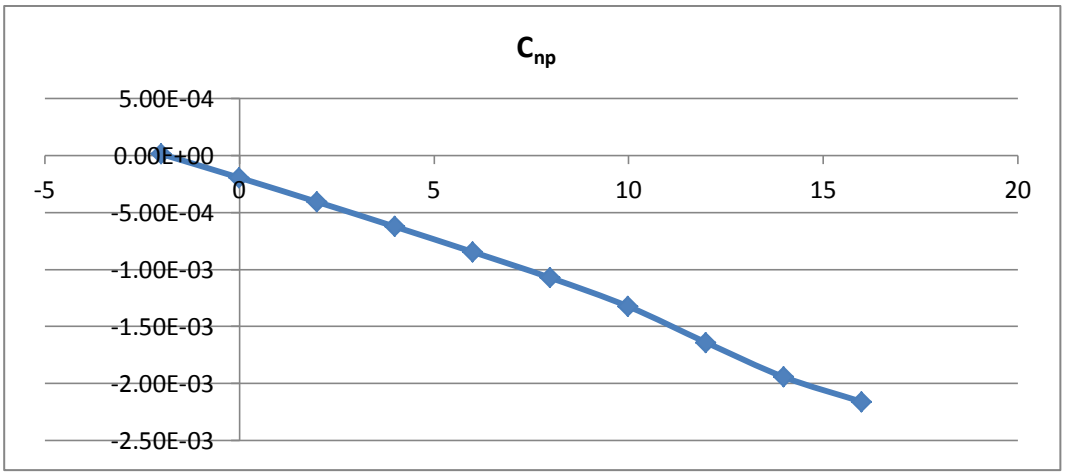

Figure 3-20: Side force coefficient due to roll rate derivative (C_{n_p}).

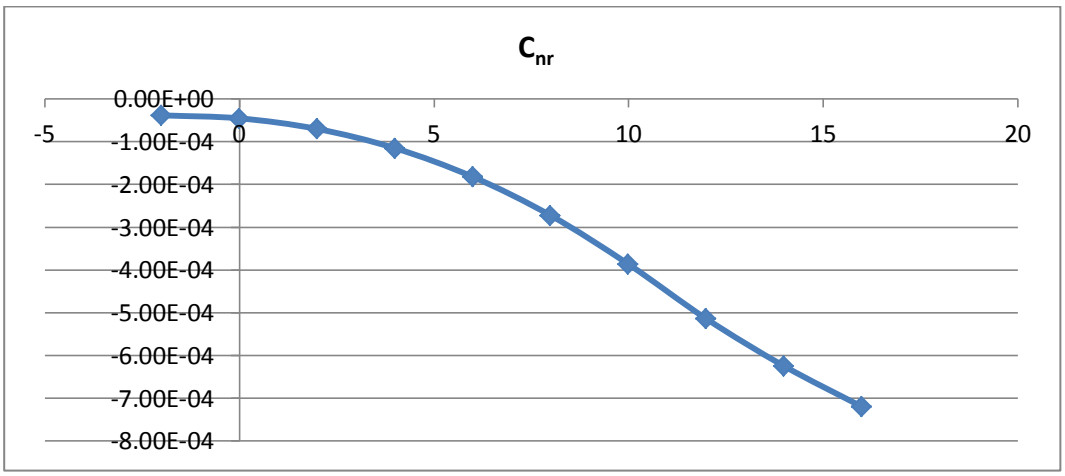

Figure 3-21: Side force coefficient due to yaw rate derivative (C_{n_r}).

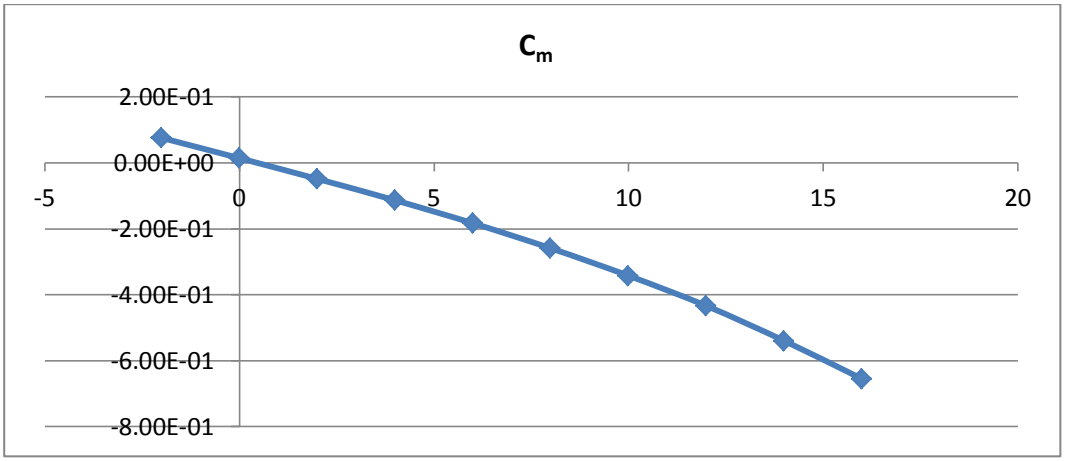

Figure 3-22: Pitching moment coefficient due to basic geometry (C_{m_α}).

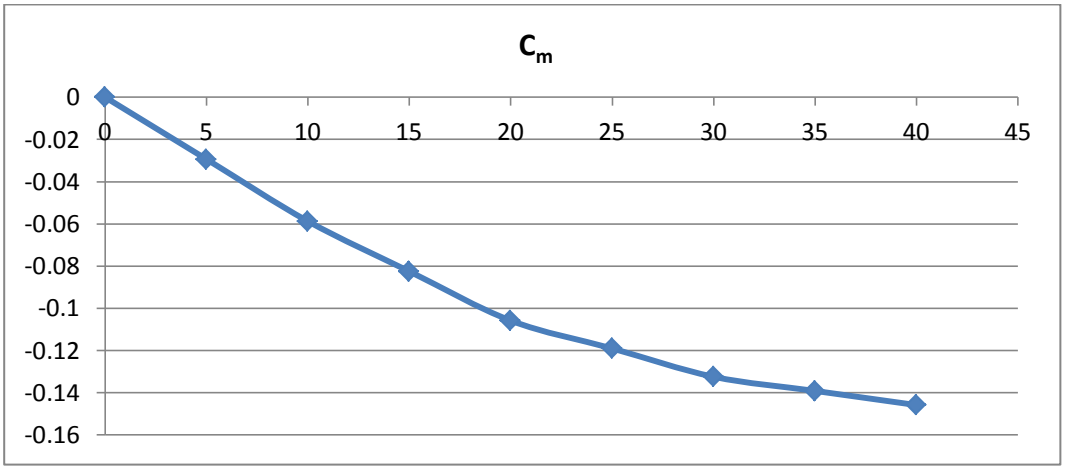

Figure 3-23: Pitching moment coefficient due to flap deflection ($C_{m_{\delta f}}$).

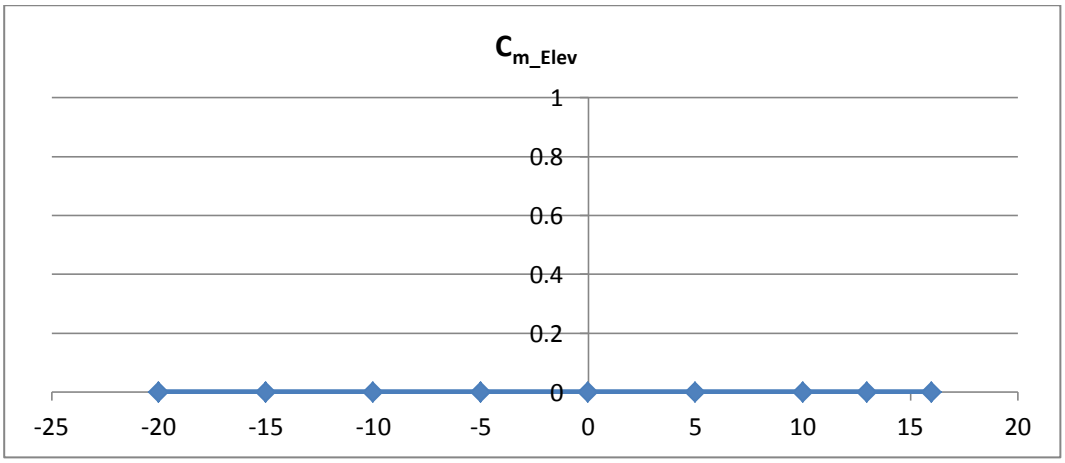

Figure 3-24: Pitching moment coefficient due to elevator deflection ($C_{m_{\delta e}}$).

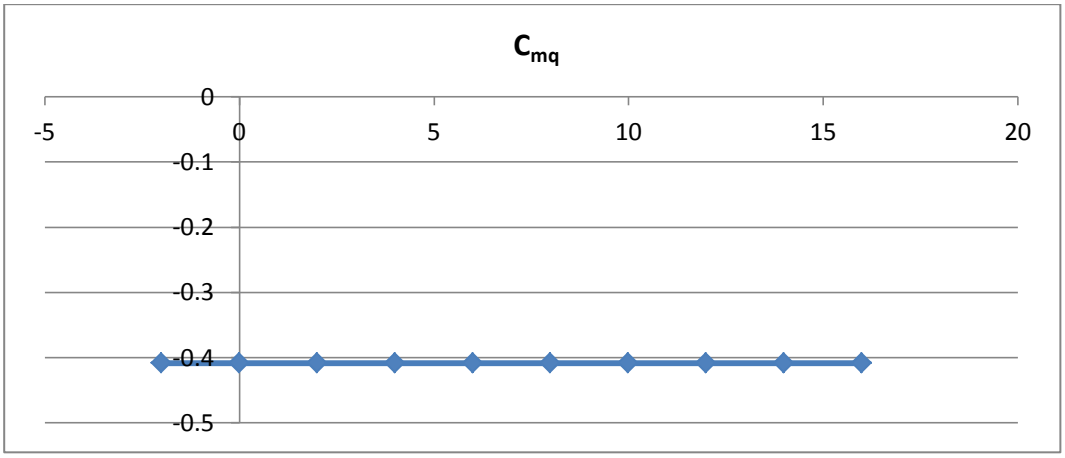

Figure 3-25: Pitching moment coefficient due to pitch rate derivative (C_{m_q}).

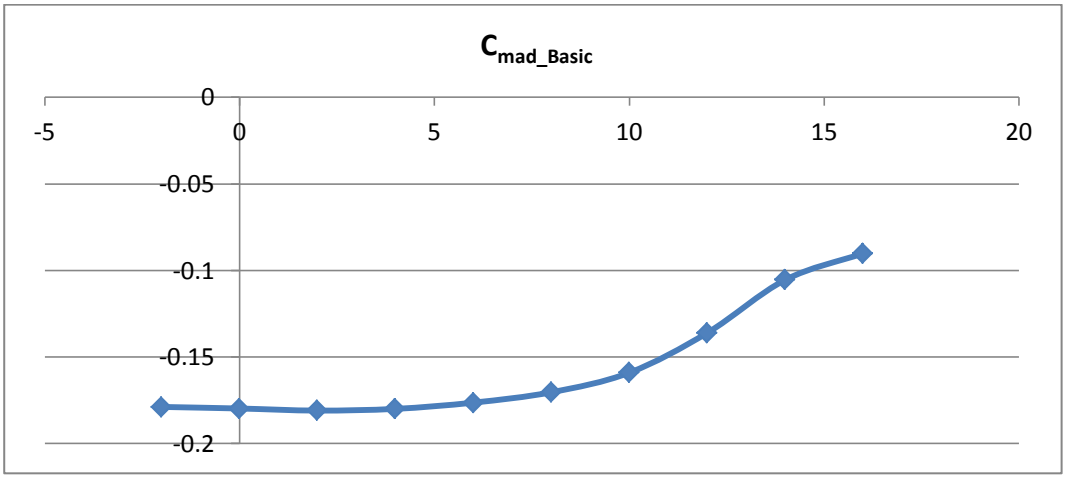

Figure 3-26: Pitching moment coefficient due to angle of attack rate derivative ($C_{m_{\alpha dot}}$).

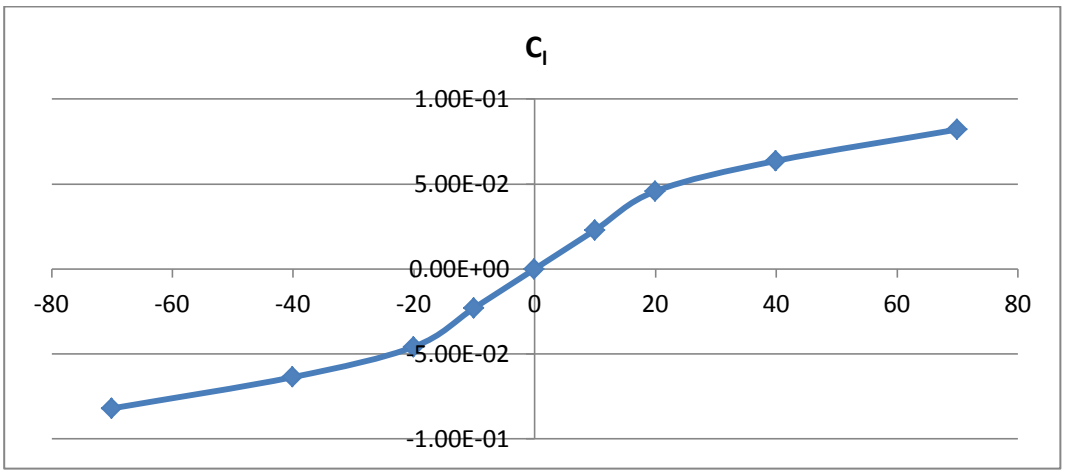

Figure 3-27: Rolling moment coefficient due to aileron deflection ($C_{l_{\delta a}}$).

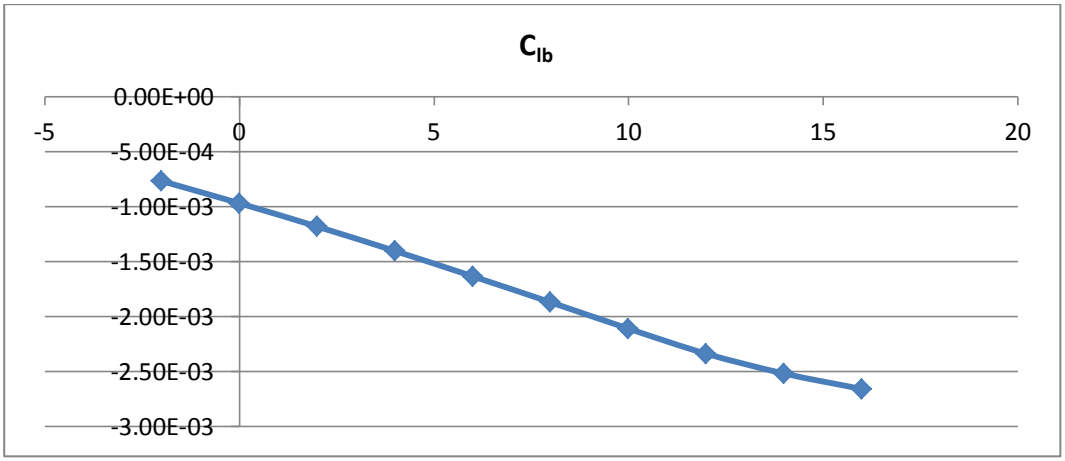

Figure 3-28: Rolling moment coefficient due to sideslip (C_{l_β}).

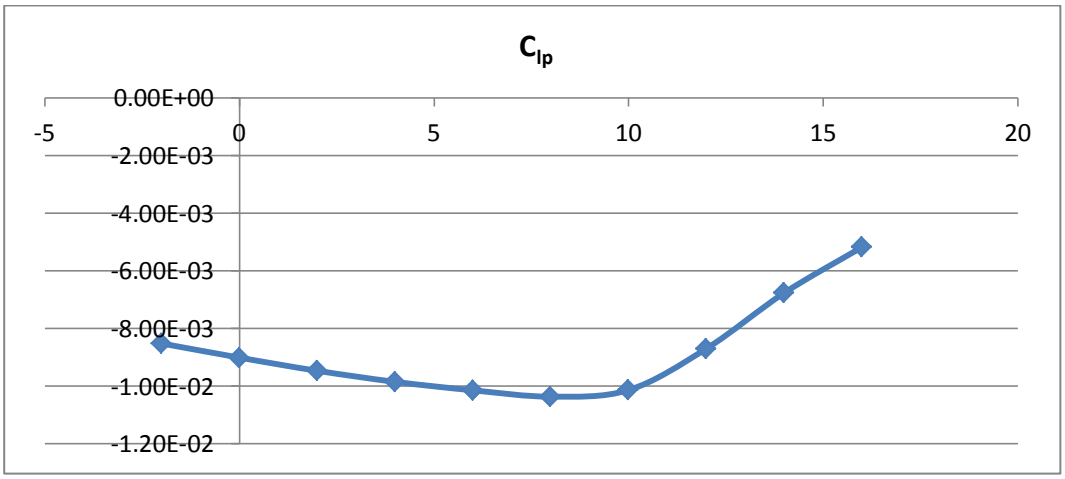

Figure 3-29: Rolling moment coefficient due to roll rate derivative (C_{l_p}).

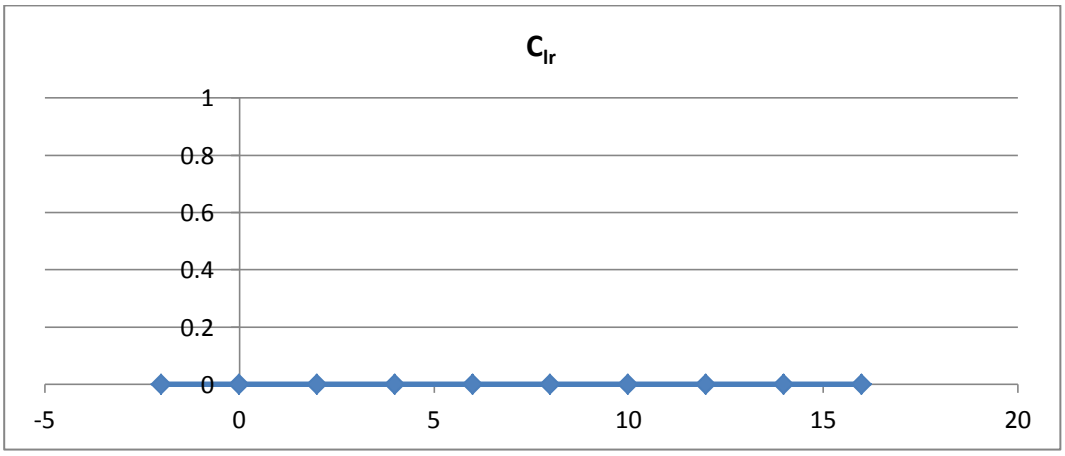

Figure 3-30: Rolling moment coefficient due to yaw rate derivative (C_{l_r}).

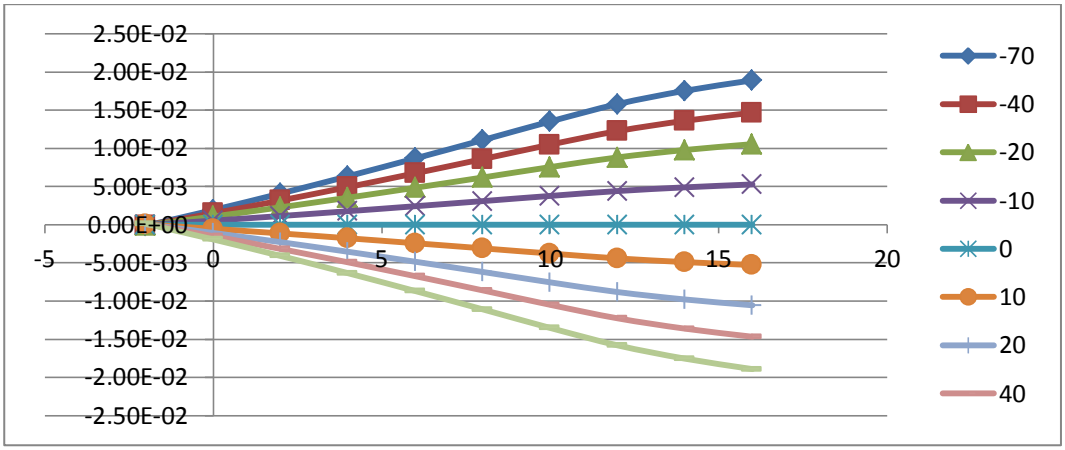

Figure 3-31: Yawing moment coefficient due to aileron deflection ($C_{y_{\delta a}}$).

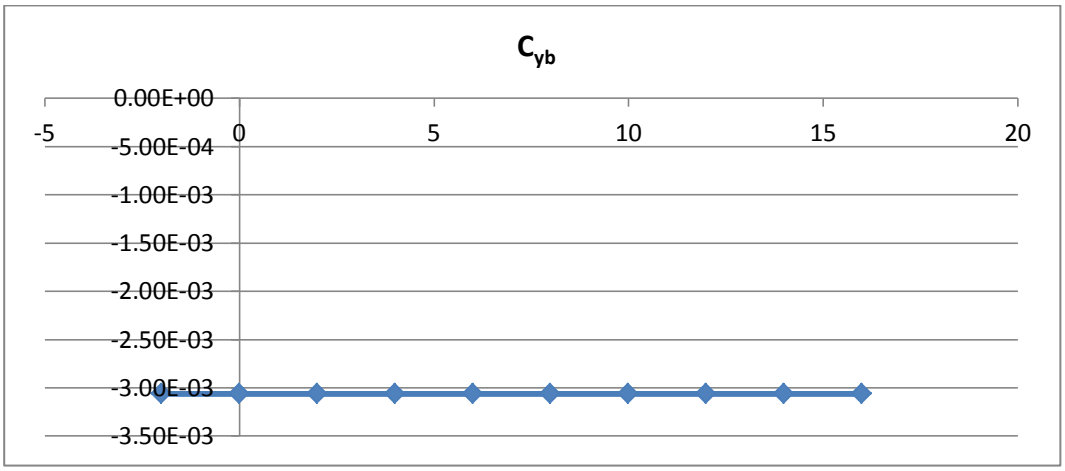

Figure 3-32: Yawing moment coefficient due to sideslip (C_{y_β}).

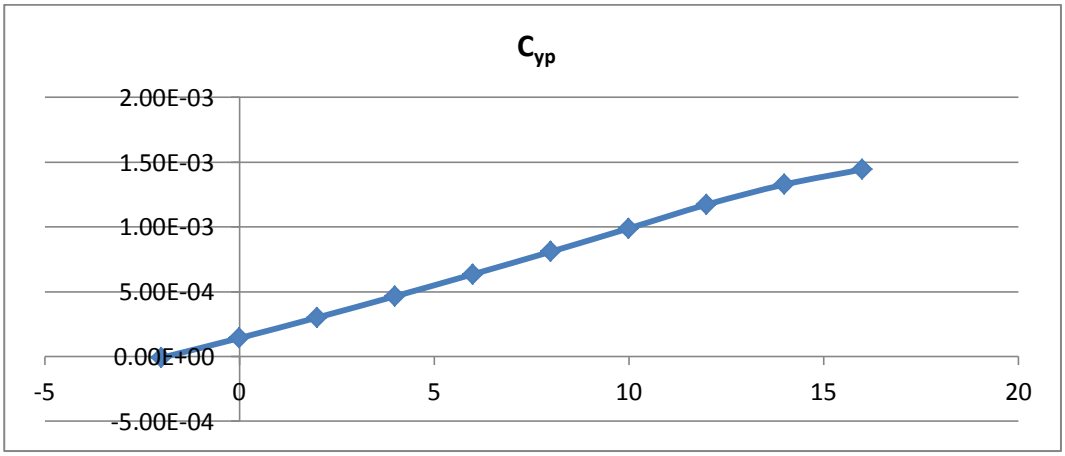

Figure 3-33: Yawing moment coefficient due to roll rate derivative (C_{y_p}).

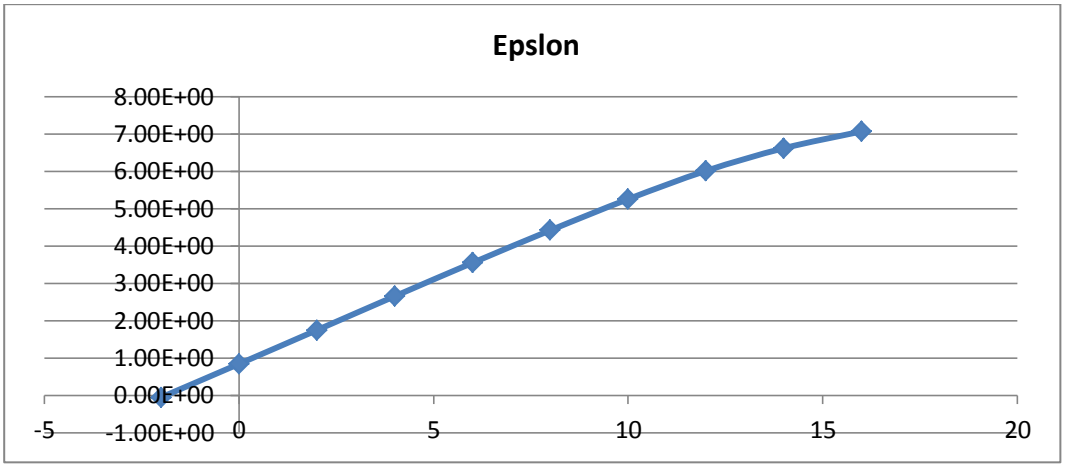

Figure 3-34: Horizontal tail downwash angle (ε).

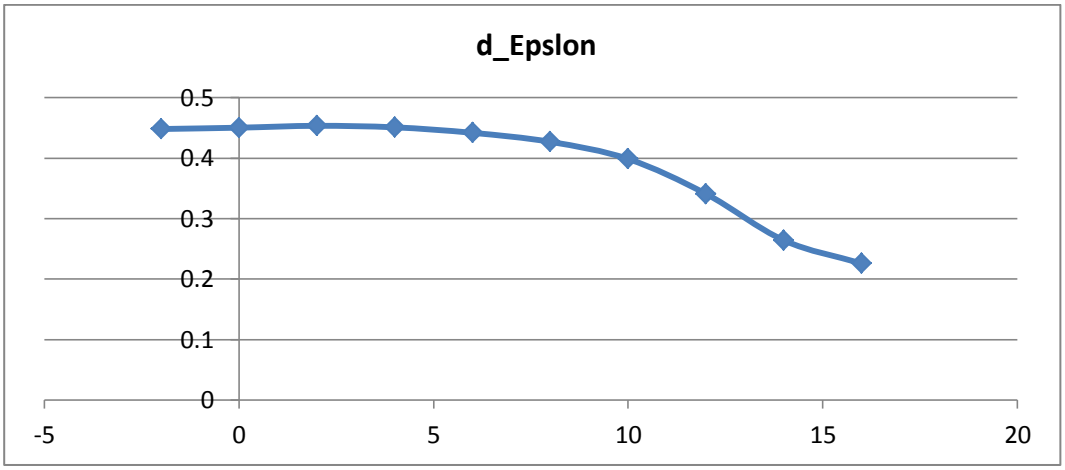

Figure 3-35: Derivative of downwash angle (δε/δα).

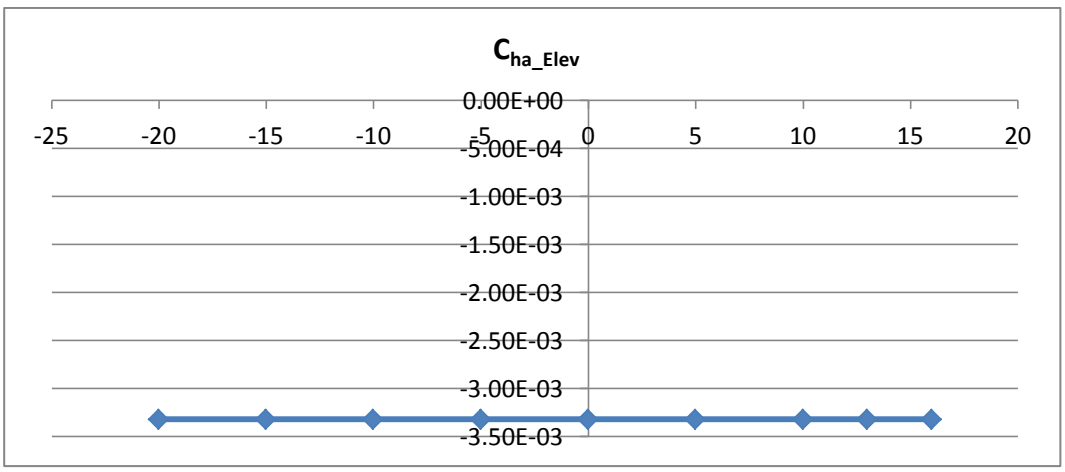

Figure 3-36: Elevator-surface hinge-moment derivative with respect to alpha (C_{h_α}).

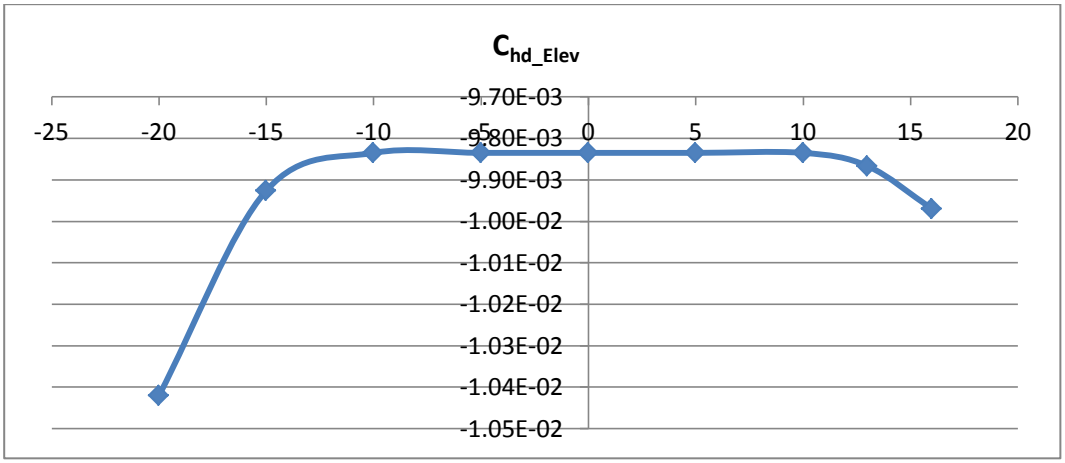

Figure 3-37: Elevator-surface hinge-moment derivative due to elevator deflection (C_{h_δ}).

3.5 Cost Analysis

For the costs analysis the following prices are for total production of 1000 aircrafts and costs are in US$:

Development support cost C_D	2098267.23
Flight test cost C_F	1709483.22
Manufacturing materials cost C_M	33849510.98

Single engine cost	10000	US$
Total Engine cost, C_eng	10000000	US$
Avionics cost per aircraft	3560.57	US$
Total avionics cost, C_avionics	3560570	US$

The total cost of a single aircraft is $51217.83.

The total cost of all aircrafts is $51217831.43.

CHAPTER 4

Detailed Design and Manufacturing

4.1 Introduction

The detailed design involves generating the detailed structural design and the aircraft systems design. The detailed design step was done simultaneously with the manufacturing of the aircraft to avoid any changes because of the availability of the material or accessories and ability of fabrication with the available tools, equipment and skills. Since 2009, we started the preparation of the building site, searching for the available material and spare parts in the local market and requesting tools, materials and the engine. This step started in January 2010 and took about 3000 working hour. Many drawings to be made for this aircraft by a drawing team are in progress.

4.2 Building material

Aluminium alloy 6063 T6 was used in the primary structures such as spars, rips and frames. This was initially provided - in 6 meters long profiles - by ALIPCO (Aluminium factory in Dammam First Industrial City). The list of the received profiles and their specifications is shown in Table 4-1. The total profiles weight that was used

in the aircraft building is 113.68 kg. Due to cutouts, just about 95% was used which is 108kg (238 lb). For material specifications see Appendix A.1

Profile no.	Alloy	TEMP	Weight gram/m	Length m	No. of pieces	shape	Dimensions mm	Total weight kg
67588	6063	T6	1525	6	2	C	150x2.5x50x2	18.3
67575	6063	T6	907	6	2	C	64x22x3	10.88
60016	6063	T6	159	6	20	L	30x30x1	19.08
60035	6063	T6	421	6	8	L	40x40x2	20.208
60010	6063	T6	173	6	10	L	25x25x1.3	10.38
60045	6063	T6	786	6	3	L	50x50x3	14.148
60001	6063	T6	71	6	4	L	15x15x0.9	1.7
64021	6063	T6	559	6	1	O	25x3	3.354
64024	6063	T6	475	6	1	O	30x2	2.85
64106	6063	T6	775	6	2	O	50x2	9.3
64010	6063	T6	93	6	1	O	12x1	0.558
67004	6063	T6	243	6	2	Z	13x15x2	2.916
The total weight of profiles were used (kg)								113.68

Table 4-1: The profiles were used in the construction of the aircraft.

Because Aluminium alloy 2024 sheets are not available locally, we chose alloy 1050 (temp H24) which has almost similar properties. See Appendix A.1 for material properties. Different thicknesses of sheets were used in construction such as 0.5 mm, 0.6 mm, 0.8 mm, 1mm, 1.5 mm, 2 mm and 3 mm. The used sheets in construction of the aircraft are listed in Table 4-2. The total sheets weight that was

used in the aircraft building is 119 kg. Due to cuts, just about 90% of sheets weight was used which is 107.1kg (236.12 lb). For material specifications see Appendix A.2.

Sheet thickness/ mm	Weight/ meter	Area of sheet/m	Total weight
0.5	1.36	27.4	33.18
0.6	1.632	24.6	45.04
0.8	2.176	6.3	13.71
1	2.72	2.5	6.8
1.5	4.08	2.7	11.02
2	5.44	1.1	5.98
3	8.16	0.4	3.264
The total weight of sheets were used (kg)			119

Table 4-2: The sheets were used in the construction of the aircraft.

Steel sheets and profiles were also used for undercarriage, flight control components and engine mounts.

4.3 Building tools and equipment

The building site was prepared by providing the following main tools and equipment (see Figure 4-1):

1. Sheet cutter (shear cut)
2. Sheet bender

3. Pipe bender
4. Hydraulic press
5. Air compressor
6. Profiles cuter

Figure 4-1: Shear cuter (left) and sheet bender (right).

In addition to that, some hand tools were used such as electrical drills, pneumatic drills, pneumatic riveter, steel welding machine, grinders and hole saw. Some other hand tools and keys such as shear plier, vice grip, g clamps, electrical pliers and wrenches. Also, Personal protection equipment such as overalls, dust masks, safety goggles and safety shoes were used during building process.

4.4 Aircraft Components and Systems Details

In this section, I will give some details about each part or system in the aircraft. The aircraft was built in two major parts to be transportable:

1. Fuselage, tail, engine and undercarriage in one piece.
2. Wing which is a separate piece.

The assembly of these major parts should not take more than half an hour and the aircraft will be ready to fly.

4.4.1 Fuselage details

The fuselage structure is as important as the wing, and many designers have come short because they neglected the fuselage. The fuselage structure contains so many details because all other aircraft components are jointed to it such as engine, wing, tail and undercarriage. Then, the fuselage was the first part to be constructed and to assemble all other parts to it. The fuselage is usually more difficult to analyze than the wing. It can be divided into two main sections:

- Front fuselage which is from the firewall to the tail boom which should the strongest part in the aircraft because it has to carry the hard landing loads, engine thrust and vibration, and the aerodynamic loads caused by the wing and tail.
- Rear fuselage which is mainly the tail boom which carry the aerodynamic loads and the weight of the tail.

In the primary structure, L shape profiles were used as shown in Figure 4.2. For the front fuselage, profile 60045 (50x50x3mm) was used to carry these large loads

and to minimizing the damage to the crew in case of crash. The front fuselage is formed of four frames as numbered in Figure 4.2.

Figure 4-2: The primary structure of the front fuselage.

The joinning points with the other components were supported well. As seen in Figure 4-3, points a,b,c and d are wing-fuselage joints and loads are transferred to fram 3 and fram 4. Also, main landing gears are mounted to frames 3 and 4 throgh points e, f, g and h and this explains why frames 3 and 4 are suported well. The rear fuselage is attached to the front fuselage at frame 4 as shown in Figure 4-4.

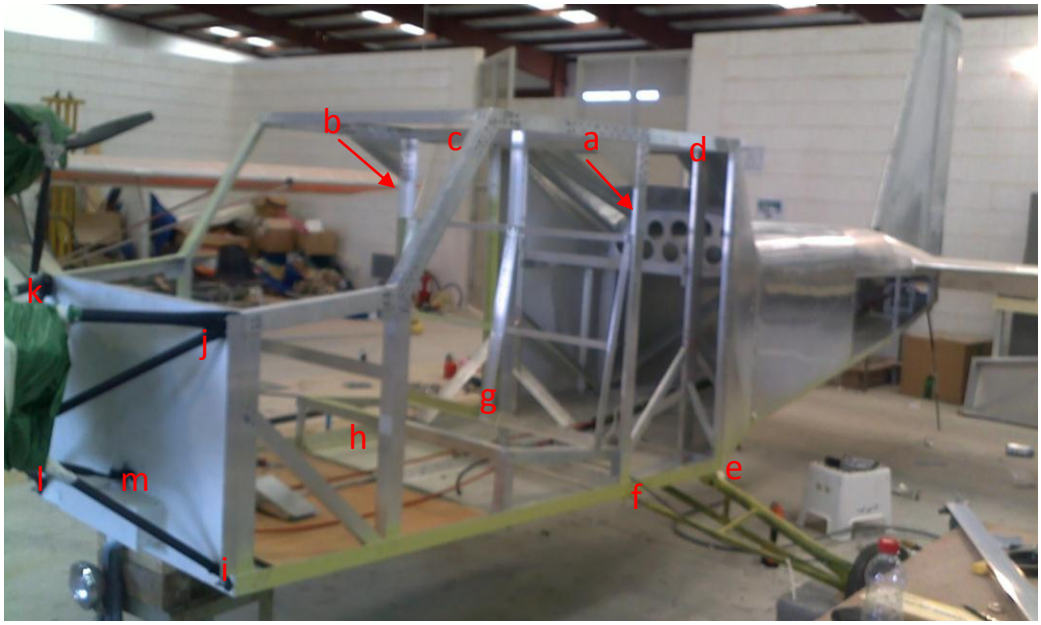

Figure 4-3: The mounting points to the front fuselage.

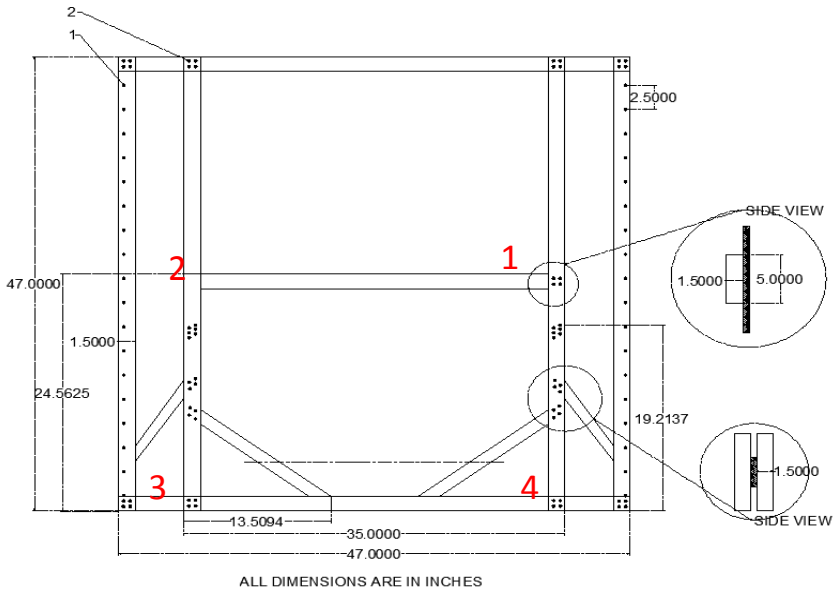

Figure 4-4: Frame 4 details.

Frame 1 is also importnt because it carrys the engine at points i, j, k and l and nose landing gear loads point m. Figure 4-5 gives more details about frame which is the fire wall of the engine.

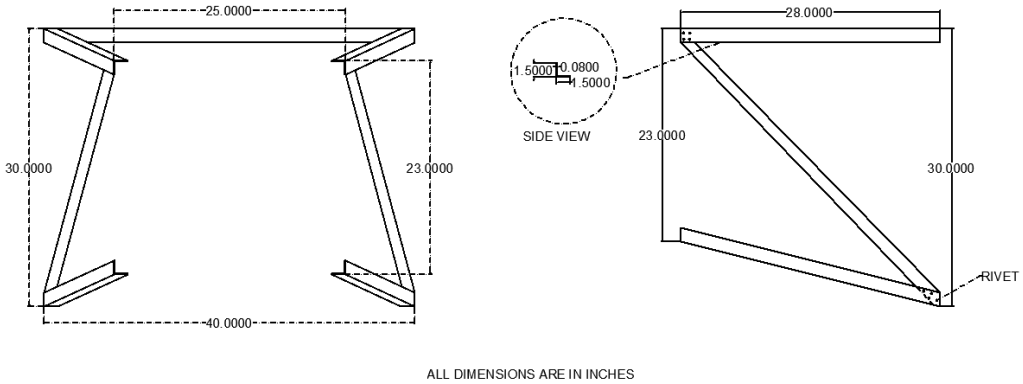

Figure 4-5: Frame 1 supports.

For the rear fuselage, profile 60035 (40x40x2mm) was used to carry the aerodynamic loads of the vertical and horizontal tails and there weights. As shown in Figure 4-6, the rear fuselage is formed of four frames (5, 6, 7 and 8) with larger spacing in between them and connected to each other by four longerons of the same profile. These longerons connect the rear fuselage to the front fuselage at frame 4 at 4 points as shown in Figure 4-4. The two upper longerons are attached perpendicular to frame 4 at points 1 and 2 and the lower two are attached to frame 4 with angle of 10°.

Figure 4-6: Rear fuselage.

To avoid any tail hit damage, a stringer made of hardened steel that works as a spring is fitted to the bottom side of frame 8. See Figure 4-7.

Figure 4-7: Tail hit stringer.

The fuselage primary structure is coated with 0.6 mm aluminium sheets from the sides and the top. 1mm sheets were used to cover the bottom side of the front fuselage and 0.8 mm sheets to cover the bottom side of rear fuselage.

Two large doors with large plexiglass windows are hinged to frame 2 with secure locking mechanism (see Figure 4-8). Air sealing tape is put to reduce the noise caused by air flow.

Figure 4-8: The aircraft doors.

4.4.2 Wing details

The aircraft wing is the main lift device which should carry all loads during maneuvers. The structure of the wing is critical and has a lot of details due to the limitation of the wing thickness (t/c=12%). The wing box structure is formed mainly of the following components (see Figure 4-9):

- The main spar which is located at the thickest point of the wing at 0.25 of the chord length.
- The secondary (rear) spar carries the flaps and ailerons hinges.
- Two stringers in the middle supporting the upper and lower skins.
- 18 flanged ribs connect the above structural components together.

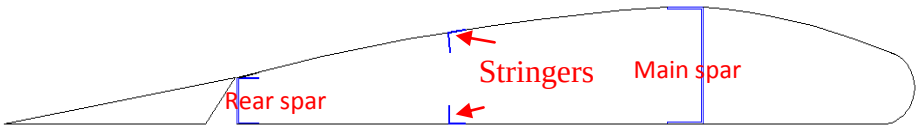

Figure 4-9: Wing cross section.

For the main spar profile No. 67588 (150x2.5x50x2) for properties of the cross section see figure 4-10. Profile No. 67575 was used for the rear spar which flabs and ailerons are hinged to it. Profile No. 60016 was used for both stringers and as flanges of ribs. Figure 4-11 gives good illustration of how they are assembled.

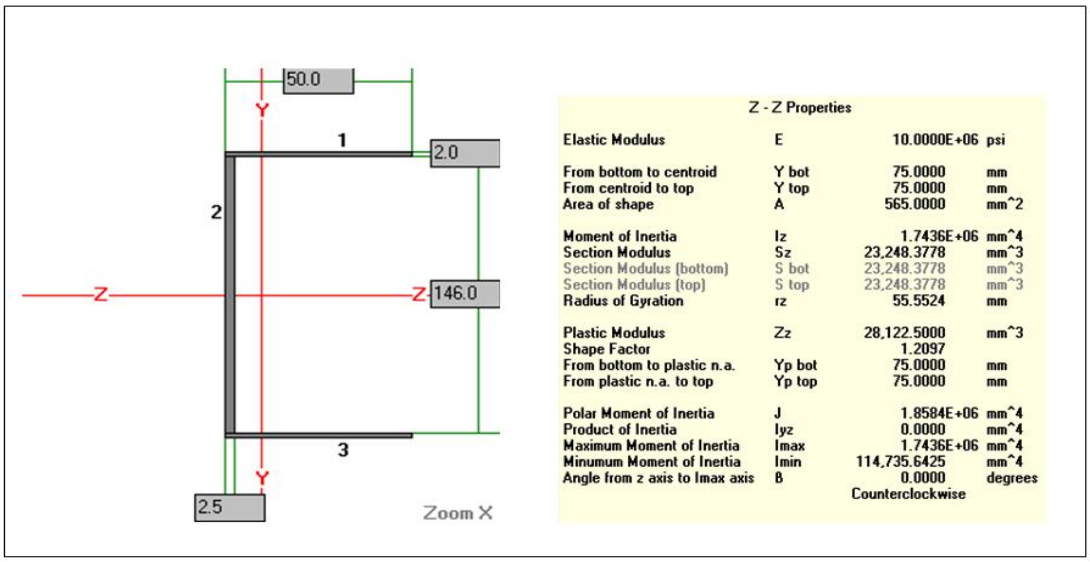

Figure 4-10: Main spar cross section.

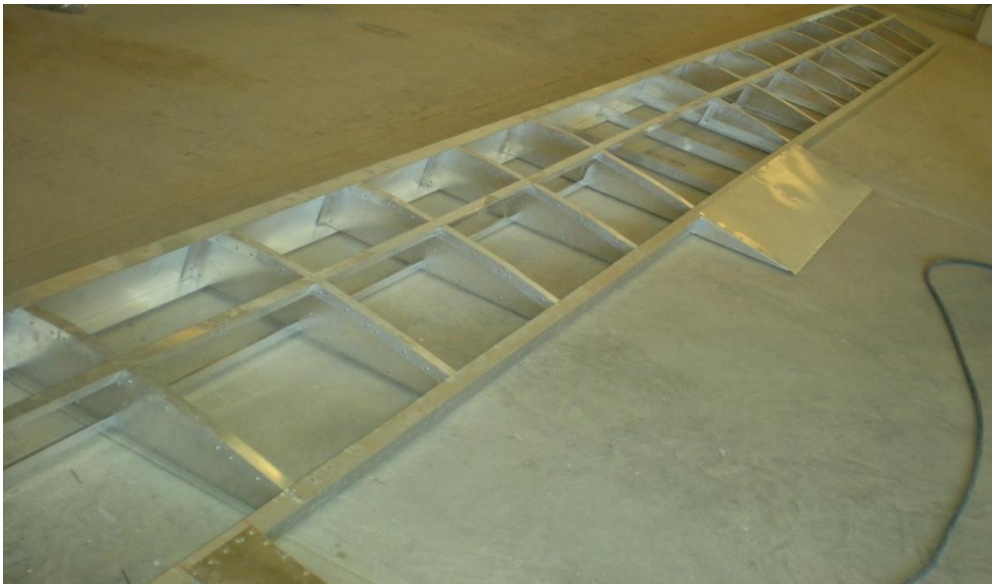

Figure 4-11: The wing box structure.

After assembling the wing box, lightening holes were made in the main spar and ribs as shown in Figure 4-12. The purpose of these holes is to reduce the weight especialy for the front spar web which is 2.5mm thick.

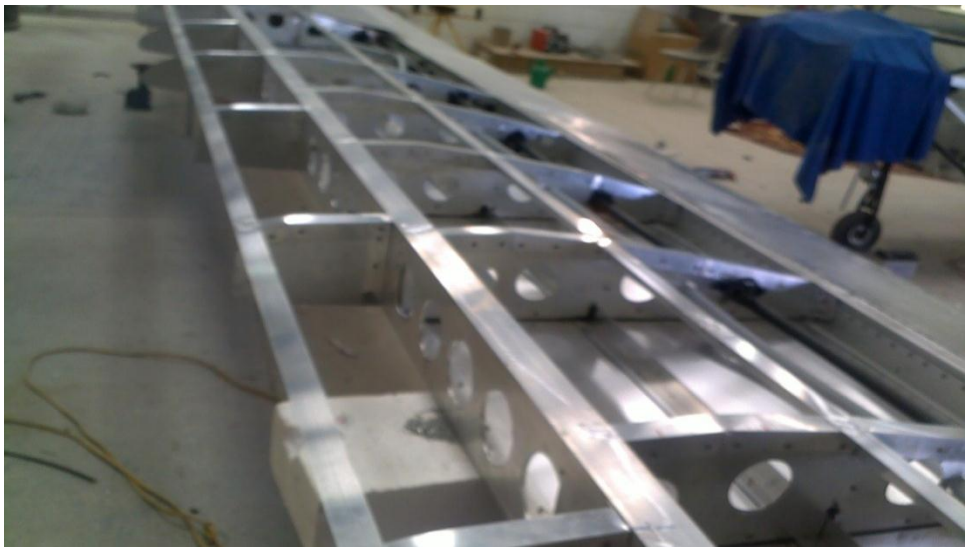

Figure 4-12: The lightening holes.

After that, the formers of the leading edge and the leading edge were installed with taking into cosideration the rotating leading edges cylinders (see Figure 4-13). Then, the wing was coated with aluminium sheets 0.5 mm thick for the lower side but for the upper side 0.8 mm thick sheets were used to be prepaired for ataching the solar cells on it.

Figure 4-13: The wing after coating the trailing edge and the lower surface.

Two flaps 215x33 cm each and two ailerons 165x33 cm each are hinged directly to the rear spar. The flabs and ailerons are formed of flanged formers connected together by two stringers of profile No. 60001 as shown in Figure 4-14. From the figure, you can see two formers facing each other and riveted to a thick rectangular sheet which is prepared for holding the control horn. Using 0.8 mm sheets, the flaps and ailerons were coated and then fitted in slots. Horner wing tip design was used as mentioned in the conceptual design phase. The tip was fabricated of 0.6 mm aluminium sheet (see Figure 4-15).

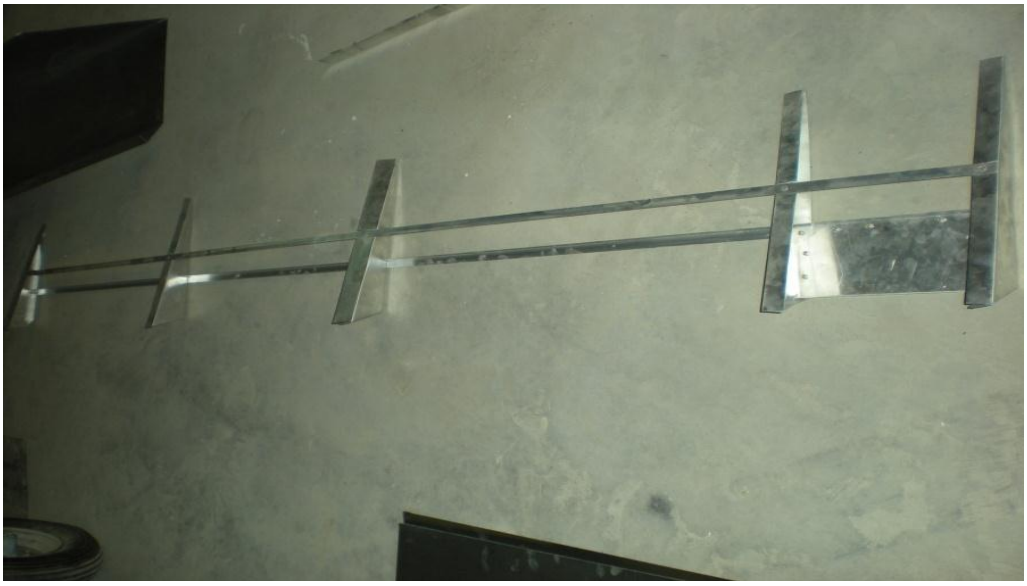

Figure 4-14: The internal structure of the flaps and ailerons.

Figure 4-15: The Horner wing tip design.

The wing is mounted to the fuselage by 4 bolts 10x30 mm drilled through the main and rear spar. In addition to that, two struts of profile No. 64106 are supporting the wing to the main landing gear (see figure 4-16). The struts upper end brackets are bolted to the main spar using two bolts 8x30 mm at 240 cm from the fuselage where the lower bracket is welded to main landing gear.

Figure 4-16: The wing after installation to fuselage.

4.4.3 Empennage

The empennage or tail structures are designed to carry the full loads of the controls during flight. The internal structure of the horizontal and vertical tails is formed of profile No. 60016. Figures 4-17 and 4-18 give an idea about the tail structure.

Figure 4-17: Horizontal tail structure.

Figure 4-18: Vertical tail structure.

The horizontal and vertical tails internal structures were covered with 0.6 mm aluminum sheets. The tail is mounted the rear fuselage at four points as shown in Figure 4-19. At point 1, a plate 3 mm was riveted frame 8 of the fuselage, horizontal and vertical tails. At point 2, the vertical tail is mounted to frame 7 and to the horizontal tail at point 3. The horizontal tail is mounted also to the two upper longerons of the rear fuselage at point 4 with two 10x80 mm bolts.

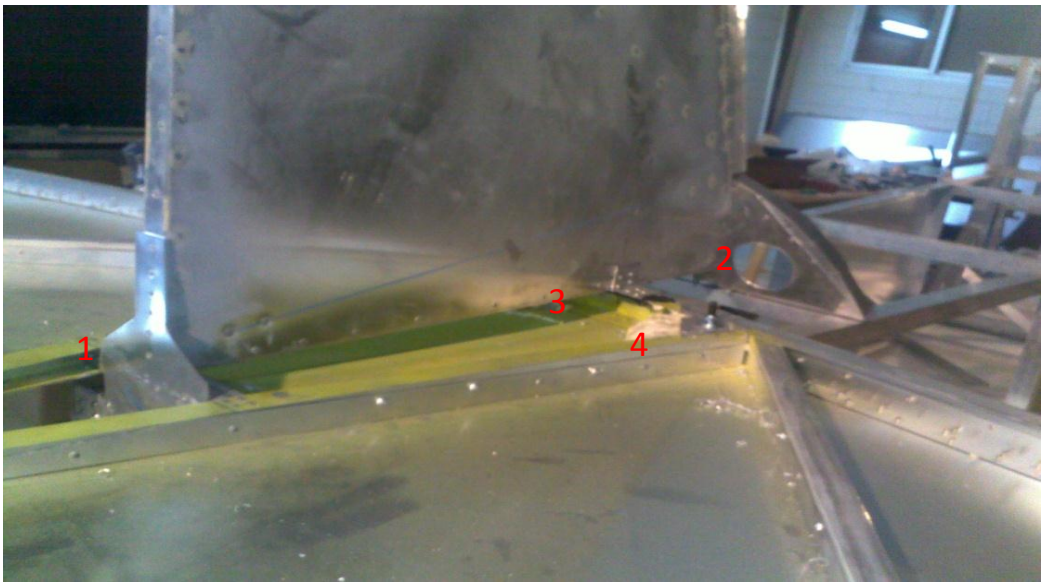

Figure 4-19: The tail mounts.

The rudder was formed of 0.8 mm sheet which was folded and then riveted to pipe of profile No. 64024. The pipe allows rudder to rotate and gives the round leading edge for rudder. The elevator is formed of 0.8 mm sheet that was folded on three formers at root and tips and then hinged to horizontal tail as shown below.

Figure 4-20: The tail after fitting on fuselage.

4.4.4 Undercarriage

The undercarriage must be robust enough to handle all types of landings, and in particular, hard landings of up to 4 g's. Tricycle configuration is used, two mains wheels and a nose wheel. For the main strut, a 38x4 mm steel pipe was used as one piece connecting the main wheels and formed using hydraulic pipe bender. Two pipes 30x2 mm were welded to the main strut and supported with a small member in the middle as shown in Figure 4-21. Two brakes sets were fixed at end of the main strut using 4 bolts 12x30 mm each (see Figure 4-22).

The main strut is bolted to two brackets at the lower corners of frame 4 of the fuselage and the secondary struts are connected to two brackets at the lower corners of frame 3. The ends of main strut are linked together with a 5mm flexible wire that allow for limited flexibility. Two wheels 16 in each are used as mains.

Figure 4-21: The main landing gears.

Figure 4-22: The brake components.

The nose leg is fabricated from 30x2mm steel pipes as shown in Figure 4-23. Two brackets are used to fix the nose leg to frame 1 of fuselage and allow for steering. Two steering horns were drilled and welded in the main leg in between the two brackets.

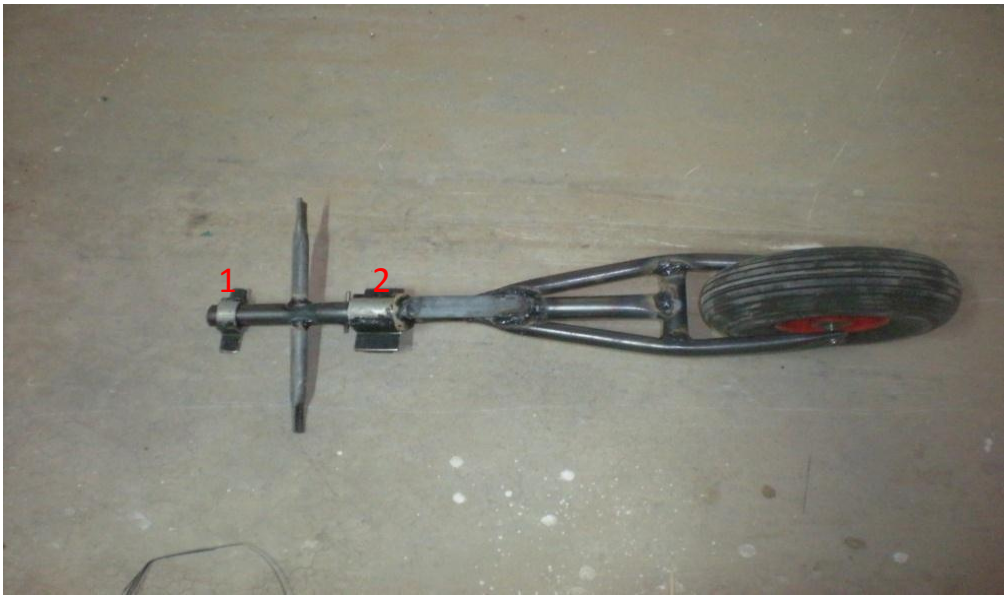

Figure 4-23: The nose landing gear.

4.4.5 Power plant

The engine was supplied in pieces with the assembly and installation manuals as shown in Figure 4-24. The assemblly process took about 50 working hours. The engine is equiped with a starter that makes the starting easy and quick. The engine mount was fabricated of 25x2mm steel pipes which are bolted together and then welded to avoid any welding cracks due engine vibration (see Figure 4-25). The engine is bolted to the mount with four bolts 10x70 mm each and then the mount is bolted to frame 1 of fuselage with four bolts 10x30 mm each.

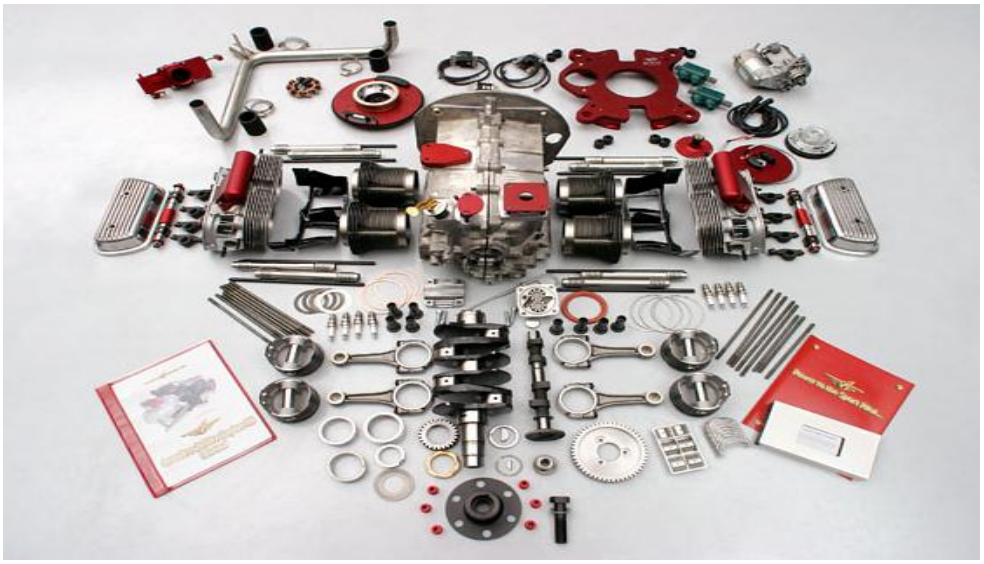

Figure 4-24: The engine supplied parts.

Figure 4-25: The engine mount.

The engine wiring diagrams that were implemented are shown in Figure 4-26 where some of the components and wires were found in the local market. The firewall layout is shown in Figure 4-27 which located at frame 1 of the fuselage. The mount depth gives good space for maintenance and cooling.

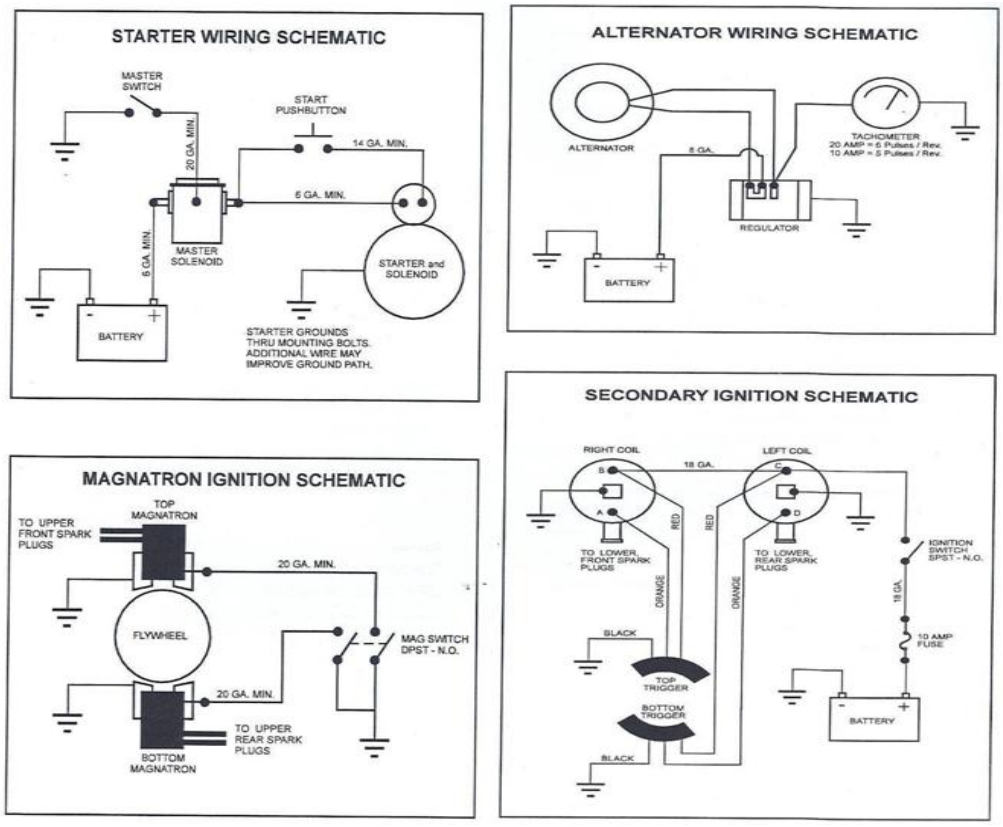

Figure 4-26: The engine wiring diagrams [46].

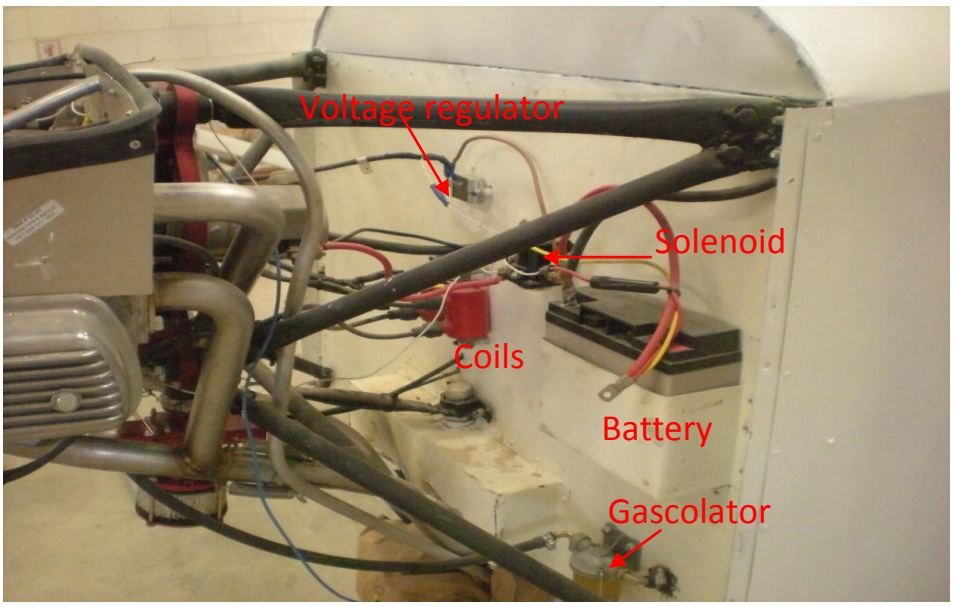

Figure 4-27: The firewall layout.

The engine was supplied also with baffle fence system to cool the engine cylinders.

See Figure 4-28.

Figure 4-28: The baffle fence system.

Engine cowling was formed of 0.8 mm thick sheets and profile No. 60001 stringers. In the design of the engine cowling, air cooling, ventilation and access for maintenance was taking into consideration. See Figure 4-29. The propeller and spinner are bolted to the engine shaft with six bolts 8x100 mm each.

Figure 4-29: The engine cowling design.

The engine control panel contains the following (see Figure 4-28):

1. Engine starting button.
2. 3 toggle switches for engine circuits.
3. Engine RPM indicator.
4. Engine oil pressure gage.
5. Engine temperature gage.
6. Fuel level gage.
7. Battery voltage gage.
8. Throttle lever (in the middle).
9. Fuel burning balancer (right to throttle lever).

Figure 4-30: The engine control and instrumentation panel.

4.4.6 Fuel system

The gravity feed fuel system is used in this project which is the safest and most reliable system (see Figure 4-31). The tank was made of 0.8 mm aluminum sheets that were welded together (see Figure 4-32). The capacity of the tank is 90 lb and is equipped with level stack to send the level to the fuel level gage.

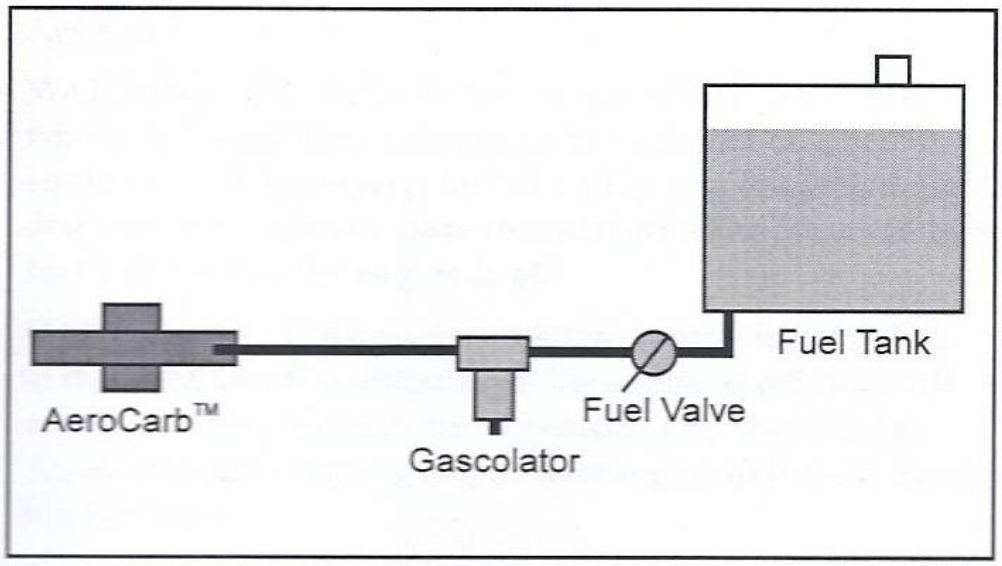

Figure 4-31: The fuel system.

Figure 4-32: The fuel tank.

4.4.7 Flight control System

For the flight control linkages, the solid push-pull linkage pattern is used. The flight control inputs by the pilot are through the following (see Figure 4-33):

- Four foot pedals two for each crew for steering and rudder control.
- Two control sticks to control elevator and ailerons.

- Flap lever to move flaps.
- Brake lever to stop the aircraft during landing and engine test.

Foot pedals are linked to the nose wheel steering horns through solid linkages and connected to the rudder using two control cables (see Figure 4-34 Brake lever).

Figure 4-33: The flight control inputs.

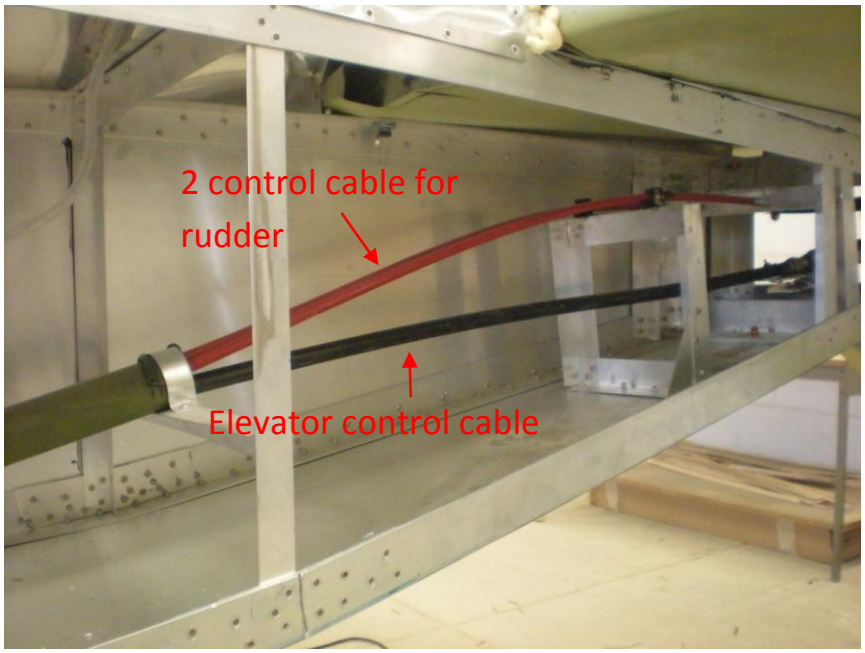

Figure 4-34: The control cables through the tail boom.

The flap lever is connected to a spring loaded torque tube behind the seats that bolted to fuselage structure. The spring keeps the flaps up if not used. The torque tube is linked to another torque tube in the wing with a control rod. See Figures 4-35 and 4-36. For ailerons control, the control stick is linked to torque tube passes underneath the seats and then to wing with a control rod as shown below. Two push-pull control rods inserted through the wing ribs to move ailerons (see Figure 4-37).

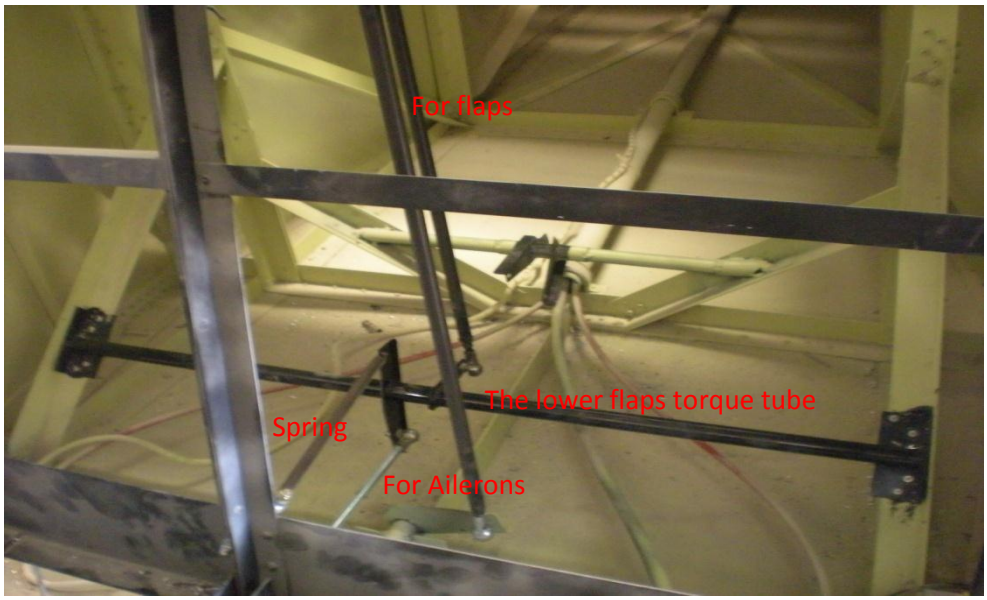

Figure 4-35: The control linkages for flaps and ailerons.

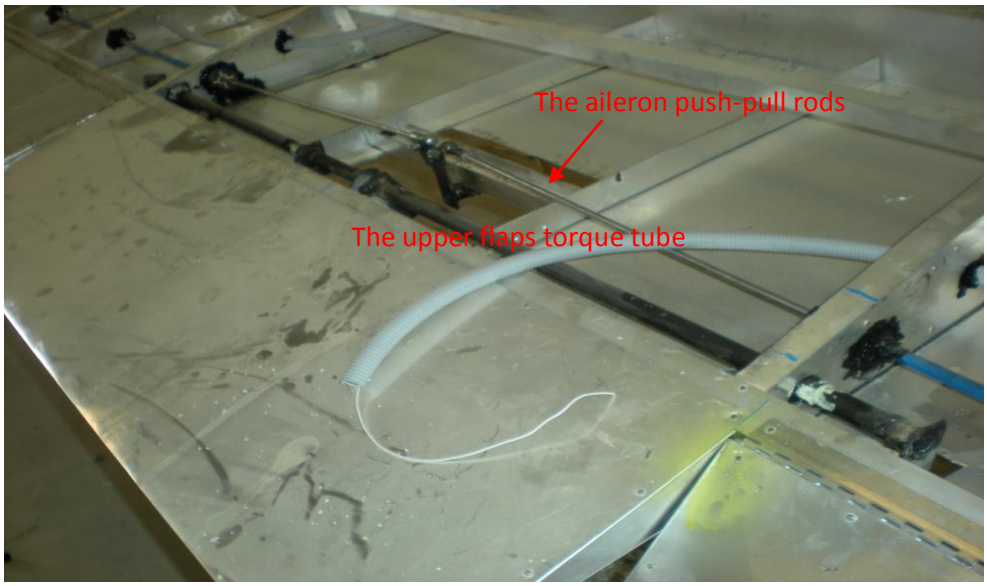

Figure 4-36: The control linkages for flaps and ailerons through wing.

Figure 4-37: The control linkages and horns for flaps (right) and ailerons (left).

4.4.8 Aircraft instrumentation

The aircraft is equipped with 2 sets of flight data indicators each set contains the following gauges (see Figure 4-38):

- Airspeed indicator
- Heading indicator
- Altimeter

Figure 4-38: The instrument's panel.

The total pressure is needed for the airspeed indicator. A pitot tube was fitted in the leading to send the total pressure the airspeed indicators using small diameter tube (see Figure 4-39).

Figure 4-39: The pitot tube.

4.4.9 Aircraft lighting

The aircraft is equipped with lights such as taxi light which is fitted on the nose leg and small lights at the wing tips and vertical tail tip (see Figure 4-40).

Figure 4-40: The aircraft lights.

4.5 Final Weights

The weight of the aircraft component was measured using hanging scales (see Figure 4-41). The final empty weight (We) is about 372 kg or 820 lb. The total takeoff weight (W_{TO}) is 1320lb then the useful weight W_u= 1320-820= 500 lb. If the crew is 400lb (2x200lb), we have 100 lb for fuel and baggage.

Figure 4-41: The way of measuring weight.

CHAPTER 5

Experimental Testing

5.1 Introduction

For all of the previous researches, the used airfoils were symmetrical. In this case, the used airfoil is nonsymmetrical which is NACA 2412. So, we need to conduct a confidence check to determine the aerodynamic characteristics such as lift and drag characteristics and the delay of the stall angle. Tests were conducted in the Aerospace Engineering Department laboratories at KFUPM in a low-speed, low-turbulence, open return- type wind tunnel where the airspeed can be varied from 1 to 40 m/s with a turbulence intensity of less than 1%. The tunnel is powered by a 5.8-kW motor that drives a centrifugal fan. The test section has a cross section of 0.8 x 0.6 m and is 2.6 m long. It is designed with large plexiglass windows on the top and sides to provide adequate illumination and viewing for visualization studies.

5.2 Testing Model

A model of NACA 2412 aerofoil was tested in the wind tunnel with a rotating leading edge cylinder. The wind tunnel was equipped with a balance which will measure the lift, drag and pitching moment of the airfoil. The model has 0.25 m chord and 0.45 m span with an aspect ratio of 1.8 which is scaled (1:5) to the aircraft wing. A plain flap with a chord of 5 cm was placed at the trailing edge of the airfoil.

Because a large gap between the rotating cylinder and the remaining stationary part of the wing would decrease the effectiveness of the rotating cylinder, so the clearance was kept within 2 mm. The gap in-between the cylinder and the cylinder cavity walls was kept 2 mm because this was found by Chaplin in his study for the best lift characteristics[41]. A schematic diagram is shown in Figure 5-1.

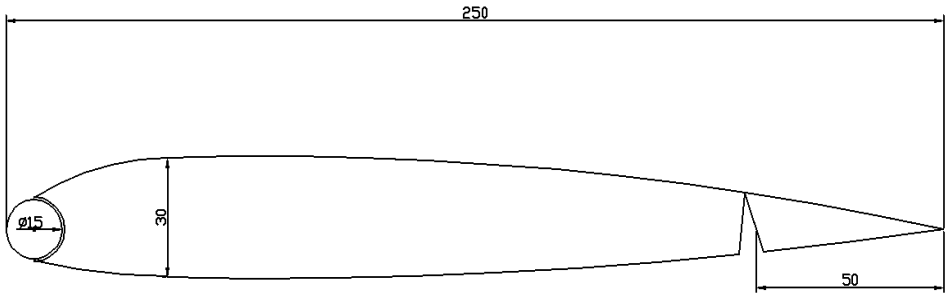

Figure 5-1: A schematic diagram of the model (in millimeters).

A 15 mm diameter hollow aluminium cylinder about 1.5 mm thick was mounted between two high-speed ball bearings and driven by a variable high speed electric motor mounted on the side of the model and connected to the cylinder by a 3 mm shaft. The maximum rotation speed of the motor was 22,000 rpm, which was measured using an optical-digital tachometer. The motor was connected to a constant 12V transformer with a variable speed selector (see Figure 5-2).

The model is scaled to the aircraft wing (1:5) and made from wood and is painted black to minimize light reflections. Measurements were conducted at a freestream velocity of 5 m/s. The angle of attack and flap deflection angles were varied from 0° to 25° and from 0° to 40°, respectively. Different rotation speeds (0–

22,000 rpm), corresponding to U_c / U = 0–3, were used to rotate the leading-edge cylinder directly. The Reynolds number was 8.56×10^4 based on the model chord.

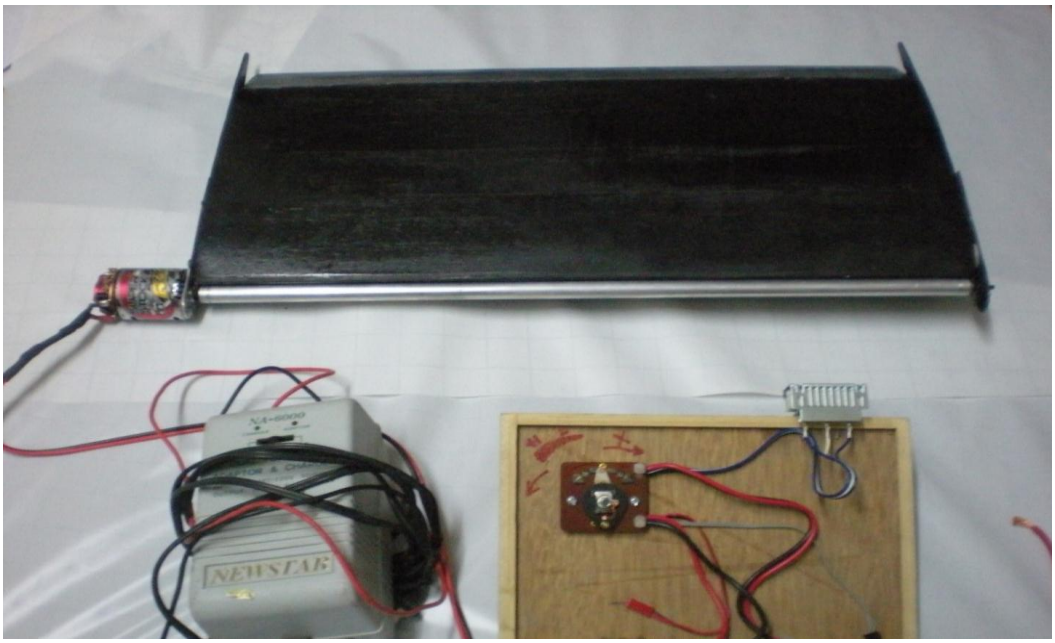

Figure 5-2: Photograph of the testing model, variable speed selector and the 220-110V to 12V transformer.

5.3 Methods of Measurements

The wind tunnel testing was complex due to the large amount of measurements needed for a single set of results. The wind speed was measured using a pitot-static tube positioned upstream of the airfoil at the beginning of the test section. This measures the difference between the total and static pressure to get the dynamic pressure. Therefore, once the dynamic pressure was known the wind velocity could be calculated from the following equation: $q = {}^1/_2 \, \rho \, U^2$.

The angle of attack can be selected by entering the required angle of attack in the balance software which sends a signal to the balance servos that are fitted underneath the wind tunnel testing section. The balance is connected to the model adaptor by push-pull rod and by the vertical movement of the rod we get a wide range of angle of attack. See Figure 5-3.

Figure 5-3: The testing model in the wind tunnel.

The ratio of cylinder velocity to the wind freestream velocity (U_c/U) can be calculated by finding the angular velocity (RPM) which was measured using an opto-tachometer and the wind free stream velocity. Some preparations to be made before testing to predetermine a wind speed and variable cylinder speeds. First, the motor was tested to find its effective range of the angular velocity of the cylinder. The range was found to be between ω_c=120 Hz and 366.67 Hz (Rev/s) (5200-22000 RPM). Therefore, the minimum angular velocity of the cylinder to avoid vibration problems was 120 Hz (5200 RPM).

$$U_c = 2\pi R \times \omega_c$$

Where R is the cylinder outer radius and equals (0.0075m)

$$U_c = \frac{2\pi(0.0075) \times RPM}{60} = 0.000785 \times \text{RPM}$$

Table 5-1 gives the corresponding cylinder surface velocity to rev/min. if we choose the wind free stream velocity to be fixed at 5 m/s, $U_c/U \approx 1$ at 6400 RPM (ω_c=106 Rev/s), $U_c/U \approx 2$ at 12800 RPM (ω_c= 213 Rev/s) and $U_c/U \approx 3$ at 19100 RPM (ω_c=318 Rev/s) . For (U_c/U) equal to 1 the wind speed would be approximately 5 m/s. The wind speed was chosen to remain constant for all sets of results at 5 m/s, this corresponded to a Reynolds number (based upon the chord length) of 8.56×10^4.

RPM	U
5000	3.925
6000	4.71
6400	5.024
7000	5.495
8000	6.28
9000	7.065
10000	7.85
11000	8.635
12000	9.42
12800	10.048
13000	10.205
14000	10.99
15000	11.775
16000	12.56
17000	13.345
18000	14.13
19000	14.915
19100	14.9935
20000	15.7

Table 5-1: The corresponding cylinder surface velocity to RPM.

The lift and drag measurements were taken from the balance software at each angle of attack and produced in form of coefficients. The angle of attack was varied between zero and 25 degrees in increment of 5 degrees from 0 to 10 and increment of 2 degrees above 10 degrees. At each angle of attack the lift and drag coefficients were measured and entered in a spread sheet to produce the required graphs.

5.4 Wind Tunnel Investigations

The test can be divided into two parts:

1. Clean configuration (without using flaps).
2. Using flaps.

5.4.1 Aerodynamic characteristics without using flaps

1. The lift characteristics

The graph in Figure 5-4 shows the lift coefficient against angle of attack of testing model (clean configuration) at $U_c/U=0$ when the cylinder is not spinning. The graph shows that the stall angle was around 14 degrees angle of attack and the maximum lift coefficient is 1.152.

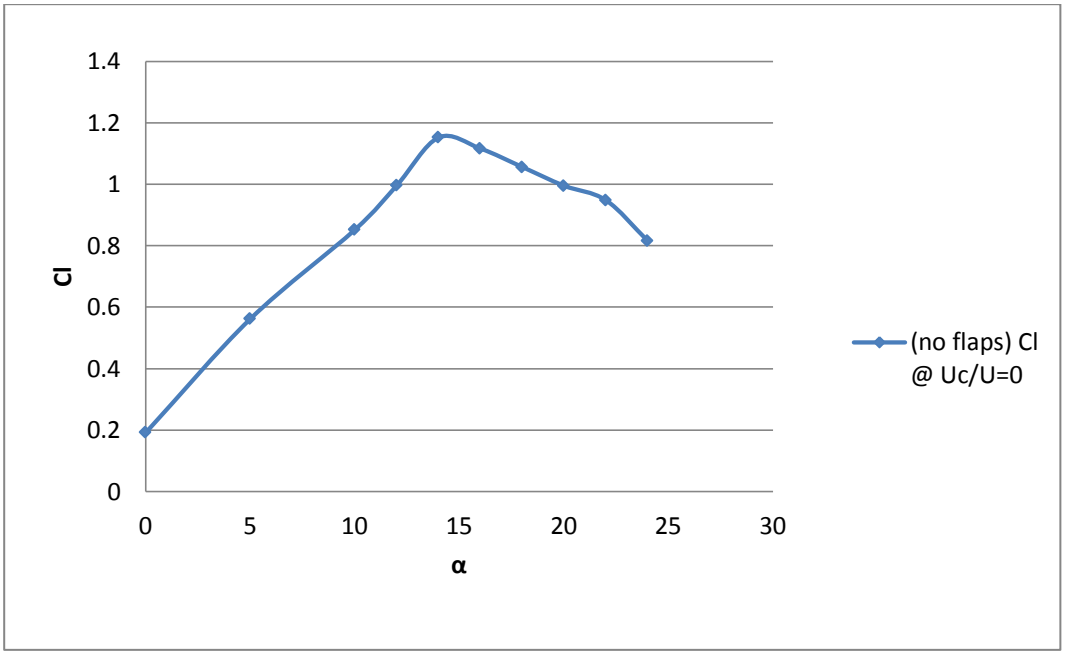

Figure 5-4: C_L curve at $U_c/U=0$.

The graph in Figure 5-5 shows the lift coefficient against angle of attack for the testing model at U_c/U= 0, 1, 2 and 3. The graph shows that the lift coefficient increases as the rotation speed increases for the same angle of attack. For the cylinder rotating at U_c / U = 3, the maximum lift coefficient is about 2.11 at α = 22. This produces an increase in the lift coefficient of about 83%. Also, the stall angle was delayed by 8 degrees. The above results show that the effects of MSBC are significant and promising. The increase in lift coefficient and stall angle of attack would improve the maneuverability and performance of the airplane especially for STOL aircraft.

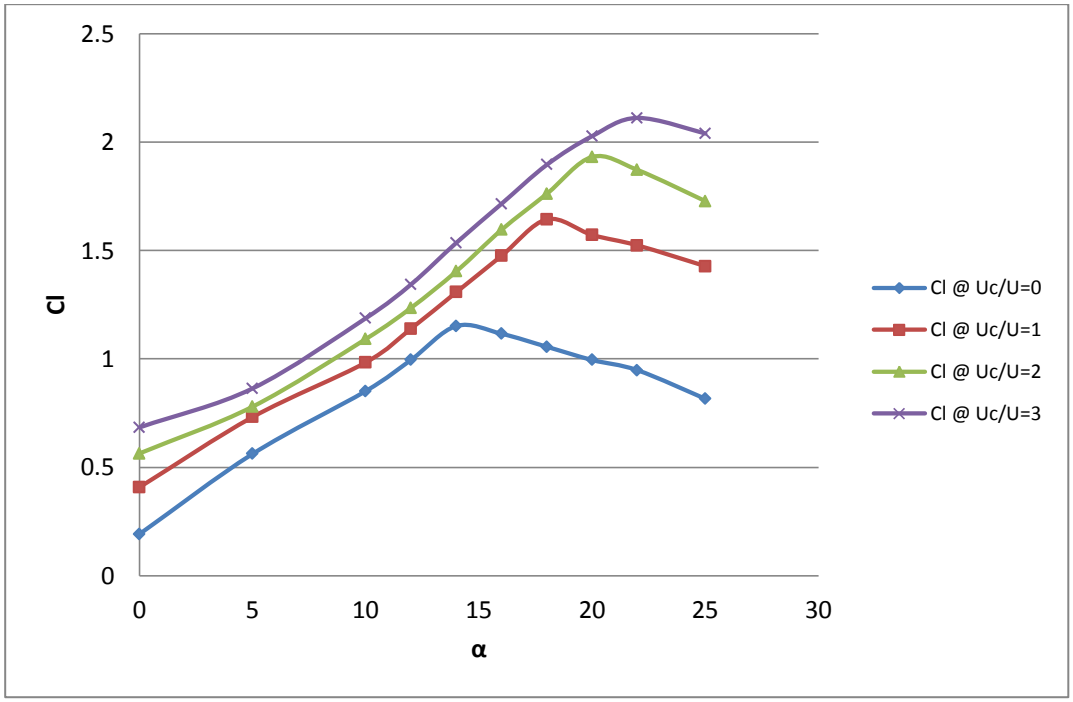

Figure 5-5: C_L curves at U_c/U=0-3.

2. Drag characteristics

The graph in figure 5-6 shows the drag coefficient against angle of attack for the testing model at U_c/U= 0, 1, 2 and 3. The graph shows almost linear rise in the drag coefficient as the rotation speed increases at the same angle of attack because of the pressure drag and skin friction drag in addition to the induced drag (caused by lift) which is proportional to the sine component of the lift force. The drag coefficient for the airfoil at a = 0 deg for different U_c /U is around 0.08.

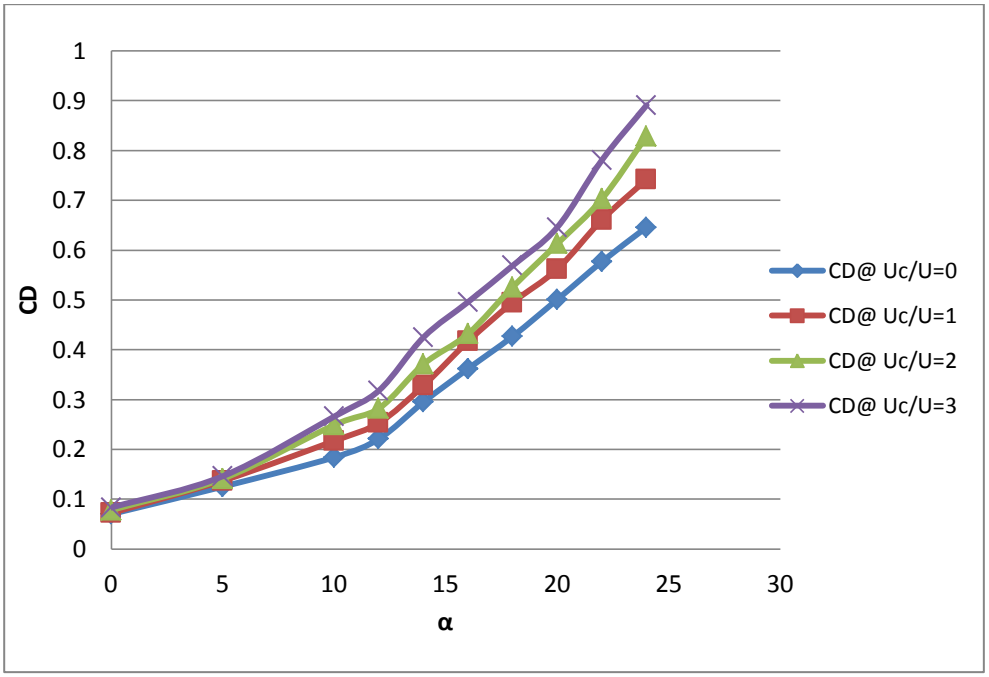

Figure 5-6: C_D curves at U_c/U=0-3

3. Lift/drag ratio characteristics

The aerodynamic efficiency of the wing can be measured using the lift-to-drag ratio. L/D at $\alpha = 0$ is 2.743 for U_c/U =0 and 8.241 for U_c/U =3 that shows the improvement in L/D more than 3 times due to increasing the cylinder rotation from $U_c/U = 0$ to 3 at zero angle of attack. The graph in Figure 5-7 shows that the maximum L/D for the airfoil occurs at zero angle of attack. Therefore, the effective range of the leading-edge rotating cylinder is at low angles of attack which reduce the need for higher angles of attack for STOL aircraft.

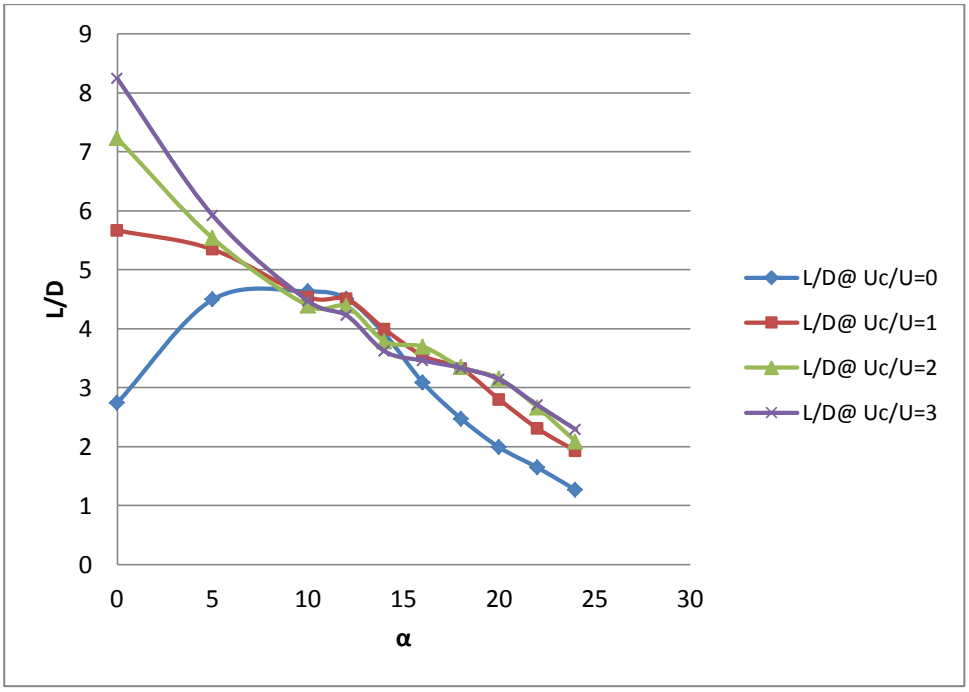

Figure 5-7: L/D curves at U_c/U=0-3

5.4.2 Aerodynamic characteristics using flaps

1. Lift characteristics

In this step, the leading edge rotating cylinder was used with another high lift device which is a plain flap. The flap was deflected at $\delta = 40°$ and the lift and drag forces were measured at each angle of attack. The graph in Figure 5-8 shows the lift coefficient against angle of attack of the testing model at $U_c/U = 0$ when the cylinder is not spinning with and without flap. The graph shows that when using the flap, the lift curve was shifted upward without any change in the slope. The stall angle was around 14 degrees angle of attack and the maximum lift coefficient is 1.42 when using flap.

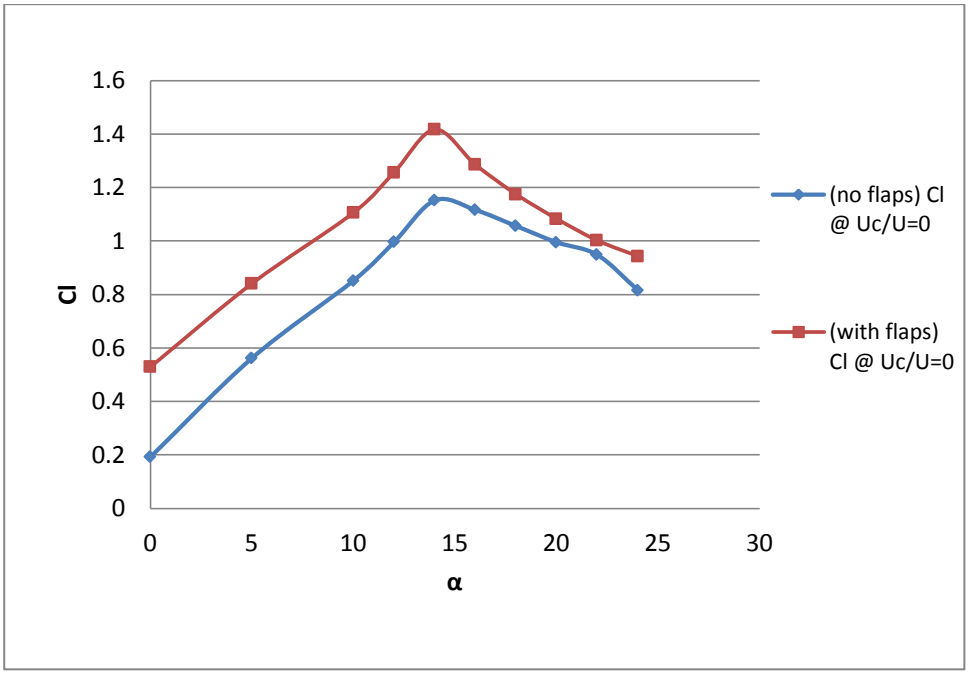

Figure 5-8: A comparison between C_L curves at $U_c/U=0$ with flap down and up.

The graph in Figure 5-9 shows the lift coefficient against angle of attack for the testing model at U_c/U= 0, 1, 2 and 3 when the flap is deflected at δ=40°. The graph shows that the lift coefficient increases as the rotation speed increases for the same angle of attack. For the cylinder rotating at U_c / U = 3 and δ=40°, the maximum lift coefficient is about 2.43 at α = 22. In comparison to the maximum lift coefficient at $U_c/U=0$ and δ=0°, the improvement in the lift coefficient is about 111%. If the flaps and rotating leading edge are used together as lift enhancement devices, the landing and takeoff distance will be shortened and that will lead to an improvement in performance and industry of the STOL aircraft.

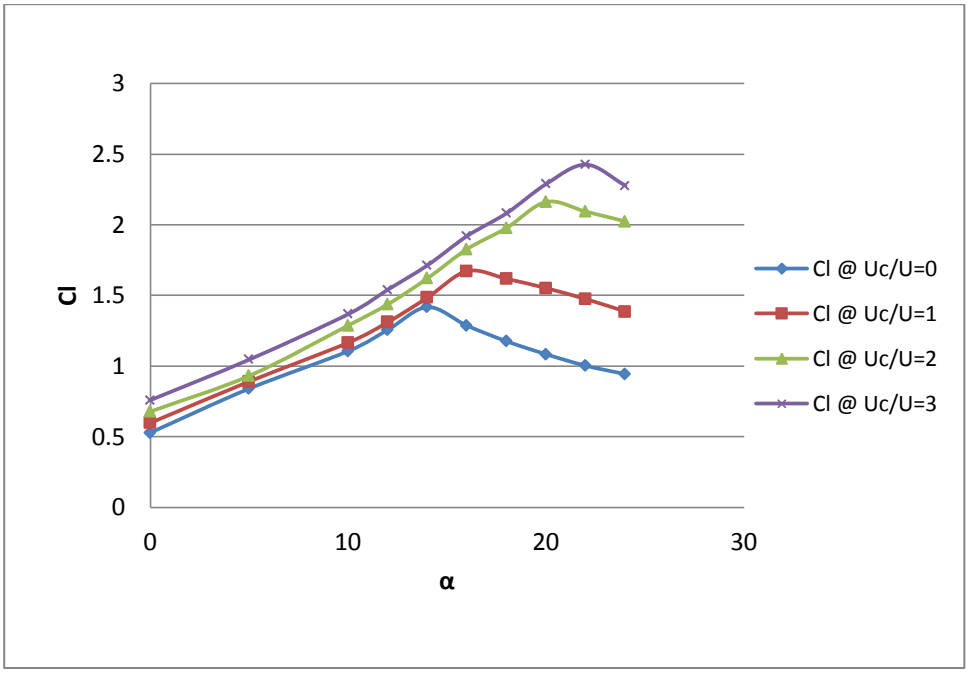

Figure 5-9: C_L curves at U_c/U=0-3 (at δ=40°).

2. Drag characteristics

The graph in Figure 5-10 shows the drag coefficient against angle of attack for the testing model at U_c/U= 0, 1, 2 and 3 when the flap is deflected at δ=40°. The graph shows almost linear rise in the drag coefficient as the rotation speed increases at the same angle of attack because of the pressure drag and skin friction drag in addition to the induced drag (caused by lift) which is proportional to the sine component of the lift force. The drag coefficient for the airfoil at a = 0 deg for different U_c /U is almost 0.15.

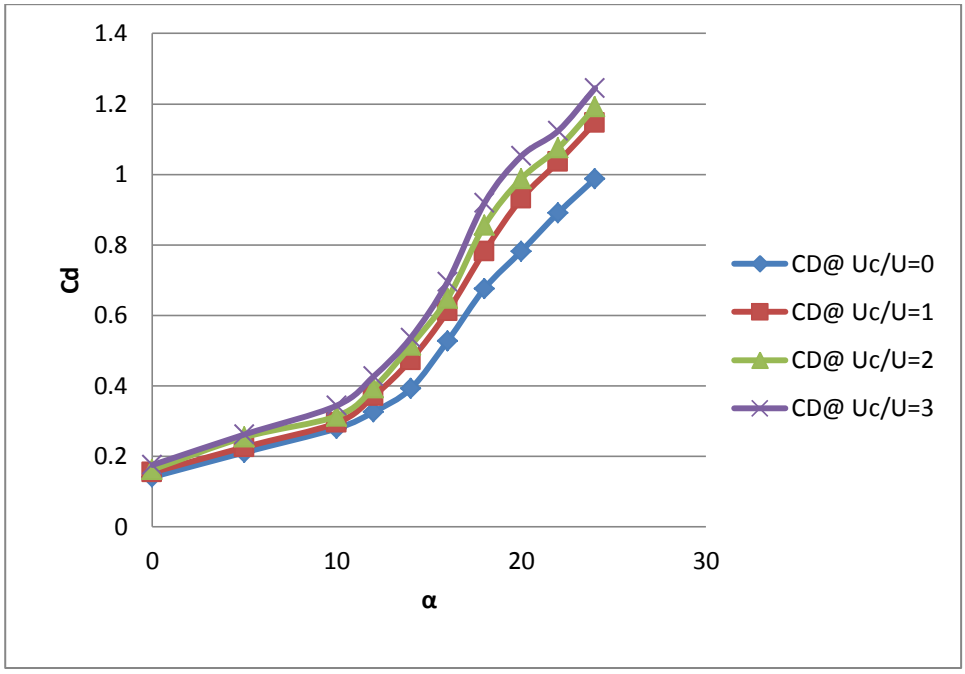

Figure 5-10: C_D curves at U_c/U=0-3 (at δ=40°).

3. Lift/drag ratio characteristics

The graph in figure 5-11 shows that the lift to drag ratio at α = 0 is 3.29 for U_c/U =0 and 3.88 for U_c/U =3. Note that the maximum L/D for the airfoil occurs at zero angle of attack. Also, from the figure, we can observe that the L/D rate is almost 4 below 10° and then drops after that. Therefore, the most effective range of the leading-edge rotating cylinder is at low angles of attack which reduce the need for higher angles of attack for STOL aircraft.

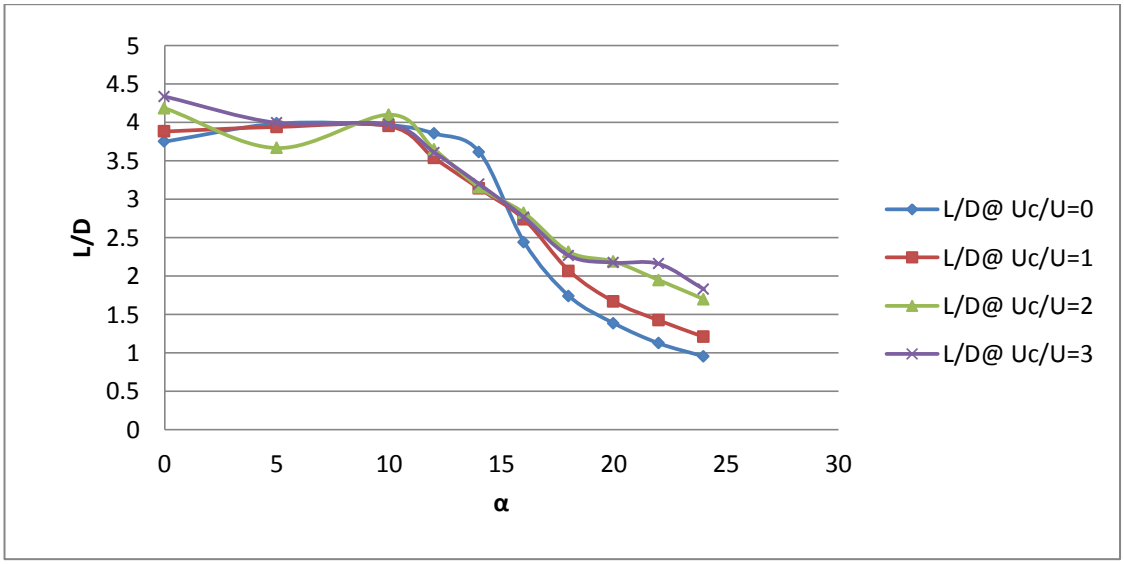

Figure 5-11: L/D curves at U_c/U=0-3 (at δ=40°).

5.6 Fixing the rotating cylinder on the aircraft

5.6.1 Preparation of the wing leading edge

The wing was prepared to contain two rotating cylinders at the leading edge along the flaps portion of the wing. The cavity of the cylinders in the leading edge was taken into consideration through the design and fabrication steps of the wing. Figure 5-12 shows the prepared cavity for rotating cylinders. A high speed bearing was fitted to outboard end of the cylinder cavity on each side of the wing. These bearings were fixed by a flanged cap to the wing ribs see Figure 5-13. The gap in-between the cylinder and the cylinder cavity wall was kept at 5mm to avoid any touchiness especially at high rotation speeds.

Figure 5-12: The prepared slot for the rotating cylinder.

Figure 5-13: The outboard end bearing and its housing.

5.6.2 Rotating cylinders design

Two aluminium alloy 6063 T6 54 mm outer diameter pipes were cut into 2.15 meters long each. Two machined bushings (see Figure 5-14) were fitted to each side of each rotating cylinder. An 8mm diameter shaft and 10 cm long was fitted to the bushings in the outboard side of each cylinder using a shaft lock screw. The shaft goes through the bearing to allow the cylinder rotation and to fix the cylinder to the wing. Two 12V D.C twin-high speed motors were fixed to the inboard sides of the cylinder cavity, connected directly to the cylinders bushings using a shaft lock screw (see Figure 5-15). These motors are manufactured by CMACMA Technologies each one weighs 2 pounds and rotates up to 16600 RPM. (see Figure 5-16).

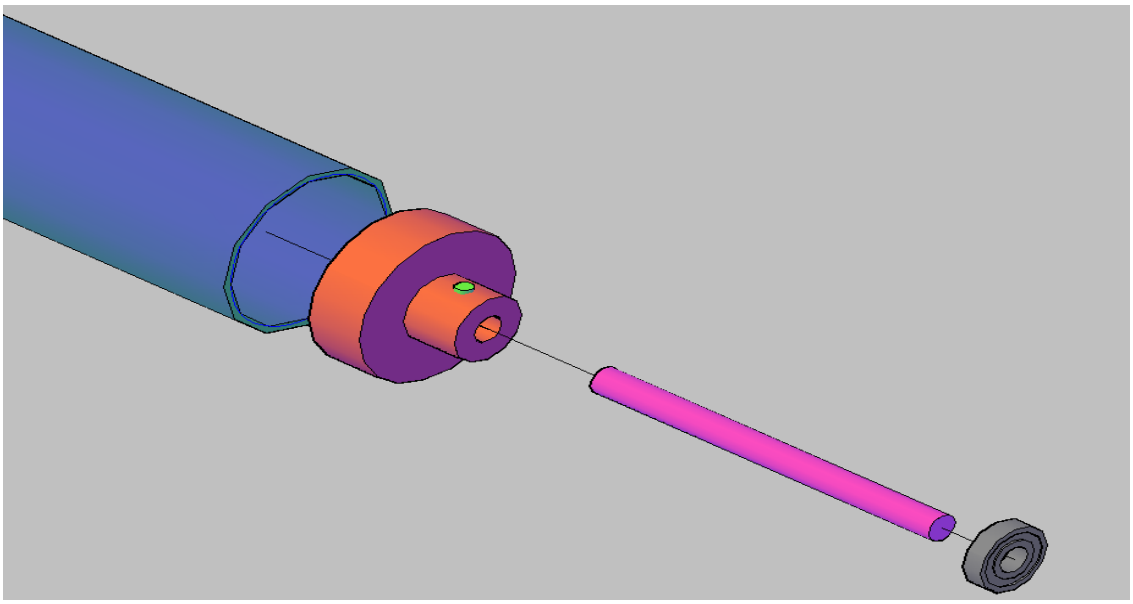

Figure 5-14: The outboard end of the rotating cylinder.

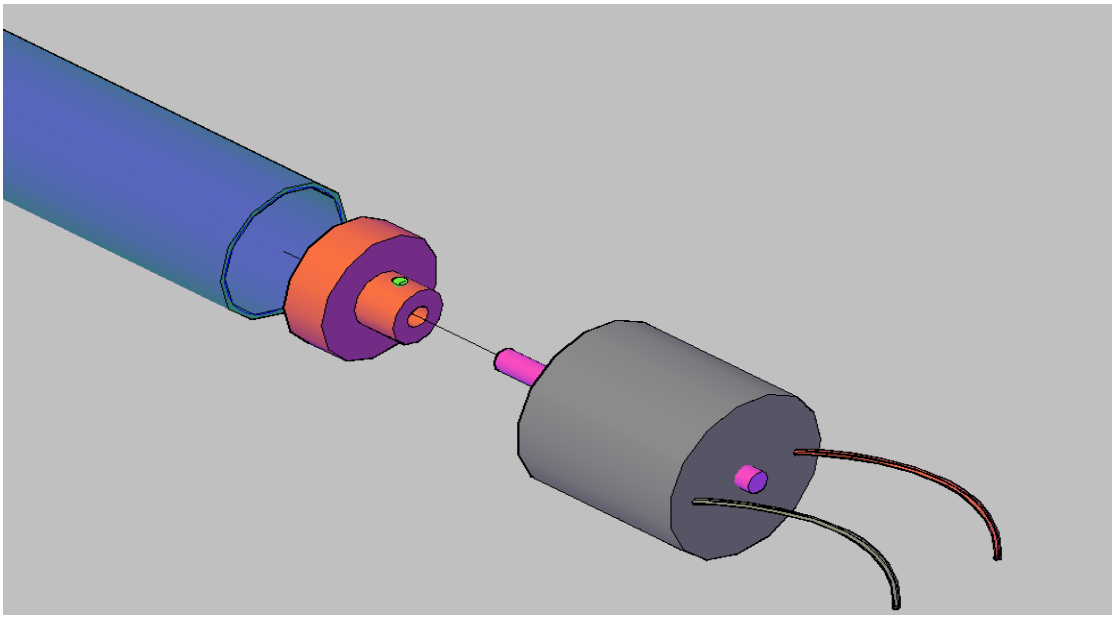

Figure 5-15: The inboard end of the rotating cylinder.

Figure 5-16: The motors used for rotating cylinder.

5.6.3 Rotating cylinders power source

Two options were negotiated as power sources for the rotating cylinders. The first option is to use the wind force by fitting ramp air turbine or fan in the middle (above the cockpit) where the speed can be controlled by a governor and transferred by a set of gears and shafts. The second option is to use the solar energy cells that charge a battery where the speed can be controlled by a variable speed controller or speed selector. The first option was ignored due to the complexity of the system and the cost. The second one was preferred because of the simplicity and cost. In this case, both motors were wired in parallel and connected to 2x12V battery (12APH).These batteries are connected in parallel to the main aircraft battery and charged using both the engine electricity and the solar cells.

Two flexible solar panels (Power Film 20 Watt) were ordered to be fitted to the upper surface of the wing (see Figure 5-17). These solar panels are equipped with blocking diodes which equip this panel to charge a 12V battery. The panels have the following specifications:

- Operating Voltage: 15.4V
- Operating Current: 1.2A
- Weight: 3 lb
- Dimensions: 12 x 73 inches

These two panels will be connected in parallel to provide 2.4 A which can give enough power to rotate the cylinders directly or charge an empty 12 APH battery in 5 hours.

Figure 5-17: Flexible solar panels (Power Film 20 Watt)

5.6.4 Operating the rotating cylinder

The rotation speeds can be controlled using a three-position switch to select low (9,500 RPM), high (16,600 RPM) and off positions.

1. For low rotation @ 9,500 RPM

Metric units were used for more accuracy and all dimensions in metric units.

The stall speed (V_s) =50mph =22.35 m/s (clean configuration)

$$U_c = \frac{2\pi R \times RPM}{60} = \frac{2\pi(0.027)\times 9500}{60} = 26.85\ m/s$$

$(U_c/U)_{low}$= 1.2

2. For high rotation @ 16,600 RPM

$$U_c = \frac{2\pi R \times RPM}{60} = \frac{2\pi(0.027) \times 16600}{60} = 46.91\ m/s$$

$(U_c/U)_{high}$= 2.1

When these cylinders are operated at stall speed, the lift coefficient will increase that will result in a reduction of stall speed (Vs < 50 mph) and shorter runway. A flight test will be needed for testing the improvement in aerodynamic characteristics and control.

The expected improvement in maximum coefficient of lift using the rotating cylinder - at$(U_c/U)_{high}$= 2.1- can be calculated as follows:

C_{Lmax} flaps down = C_{Lmax} clean + 1/2 C_{Lmax} with LERC where C_{Lmax} clean= 1 .6

= [1.6/2] + [2.25/2] = 1.925

The C_{Lmax} increased from 1.6 to 1. 925 (20%)

Then the dynamic pressure q= W/ Sw x C_{Lmax}

$$q = \frac{W}{S_w C_{L_{max}}} = \frac{1320}{138*1.925} = 4.96 \text{ psf}$$

where $q = \frac{\rho v^2}{2} = \frac{v^2}{391}$ at sea level conditions

(*q* is in 'psf' Pounds per square feet. when V is In mph)

Then: V_s= 44 mph (where V_s= 50 mph without using LERC)

So, the new stall speed is reduced by 12%. For better improvement U_c/U should be increased.

CHAPTER 6

Conclusion

6.1 The aircraft specifications

The final characteristics are listed in Table 6-1. The aircraft now is ready to fly after doing some ground checks for all of its systems. The aircraft will be introduced for certification and the aircraft will be ready for flying soon. The leading edge rotating cylinders can be tried and feedback from the pilot and measurements can be obtained.

Figure 6-1: The aircraft.

SPECIFICATIONS	
General	
seats	**2**
Weights	
Empty Weight	**820 lbs**
Gross Weight	**1320 lbs**
Fuel Capacity	**90lb**
Useful Load	**500lb**
Geometry	
Wing Span	**32 ft**
Wing Area	**138ft^2**
Aspect ratio	**7.42**
Length	**23 ft**
Height (At Wing)	**9.6 ft**
Engine	**Aerovee 2.1**
Horse Power	**80**
Fuel Consumption (80%)	**3.5Gal/hr**
Performance	
Stall speed	**50mph**
Cruise Speed	**112 mph**
Never Exceed Speed	
Maximum Speed	**124 mph**
service celling	**11,000ft**
Range (with reserve)	370**miles**
wing laoding	**10.24**
Rate Of Climb	**843 ft/min**
Take Off Roll	560 **ft**
Landing Ground Roll	**687 ft**
TO Distance - 50 ft obstacle	**732 ft**

Table 6-1: The aircraft specifications.

6.2 Comparison to the results for symmetric airfoil NACA 0024

If we compare the results of this study to the results that was conducted by Dr. Ahmed Al Garni and his team for symmetric airfoil NACA 0024 (see Figures 6-2 and 6-3), we can observe the following:

- For airfoil NACA 0024 at U_c / U = 3:

The Reynolds number was 6.5×10^4 based on the model chord.

  - 88% increase in lift (from 0.85 to 1.6) due to the cylinder rotation at δ = 0°.
  - 124% increase in lift (from 0.85 to 1.9) due to the combined effects of the cylinder rotation and flap deflection at δ = 30°. (See Figures 6-2 and 6-3).
  - About 20° increase in stall angle (160%).

- For airfoil NACA 2412 at U_c / U = 3:

  The Reynolds number was 8.56×10^4 based on the model chord.

- 83% increase in lift (from 1.15 to 2.11) due to the cylinder rotation at δ = 0°.
- 111% increase in lift (from 1.15 to 2.43) due to the combined effects of the cylinder rotation and flap deflection at δ = 40°.
- 8 degrees delay in stall angle (57% increase)

The differences in results are due the following:

- airfoil type (cambered and symmetric)
- Rotating cylinder size
- flap size and deflection angle
- testing model conditions
- testing tools and facilities.

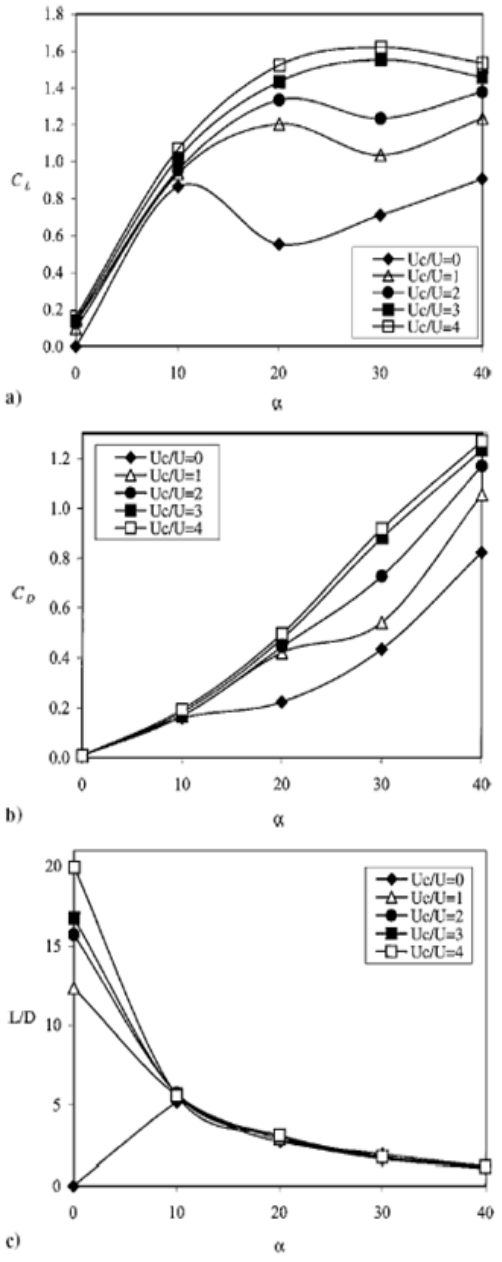

Figure 6-2: Effect of leading-edge rotating cylinder at δ = 0° on the aerodynamics characteristics of NACA 0024.[40]

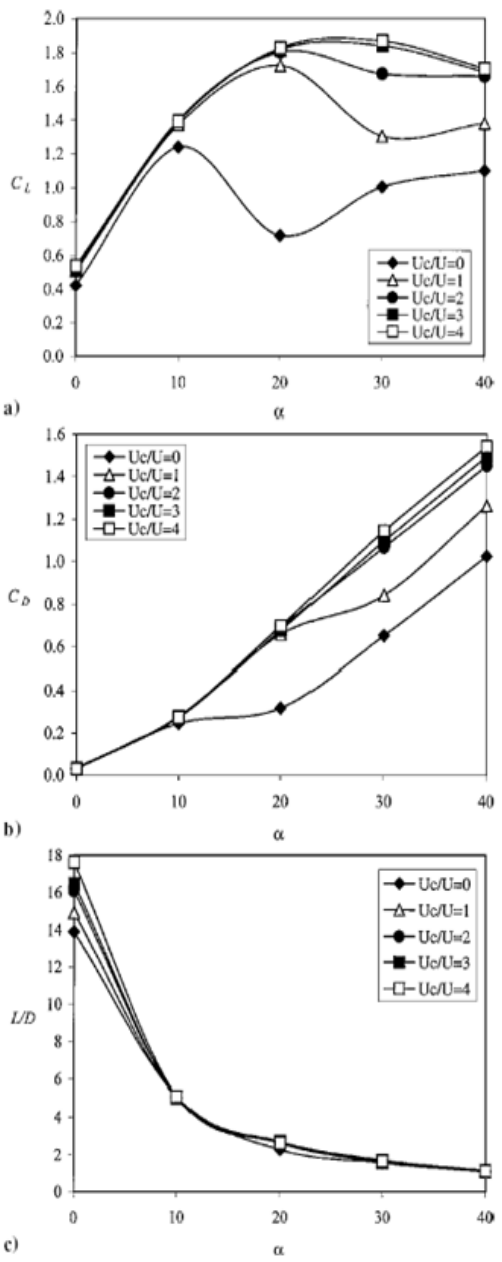

Figure 6-3: Effect of leading-edge rotating cylinder at δ = 30° on the aerodynamics characteristics of NACA 0024. [40]

6.3 Conclusion

The experimental investigation showed some very important and interesting results regarding the leading edge rotating cylinder which is promising as a successful high lift device. The maximum lift coefficient was increased by 83% for clean configuration (flap up) and 111% when using flap at cylinder rotation $U_c/U=3$. The lift to drag ratio increased by 3 times with cylinder rotation $U_c/U=3$ at zero angle of attack and the stall angle was delayed by 8 degrees. The increase in lift coefficient and the delay of the stall angle of attack would improve the maneuverability and performance of the airplane especially for STOL aircraft. The test showed that the most effective range of the leading-edge rotating cylinder is at low angles of attack which reduce the need for higher angles of attack for STOL aircraft. The expected improvement in maximum coefficient of lift of our aircraft using the rotating cylinder at $(U_c/U)_{high}=2.1$ will be 20% (from 1.6 to 1.92). The stall speed will be reduced from 50 mph to 44 mph and this will shorten the runway.

Due to the improvements in the aerodynamic characteristics such as lift and lift to drag ratio and delay of the stall angle, this technology will be more attractive for the aerospace industry in the future. By comparing these results for the rotating leading edge cylinder concept for the cambered to the symmetric airfoil, we can say that this technology is more recommended for symmetric airfoils. This is very promising and the results of this project give great indications that there is huge potential for this method of flow control.

6.4 Recommendations for further research

This thesis has covered one of the applications of moving surface boundary layer control to a streamlined body. More research and time is needed in this field to consolidate and extrapolate the findings of this project and the following suggestions are made for further areas of study:

- The effect of adding more rotating cylinders could be experimentally analyzed. These cylinders would be added to the top surface of the airfoil or at the trailing edge.
- The sensitivity of the gap distance could be investigated for an optimum gap for L/D ratio.
- The effects of surface roughness could be investigated.
- Computational methods and flow visualization methods could be carried out involving more models.

References

1. Wygnanski, I., & Newman, B.G., "The Effect of Jet Entrainment on lift and Moment for a Thin Airfoil with Blowing" *Aeronautical Quarterly,* Vol.15, 1964, p122
2. Helen Heapc and Bill Crowther," A Review Of Current Leading Edge Device Technology And Of Options ForInnovation Based On Flow Control" University of Manchester, UK,2003.
3. Flaig, A. & Hilbig, R, "High lift design for large civil aircraft." High Lift Aerodynamics AGARD. CP515, Sept 1993, pp31-1 31-12
4. HELIX Consortium, "Innovative Aerodynamic High Lift Concepts" Project number GRD1-2000- 25205, Version 1.3 pp 10.
5. Modi, V. J., Mokhtarian, F., Fernando, M. S. U. K., and Yokomizo, T.,"Moving Surface Boundary-Layer Control as Applied to Two-Dimensional Airfoils," *Journal of Aircraft*, Vol. 28, No. 2, 1991, pp. 104–112.
6. Gad-el-Hak, M., "Flow Control passive, active and reactive flow management," Cambridge University Press, 2000, pp25.
7. Bin Ying, "Boundary-Layer Control of Bluff Bodies With Application to Drag Reduction of Tractor-Trailer Truck Configurations," *M.A.Sc. Thesis,* University of British Columbia, Dec. 1991.
8. Ming, C., Qiang, Y., and Li-Shi, L., "Simulation of flow past a rotating circular cylinder near a plane wall," *International Journal of Computational Fluid Dynamics,* Vol. 20, No. 6, 2006, pp. 391-400.
9. Goldstein, S., *Modem Developments in Fluid Mechanics,* Vols. I and II, Oxford University Press, 1938.
10. Lachmann, GV.,*Boundary Layer and Flow Control,* Vols.I and Il, Pergamon Press, 1961.
11. Rosenhead, L., *Laminar Boundary Layers,* Oxford University press, 1966.
12. Schlichting, H., *Boundary Layer Theory,* McGraw-Hill Book Company, 1968.
13. Chang, P.K., *Separation of Flow,* Pergamon Press, 1970.

14. Magnus, G, "Ueber die Verdichtung der Gase an der Oberflache Glatter Kerper,"Poggendorfs Annalen der Physik und Chemie, Vol. 88, No.1, 1853, pp 604-610.

15. Swanson, W.M., "The Magnus Effect: A Summary of Investigation to Date," *Transactions of the ASME, Journal of Basic Engineering*, Vol. 83, September 1961, pp. 461-470.

16. Ericsson, L.E., "Moving Wall Effects inUnsteady Flow", *Journal of Aircraft,* Vol. 25,No.11, Nov 1988, pp 977-990.

17. L. Rayleigh, *On the irregular flight of a tennis ball,* Messenger of Mathematics,**7** (1877), 14-16.

18. Betz, A., "History of Boundary-Layer Control in Germany," *Boundary-Layer and Flow Control,* Editor: G.V. Lachmann, Pergamon Press, New York, Vol. I, pp. 1-20.

19. Flettner, A., "The Flettner rotor Ship," *Engineering,* Vol. 19, January 1925, pp. 117-120.

20. Benjamini I. Triplett, "Aerodynamics of an Airfoil with Plain Flap in Presence of Momentum Injection," *Master Thesis,* University of British Columbia, Canada, 2000.

21. Favre, A., "Contribution a l'Etude Experimentale des Mouvements Hydrodynamiques a Deux Dimensions," Thesis presented to the University of Paris, 1938.

22. Alvarez-Calderon, A., and Arnold, F. R., "A Study of the Aerodynamic Characteristics of a High Lift Device Based on Rotating Cylinder Flap, "Stanford University Technical Report RCF-1, 1961.

23. Brown, D.A., "Peruvians Study Rotating-Cylinder Flap," *Aviation Week and Technology*, Vol. 88, No. 23, December 1964, pp. 70-76.Tennant, J. S., Johnson, W. S., & Korthapalli, A., "Rotating Cylinder for Circulation Control on an Airfoil," *Journal of Hydronautics,* Vol. 10, 1976, pp. 102--105.

24. Brooks, J. D., "The Effect of a Rotating Cylinder at the Leading and Trailing Edges of a Hydrofoil," U.S. Naval Ordnance Test Station,NAVWEPS Rept. 8042, April 1963.

25. Steele, B. N and Harding, M. H., “The Application of Rotating Cylinder to Ship Maneuvering,” National Physical Laboratory, Ship Division, UK, Report No. 148, Dec 1970.
26. Cichy, D. R., Harris, J. W., and MacKay, J. K., "Flight Tests of a Rotating Cylinder Flap on a North American Rockwell YOV-10AAircraft," NASA CR-2135, Nov. 1972.
27. Sandeep R., "Aerodynamics and Dynamics of Bluff Bodies in Presence of the Moving Surface Boundary-Layer Control," *Doctoral Thesis*, University of British Columbia, Dec. 1996.
28. Theo Thomson, M., " A Comparative Study of the Aerodynamic Characteristics of a Modified Symmetrical Airfoil Section Fitted with Leading and Trailing Edge Flow Control Devices In and Out of Ground Effect," School of Engineering and Design, Brunel University, 2006.
29. Tennant, J. S., “The Theory of Moving Wall Boundary Layer Control and its Experimental Application to Subsonic Diffusers,” Ph.D. Dissertation, Clemson Univ., Clemson, SC, May 1971.
30. Johnson, W. S., Tennant, J. S., and Stamps, R. E., "Leading EdgeRotating Cylinder for Boundary-layer Control on Lifting Surfaces," *Journal of Hydrodynamics*, Vol. 9, No. 2, April 1975, pp. 76-78.
31. Modi, V. J., Sun, J. L. C., Akutsu, T., Lake, P., McMillian, K., Swinton,P. G., and Mullins, D., "Moving Surface Boundary-layer Control for Aircraft Operation at High Incidence," *Journal of Aircraft*, AIAA, Vol.18, No. 11, November 1981, pp. 963-968.
32. Mokhtarian, F., and Modi, V. J., "Fluid Dynamics of Airfoil with Moving Surface Boundary-layer Control," *AIAA Atmospheric Flight Mechanics Conference*, August 1986, paper No. 86-2184-CP; also *Journal of Aircraft*, Vol. 25, No. 2, February 1988, pp. 163-169.
33. Mokhtarian, F., Modi, V. J., and Yokomizo, T., "Rotating Air Scoop as Airfoil Boundary-layer Control," *Journal of Aircraft*, AIAA, Vol. 25, No.10, October 1988, pp. 973-975.
34. Modi, V. J., Munshi, S. R., Bandyopadhyay, G., and Yokomizo, T.,“High-Performance Airfoil with Moving Surface Boundary-Layer Control,”*Journal of Aircraft*, Vol. 35, No. 4, 1998, pp. 544–553.

35. Modi, V.J., "Moving Surface Boundary-Layer Control: A Review," *Journal of Fluids and Structures*, Vol. 11, No. 6, 1997/8, pp. 627-663.
36. Modi, V.J., Fernando, M.S.UK & Yokomizo, T., "Moving Surface Boundary Layer Control: Studies with Bluff Bodies and Application," *AIAA Journal*, Vol. 29, No.9, Sept 1991, pp 1400 -1406.
37. Hassan, A.A. & Sankar, L.N., "Separationcontrol Using Moving Surface Effects: A Numerical Simulation," *Journal of Aircraft*, Vol. 29, No.1, Jan - Feb 1992, pp 131-139.
38. Gerontakos, P. and Lee, T., "Near Wake Behind an Airfoil with Leading-Edge Flow Control," *Journal of Aircraft*, Vol. 42, No. 2, 2005, pp. 561--567.
39. Sayers, A. T., "Lift Coefficient and Flow Visualization on Leading Edge Rotating Cylinder Rudder," *International Journal of Mechanical Engineering Education*, Vol. 7, No. 2, 1979, pp. 75–79.
40. Ahmed Z. Al-Garni, Abdullah M. Al-Garni, Saad A. Ahmed and Ahmet Z. Sahin.," Flow Control for an Airfoil with Leading-Edge Rotation" *Journal of Aircraft*, Vol. 37, No. 4, July–August 2000.
41. Chaplin, R., Flow control over a streamlined body using a rotating leading edge, *Department of Mechanical Engineering Strathclyde University U.K.*, 2005.
42. Thomas C. Corke, Design of Aircraft, Prentice Hall, 2002.
43. Chris Heintz, "Aircraft Design Made Easy", http://www.zenithair.com/images/kit-data/ch-design-made-simple-p1.pdf
44. Chris Heintz, "Anatomy of a STOL Aircraft", http://www.zenithair.com/stolch801/design/design.html.
45. Advisory Circular, AC 120-27E, **Aircraft Weight and Balance Control**, FAA, 2005.
46. Aerovee 2.1 engine manuals and website/ http://www.aeroconversions.com.
47. DATCOM software user manual.
48. A conference to be held " experimental study of a rotating leading edge airfoil'

Appendix A

Material spesification

1- Aluminm profiles specification certification.

PRODUCTS TECHNICAL SPECIFICATIONS

الوبكو ALUPCO

QUALITY CONTROL SPECIFICATIONS AND STANDARDS:

Quality specifications in Alupco meet local and international standards such as SASO (Saudi), DIN (German), ASTM (American), BS (British) and ISO (International Standard Organization).

1. EXTRUSION:

A. ALLOYS:

Alloys and compositions according to aluminium association as shown in the following table:

ALUPCO ALLOYS				
ALLOY	6061	6063	6082	6351
ELEMENT	MIN.–MAX.	MIN.–MAX.	MIN.– MAX.	MIN.–MAX.
% SILICON	0.40 - 0.80	0.20 - 0.60	0.70 - 1.30	0.70 - 1.30
% IRON	0.70	0.35	0.50	0.50
% MAGNESIUM	0.80 - 1.20	0.45 - 0.90	0.60 - 1.20	0.40 - 0.80
%MANGANESE	0.15	0.10	0.40 - 1.00	0.40 - 0.80
% COPPER	0.15 - 0.40	0.10	0.10	0.10
% ZINC	0.25	0.10	0.20	0.20
% TITANIUM	0.15	0.10	0.10	0.20
% CHROMIUM	0.04 - 0.35	0.10	0.25	---
% OTHERS	0.15	0.15	0.15	0.15

Percent by weight except where a range is shown. All values are maximum unless minimum mentioned. Regular checks are conducted to confirm the chemical composition of the above mentioned alloys.

B. HEAT TREATMENT:

T6 - Heat treated hardened metal (artificial ageing).
T4 - Heat treated and naturally aged (for bending).

Regular tests are made after each heat treatment process to ensure conformity to specifications.

C. MECHANICAL PROPERTY:

In T6 condition, the following mechanical properties are achieved:

ALLOY PROPERTIES	6061	6063	6082	6351
MINIMUM YIELD STRENGTH (N / MM2)	240	160	260	250
MINIMUM ULTIMATE TENSILE STRENGTH (N / MM2)	260	215	310	290
MINIMUM % OF ELONGATION	8	10	8	8

Periodical checks are conducted according to the DIN standard tests. 6061, 6082 and 6351 are hard alloys used mainly for non-architectural applications and require more wall thickness than 6063 alloy with tolerances according to DIN 1748. These alloys are less suitable for anodized quality due to color variations.

2- Aluminm sheets specification certification

شركة الخليج لدرفلة الألمنيوم ش.م.ب.(م)
GULF ALUMINIUM ROLLING MILL CO. B.S.C. (c)

جارمكو GARMCO
N. Sitra Industrial Area Telex. 9786 GARMCO BN
P.O. Box 20725, Kingdom of Bahrain Fax: 17 730542 - Tel: 17 731000

TEST CERTIFICATE

SHEET 1 OF 1

CERTIFICATE & DATE	OUR ORDER NUMBER(S)
781393 08-08-2007	GS44590 03

ULTIMATE CONSIGNEE

CUSTOMER P.O. NUMBERS: D07-343

ORDER DETAIL:

PRODUCT TYPE: ALUMINIUM SHEETS MILL FINISH

ALLOY 1050 TEMPER H24 STANDARD EN 573/485

GAUGE 2.000 MM WIDTH 1219.00 MM LENGTH 2438.00 MM

CUSTOMER NAME & ADDRESS
ABDULLATIF AND MOHAMMED ALFOZAN CO.
P.O.BOX 38, ALKHOBAR 31952
SAUDI ARABIA, TEL:9663-8959094
FAX: 9663-8955305/8984848

WE HEREBY CERTIFY THAT THE MATERIAL DESCRIBED HEREIN HAS BEEN MAI UFACTURED IN ACCORDANCE WITH THE STANDARDS SPECIFIED, AND THAT SATISFIES THE STIPULATED REQUIREMENTS.

SURVEYOR

TECHNICAL MANAGER

PACKING LIST # G162499

LC NUMBER E026731

PACKAGE NUMBERS	MECHANICAL TEST SLAB #	TEST #	TENSION TEST Tensile Strength	Yield Strength	Elongation	REMARKS
	Units		N/MM2	N/MM2	%	
	Specified minimum Specified maximum		105 145	75	5.00	
1076259 1076264 1076260 1076263	872560	576478	133	128	7.05	
1076266 1076265 1076267 1076268 1076269	872565	576477	130	122	8.20	

CHEMICAL ANALYSIS

	Si	Fe	Cu	Mn	Mg	Cr	Zn	Ti	Others Each	Others Total	Al
Spec. Min.											99.50
Spec. Max.	0.250	0.400	0.050	0.050	0.050		0.050	0.030	0.030	0.100	
SLAB #											
872560	0.110	0.290						0.008	0.012	0.012	99.58
872565	0.090	0.290						0.008	0.013	0.013	99.60

ISO 9001 Control Code: TECH/DOC - 0011 Issued Date: 10/12/2006

MS 002 10/92

VITAE

1. **SAEED ABDULLAH AL AHMRI**
2. My Nationality is Saudi.
3. Born in ABHA, Saudi Arabia.
4. Address: Kingdom of Saudi Arabia, Dhahran (31261) , P. O. Box # 7889,
5. E-mail: (pir_sq2@hotmail.com).
6. Contact Number: 00966568839999.
7. Received Bachelor Degree with distinction in Aerospace Engineering from King Fahd University of Petroleum & Minerals, Dhahran, Saudi Arabia, in June 2002.
8. Joined the Royal Saudi Air Force as an Engineering Officer in Sep. 2002.
9. Received Master of Science Degree in Aerospace Engineering with emphasis on Aerodynamics, Design and Structure as a major from King Fahd University of Petroleum & Minerals, Dhahran, Saudi Arabia, in 2011.